NTNU – Trondheim
Norwegian University of
Science and Technology

Structural resistance of polar ships to ice loading

Discussion of the IACS Polar rules
considering different structural and
methodological aspects

Mustapha El Jaaba

Marine Technology (2 year)
Submission date: June 2013
Supervisor: Jørgen Amdahl, IMT

Norwegian University of Science and Technology
Department of Marine Technology

MASTER THESIS

Spring 2013

Structural resistance of polar ships to ice loading

Discussion of the IACS Polar rules considering different structural and methodological aspects

Maine Construction

Author: El Jaaba Mustapha

Supervisor: Prof. Jørgen Amdahl

NTNU

Norwegian University of Science and Technology

Department of Marine Technology

NTNU
Norwegian University of Science and Technology
Department of Marine Technology

MASTER THESIS

Abstract:

Polar shipping and offshore activities in the arctic areas are increasing constantly, due to the growing interest in the main trans-arctic routes and the development of the extraction of petroleum and gas in these regions. In this regard, huge efforts have been made to develop and improve means for gradually introducing arctic commercial navigation and resources exploitation. In the same time, stricter safety and environmental standards have been promoted by different international organizations, especially polar countries. These two trends have led in developing new designs and operational standards, with the purpose of ensuring safe and sustainable activities in the arctic areas.

Classification societies, as an important member within the maritime cluster, have had the leading role and the commitment in developing rules and standards that can help designing and operating ice-strengthened ships and ships with icebreaker abilities in a safe manner.

In this purpose, The International Association of Classification Societies (IACS) took the initiative of developing unified common Rules for Polar Ships (URI1 to URI3), in collaboration with other classification societies and skilled groups from the concerned polar countries.

Address:
NTNU
Department of Marine Technology
N-7491 Trondheim

Location
Marinteknisk Senter
O. Nielsens vei 10

Tel. +47 73 595501
Fax +47 73 595697

NTNU
Norwegian University of Science and Technology
Department of Marine Technology

Table of Contents

Address:
NTNU
Department of Marine Technology
N-7491 Trondheim

Location
Marinteknisk Senter
O. Nielsens vei 10

Tel. +47 73 595501
Fax +47 73 595697

Address:
NTNU
Department of Marine Technology
N-7491 Trondheim

Location
Marinteknisk Senter
O. Nielsens vei 10

Tel. +47 73 595501
Fax +47 73 595697

Table of Figures

Address:
NTNU
Department of Marine Technology
N-7491 Trondheim

Location
Marinteknisk Senter
O. Nielsens vei 10

Tel. +47 73 595501
Fax +47 73 595697

Table of Tables

Address:
NTNU
Department of Marine Technology
N-7491 Trondheim

Location
Marinteknisk Senter
O. Nielsens vei 10

Tel. +47 73 595501
Fax +47 73 595697

NTNU
Norwegian University of Science and Technology
Department of Marine Technology

Nomenclature

K_n	Kinetic energy
E_{crush}	Crushing energy
V_n	Normal velocity
V_{ship}	Ships velocity
F_n	The bow normal ice force
λ_n	Stem penetration in ice as defined by figure
λ_{n_m}	The stem maximum penetration in ice
M_e	Effective mass
M_{ship}	Ships displacement
Co	Mass reduction coefficient
P	Ice pressure
Po	Ice pressure (at 1 m^2) [MPa]
A	Nominal contact area of the stem and ice edge
ex	Pressure-area exponent [no units, assume ex = -0.1]
W	The ice patch width
H	The ice patch height
AR	Design patch aspect ratio
fa	Shape factor which expresses the influence of the bow shape on ice force
x	Distance from the forward perpendicular FP to the hull position under consideration
L	Ship length
CF_c	Crushing failure class factor
CF_F	Flexural failure class factor
CF_D	Load Patch Dimensions Class Factor
CF_{Dis}	Displacement Class Factor
CF_L	Longitudinal Strength class factors
h_{ice}	Ice thickness [m]
σ_f	Ice flexural strength [MPa]
Q	Ice line load
dR	Force increment
K_0	Elastic stiffness matrices
K_σ	Geometrical stiffness matrices
dr	Displacement increment
l	Frame span
σ_y	Yield stress
τ_y	Yield shear stress
σ_{cr}	Elastic critical buckling stress (Euler buckling stress)
q	Line load
Z_y	Elastic section modulus
Z_p	Plastic section modulus
Z_{pr}	Reduced plastic section modulus
M_p	Plastic bending moment
M_{pr}	Reduced plastic bending moment due to shear
h_w	Web height
t_w	Web thickness
S	Plate spacing
t_p	Attached plate thickness
b_f	Flange width
t_f	Flange thickness
A_w	Web area
A_f	Flange area
A_0	Minimum web area
z_{na}	Plastic neutral axis above the attached plate
w_e	External work due to patch load
w_i	Internal work
w	Maximum deflection

Address:
NTNU
Department of Marine Technology
N-7491 Trondheim

Location
Marinteknisk Senter
O. Nielsens vei 10

Tel. +47 73 595501
Fax +47 73 595697

NTNU
Norwegian University of Science and Technology
Department of Marine Technology

MASTER THESIS

k_w	Ratio of the web modulus
Z_w	The web plastic section modulus
b	Ice patch breadth
q_c	Line load plastic capacity
q_y	Line load elastic capacity
α	The shape factor
k_z	Ratio of z_p to Z_p
z_p	Sum of plastic section modulus of plate and flange
k_σ	Buckling factor
υ	Poisson's coefficient
E	Young's modulus
f_y	Yield strength
$\bar{\lambda}$	Reduced slenderness
m_p	Plastic moment plate capacity pr. Unit length
t	Plate field thickness
KE	The kinetic energy
PE	The potential energy
IE	The ice indentation energy
F_{IB}	Vertical ice bow force
κ	Normalized ice strength
K_h	Vertical stiffness at the bow
K_{Ice}, K_f	Stem indentation parameter in the ice
γ	Stem angle
α	Waterline angle
D	Ship displacement
A_{wp}	Water-plane area
A_v	Vertical projection of the contact area between the stem and the ice edge

Address:
NTNU
Department of Marine Technology
N-7491 Trondheim

Location
Marinteknisk Senter
O. Nielsens vei 10

Tel. +47 73 595501
Fax +47 73 595697

NTNU
Norwegian University of Science and Technology
Department of Marine Technology

MASTER THESIS

1. Introduction and Summary

Generally, the design of ships and offshore structures intended for operation in ice infested waters has been based upon elastic methods of plasticity. However, through development of knowledge regarding the true behaviour of structural components in the large deflection and post-ultimate resistance range, the achievement of more consistent utilization of strength members has become possible. Overloading in the case of ice loading is quite typical and hard to overlook.

To minimize the consequences of these overload conditions; a better understanding of structure behaviour within the plastic range has become a necessity.

Notwithstanding the plastic design method can be somewhat more complex than the elastic approach; the method may result in significant reduction in steel weight.

In this purpose, the International Association of Classification Societies, (IACS), has initiated new unified rules for Polar ships, in collaboration with the Russian Register and partly by experience from DNV and other classification societies. These rules are based mainly on plastic methods with the purpose of determining the scantlings of plating, stiffeners and girders that correspond to the structure maximum resistance as the ship is crushing the ice

In the IACS unified rules, a steel Polar Ship intended for navigation in ice-infested polar waters is assigned a class notation PCi, as described in table 1 in the IACS polar class requirement I1.

The selection of a class notation is a result of keeping the balance between statistical analysis, owners experience, ice expertise and financial/economic considerations.

Address:
NTNU
Department of Marine Technology
N-7491 Trondheim

Location
Marinteknisk Senter
O. Nielsens vei 10

Tel. +47 73 595501
Fax +47 73 595697

Table 1: Polar class description

PC1	Year-round operation in all Polar waters
PC2	Year-round operation in moderate multi-year ice conditions
PC3	Year-round operation in second-year ice which may include multiyear ice inclusions.
PC4	Year-round operation in thick first-year ice which may include old ice inclusions
PC5	Year-round operation in medium first-year ice which may include old ice inclusions
PC6	Summer/autumn operation in medium first-year ice which may include old ice inclusions
PC7	Summer/autumn operation in thin first-year ice which may include old ice inclusions

Due to the growing popularity of the IACS Polar Class rules, (UR I1), within the maritime cluster these days, it is necessary for the concerned designers and approval engineers to better understand and master the background and the different aspects that have led to these rules, which has been the main motivation for the issuance of this project.

Address:
NTNU
Department of Marine Technology
N-7491 Trondheim

Location
Marinteknisk Senter
O. Nielsens vei 10

Tel. +47 73 595501
Fax +47 73 595697

2. Scope

This report is partially dedicated to give better understanding of the background and the philosophy behind the IACS Polar Class (UR I1) requirements, and partially to discuss the rules considering different structural and methodological aspects.

To convoy the legitimacy of the IACS Polar Class (UR I1) requirements, a set of comparisons with non-linear finite element analysis are carried out considering different structural aspects.

Correspondingly, a comparison of steel weight increase as a result of increasing class from PC7 to PC1 is also carried out

To carry out non-linear finite element analysis, it has been initially suggested to use Abaqus. However, and due to the unavailability of Abaqus, it has been chosen to use USFOS instead.

In this report, it has been focused mainly on plate and frame requirements within an ice reinforced area for a ship constructed of steel and intended for navigation in ice-infested polar waters.

Address:
NTNU
Department of Marine Technology
N-7491 Trondheim

Location
Marinteknisk Senter
O. Nielsens vei 10

Tel. +47 73 595501
Fax +47 73 595697

3. Hull area extent in the IACS Polar Class rules (UR I1)

The realization of hull area extent requirements is a result of long investigations of the corresponding requirements in the Canadian Equivalent Standards, the New Edition of the Russian Register Rules, the American Bureau of Shipping and the Baltic rules. Data extracted from historical events indicating damage in certain hull areas has been also a very important input for the purpose of defining ship/ice interaction design loading scenarios. The possible Design Loading Scenarios Affecting Hull Area Extent Definitions have been sorted out by James Bond in table 3.4 [Reference 16], and reproduced in this report in table 2

Table 2: Design Loading Scenarios Affecting Hull Area Extent Definition

Design Loading Scenario	Description
Ramming 1	Ramming in level ice
Ramming 2	Ramming ridges
Ramming 3	Ramming and maneuvering in ridges and hummocks filed
Open Pack 2	Reflected impact from one floe to another
Open Pack 3	Striking a floe on the quarter during a turn
Wedging 1	wedging between two floes or a narrow lead
Dangerous 1	Striking a concealed multi-year floe or growler
Dangerous 4	Ramming a growler among whitecap wavers
Offshore 1	Breaking up ice to protect an offshore installation or shore facility
Shallow Water 1	Ice pieces strike the bottom and bilge in shallow water
Shallow Water 2	Ice pieces jam between the ship's bottom and the seabed
Shallow water 3	Ship strikes submerged ice attached to the seabed
Pressure 1	Ship stopped in pressure
Pressure 3	Ship stopped in pressure with multi-year floe or glacial ice on one side

In order to create one common hull area extent requirements, a compromise between the Canadian and Russian approach has been discussed by the Canada-Russia bilateral group. The decisions made have been taken based on the ice conditions possible in the Russian and the Canadian arctic, regulatory Policies as well as damage reports.

The Ice conditions in the Canadian arctic are quite sever during the winter, with a variety of challenging multi-year ice features, like ridges, hummocks and rafted ice up to 10 meters height. Even during the summer, southward drifting winter ice may be encountered. In addition, ice features with winter strength tend to become summer strength very late in the year, i.e. early August.

Due to this ubiquity of sever ice conditions during a long period of the year, heavy ice may be encountered in open waters during the summer with significant concentrations.

Moreover, the Canadian Government regulatory policy requires independent year round navigation in the Canadian Arctic.

The ice condition in the Canadian arctic and the northern sea route together with the regulatory policies and damage reports are the radicals behind the design loading scenario listed in table 2. The ice belt extension in each area is then based on the expectation of occurrence of these ship/ice interaction design loading scenarios.

The final result from this bilateral work was that the hull area is divided horizontally to distinguish between the Bow, Bow Intermediate, Mid-body and Stern area, and vertically to distinguish between the Ice, Lower and Bottom areas, as described by figure 1 in the IACS Unified Requirements for Polar Ships and reproduced in this report in figure 1.

Address:
NTNU
Department of Marine Technology
N-7491 Trondheim

Location
Marinteknisk Senter
O. Nielsens vei 10

Tel. +47 73 595501
Fax +47 73 595697

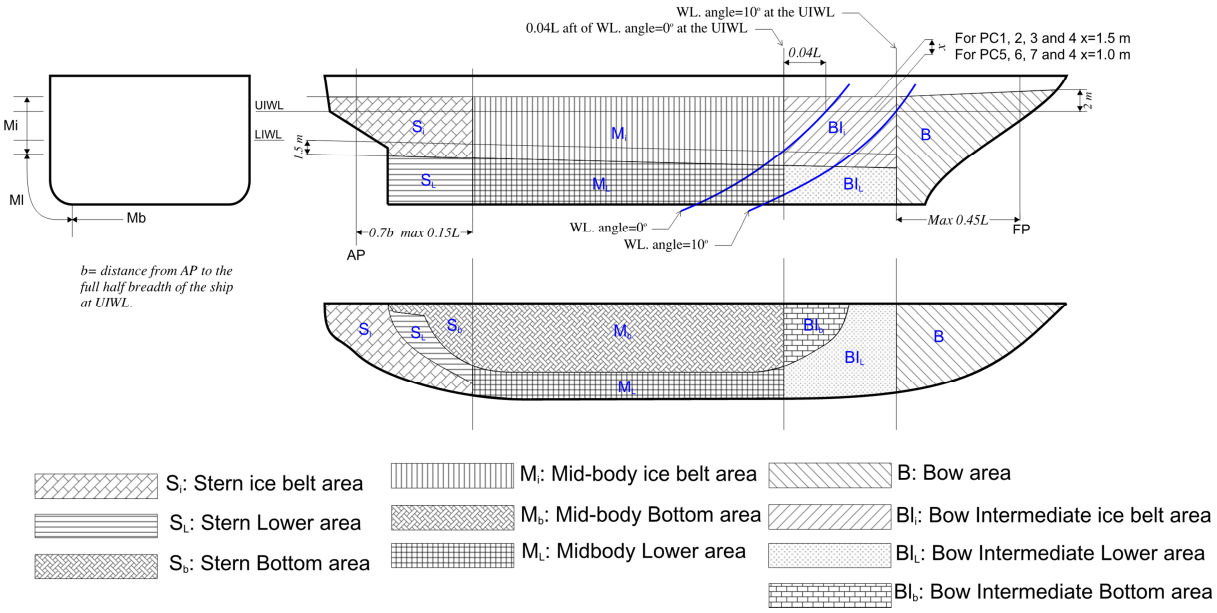

Figure 1: Hull Area Extents (IACS Requirements for Polar Class, 2011)

The division of the hull areas as shown by figure1 is then enforced by assigning the most probable loading scenarios corresponding to each area, taking in consideration ice conditions, navigational factors and damage reports. According to James Bond [Reference 16], the UR area definitions and the corresponding loading scenarios assigned to each area are as follow:

- Bow area, B:

Considering the Canadian criteria of year around independent navigation, the Bow area has to be reinforced to withstand the following load scenarios described in table 2:

- Ramming 1
- Ramming 2
- Open Pack 2
- Dangerous 1
- Dangerous 4

The bow area is defined according to IACS rules as follow:

- In the horizontal direction the bow area starts from the vertical line intersecting the upper ice water line at the point where the water line angle is 10^o and fore.
- In the vertical direction the bow area starts from the base line up to a tapered line, situated 2m above the UIWL at the stem and *x* m above the UIWL at the bow area vertical line. Fig. 1.

- Bow Intermediate area, BI:

The load scenarios considered in the BI area are:

- Wedging 1
- Ramming 2
- Dangerous 1
- Dangerous 4

The BI area is defined according to IACS rules as follow:

- In the horizontal direction, the BI area is limited by the vertical line intersecting the upper ice water line at the point where the water line angle is 10^o and the vertical line situated 0.04L aft of the point on the upper ice water line where the water line angle is 0^o. Fig.1
- In the vertical direction, the BI area is subdivided to the Bow intermediate ice-belt area, BI_i, situated between the horizontal line *x* m above the UIWL and 1.5m below the LIWL. The Bow intermediate Lower area, BI_L, lies between the horizontal line 1.5m below the LIWL and the bottom boundary where the shell is inclined 7° from the horizontal plan. And the Bow intermediate bottom area, BI_b, is from the bottom boundary and down.

- Mid-body area, M:

Based on damage reports, alarming substantial hull damage in this area, it is decided to consider the following load scenarios in the M area:

- Offshore 1
- Pressure 1

- Ramming 2
- Ramming 3
- Possibly Shallow Water 1, 2 and 3.
- Pressure 1 and 3

The M area is defined according to IACS rules as follow:

- In the horizontal direction the M area is limited by the vertical boundary line of the BI area and the vertical line situated at 70% the distance from AP to the full half breathe of the ship at UIWL, with a maximum of 0.15L from AP.
- In the vertical direction the M area is subdivided to a Mid-body ice belt area, M_i, situated between the horizontal line *x* m above the UIWL and 1.5m below the LIWL. Mid-body Lower area, M_L, is defined as the area between the horizontal line 1.5m below the LIWL and the bottom boundary where the shell is inclined 7° from the horizontal plan. And the Mid-body bottom area, M_b, is from the bottom boundary and down.

- Stern area, S:

The stern area has to be reinforced considering the fact that ships assigned high ice class, when encountering ridges, may get stopped due to this impact and in order to be able to proceed, the ship must back away and ram the ridge again. This is the reason why in the IACS polar rules the hull area factors in stern area can be higher than the hull area factors in the Mid-body area for high polar class vessels, especially for ships intended to operate astern

The S area is defined according to IACS rules as follow:

- In the horizontal direction the S area is limited by the vertical boundary line of the M area and aft.
- In the vertical direction the S area is subdivided to a Stern ice belt area, S_i, situated between the horizontal line *x* m above the UIWL and 1.5m below the LIWL. Stern Lower area, S_L, is defined as the area between the horizontal line 1.5m below the LIWL and the

bottom boundary where the shell is inclined 7° from the horizontal plan. And the Stern bottom area, S_b, is from the bottom boundary and down.

Address:
NTNU
Department of Marine Technology
N-7491 Trondheim

Location
Marinteknisk Senter
O. Nielsens vei 10

Tel. +47 73 595501
Fax +47 73 595697

4. Design Ice Load

4.1 Introduction

In this part, references are made to the document prepared by Claude Daley (2000) for the design ice load.

For a predefined hull structure shape with certain displacement and speed, the only major class dependant parameter affecting the requirement is the ice load.

Predicting the ice forces and pressures is not a straight forward issue. To meet the challenge, idealized failure models have been suggested based on systematic observations of ice-structure interactions and ice failures.

The derivation of ice load in the IACS Unified Requirements for Polar Ships (URI1 to URI3) is based on the design scenario of bow glancing collision with an infinite ice edge, i.e. the ice edge is at rest and gains no kinetic energy after collision. In this case, the total ship kinetic energy is fully transformed to a potential crushing energy at the point where maximum ice dentation is reached, i.e. maximum normal ice force. The energy equation can then be expressed as follow:

$$K_n = E_{crush} \tag{1}$$

Where:

$$E_{crush} = \int_0^{\lambda_{nm}} F_n(\lambda_n)\mathrm{d}\lambda_n \tag{2}$$

F_n =The bow normal ice force

λ_n =Stem penetration in ice as defined by figure 2

Address:
NTNU
Department of Marine Technology
N-7491 Trondheim

Location
Marinteknisk Senter
O. Nielsens vei 10

Tel. +47 73 595501
Fax +47 73 595697

λ_{n_m} is the maximum penetration in ice

$$K_n = \frac{1}{2} M_e {V_n}^2 \quad (3)$$

$M_e = effective\ mass = \frac{M_{ship}}{CO}$

M_{ship} =Ships displacement

$Co = mass\ reduction\ coefficient$

$V_n = normal\ velocity = V_{ship}.sin(\alpha)\ cos(\beta')$

$\alpha\ and\ \beta' as\ defined\ in\ figure\ 3$

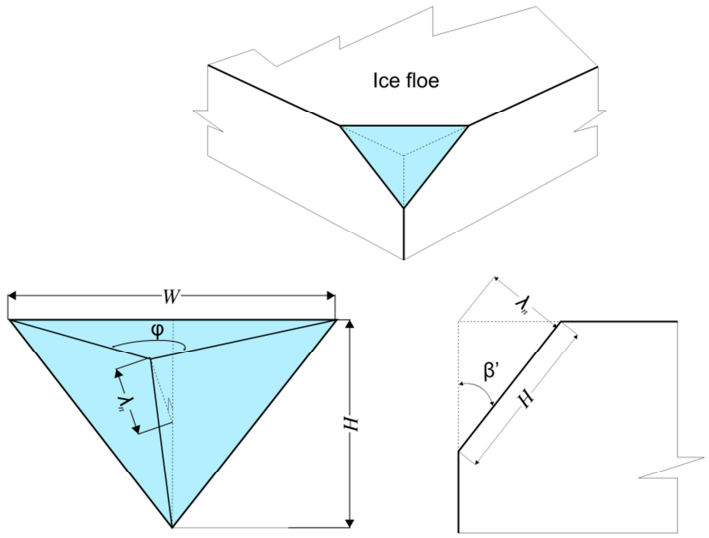

Figure 2: ice/hull overlap geometry during an oblique collision with an ice floe.

(Claude Daley, 2000)

4.2 The Total normal ice load on the bow area

The total normal ice load F_n is found by determining the nominal contact area A between the stem and the ice edge and the average ice pressure P, defined as follow:

$$P = P_0 A^{ex} \quad (4)$$

Where:

$$A = \frac{WH}{2} \quad (5)$$

$$W = \frac{2tan\left(\frac{\varphi}{2}\right)\lambda_n}{\cos(\beta')} \quad (6)$$

$$H = \frac{\lambda_n}{\sin(\beta')cos(\beta')} \quad (7)$$

P_0 is the ice pressure at 1m^2,

ex is a constant.

β' as defined by figure 3.

φ as defined by figure 2.

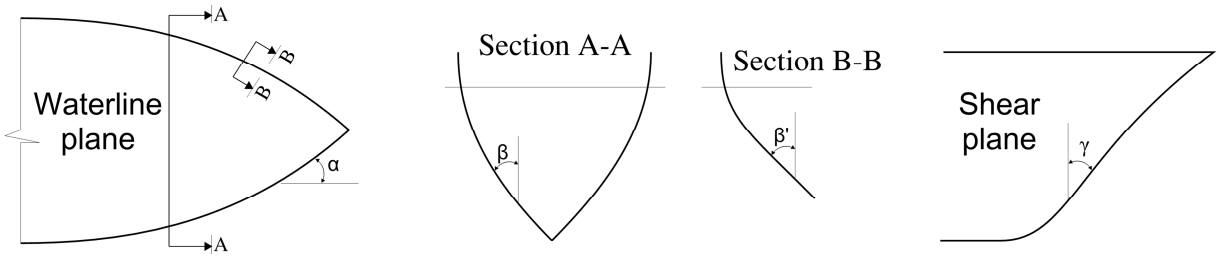

Figure 3: *Definition of hull angles*

(IACS Unified Requirements for Polar Ships)

The expression of the average ice pressure P, eq.(4), allows for expressing the normal ice force $F_n = A.P$ as a function of the normal ice dentation λ_n described by figure (2). From eq. (5), (6) and (7) F_n is obtained as follow:

$$F_n(\lambda_n) = Po\left(\frac{tan\left(\frac{\varphi}{2}\right)\lambda_n{}^2}{\sin(\beta')\cos^2(\beta')}\right)^{1+ex} \tag{8}$$

By substituting F_n with its new expression in the energy equation (1), the energy equation can then be solved to find a close form expression of the maximum normal ice dentation λ_{nm} , as follow:

$$\lambda_{n_m} = \left(\frac{\frac{1}{2}M_e V_n^2(3+2ex)}{Po\left(\frac{tan\left(\frac{\varphi}{2}\right)}{\sin(\beta')\cos^2(\beta')}\right)^{1+ex}}\right)^{\frac{1}{3+2ex}} \tag{9}$$

Considering equations (8) and (9), the final normal ice load expression is obtained as:

$$F_n = fa.Po^{\frac{1}{3+2ex}}.V_{ship}^{\frac{4+4ex}{3+2ex}}.M_{ship}^{\frac{2+2ex}{3+2ex}} \tag{10}$$

Where:

$$fa = (3+2ex)^{\frac{2+2ex}{3+2ex}}.\left(\frac{tan\left(\frac{\varphi}{2}\right)}{\sin(\beta')\cos^2(\beta')}\right)^{\frac{1+ex}{3+2ex}}.\left(\frac{1}{2CO}\left(sin(\alpha)cos(\beta')\right)^2\right)^{\frac{2+2ex}{3+2ex}} \tag{11}$$

More detailed calculation steps of the final shape factor fa can be found in reference [4]

From equation (11), it is seen that the normal ice force in the bow is a function of:

- fa : A shape factor which expresses the influence of the bow shape on ice force magnitude.
- Ice strength, a **class dependent factor**.
- Ships velocity, a **class dependent factor**.
- And the displacement of the ship at the upper ice water line.

By setting $ex = -0.1$ and $\varphi = 150^o$, the shape factor fa is simplified to be:

$$fa = \frac{\left(0.097 - 0{,}68\left(\frac{x}{L} - 0.15\right)^2\right)\alpha}{\sqrt{\beta'}} \leq 0.6 \qquad (12)$$

Where:

- α and β' as defined in figure 3
- $x =$ Distance from the forward perpendicular FP to the hull position considered within the bow area.
- $L =$ Ship length.

And the normal ice load, eq.(10) becomes:

$$F_n = fa.CF_c.M_{ship}^{0.64} \qquad (13)$$

Where CF_c is a class dependent coefficient:

$$CF_c = Po^{0.36}.V_{ship}^{1.28} \qquad (14)$$

Figure 4 shows that an ice sheet in contact with the hull structure may fail under tree different modes, crushing, shear or bending failure, or a combination of the three failure modes.

Address:
NTNU
Department of Marine Technology
N-7491 Trondheim

Location
Marinteknisk Senter
O. Nielsens vei 10

Tel. +47 73 595501
Fax +47 73 595697

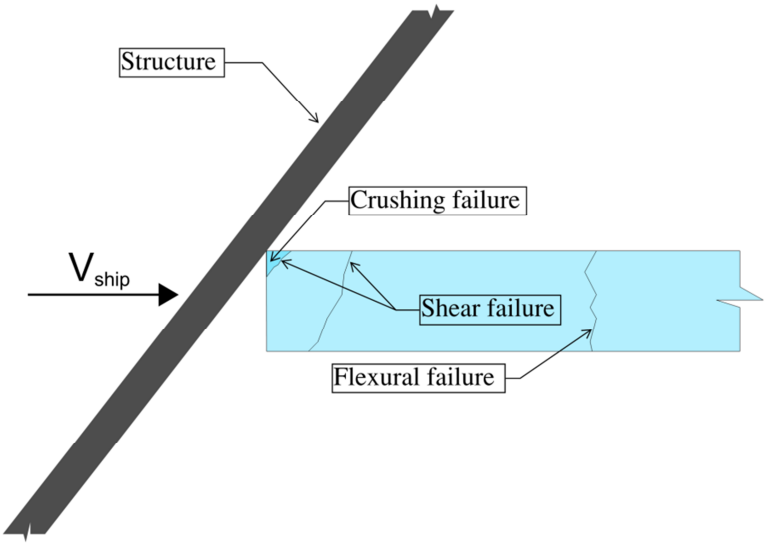

Figure 4: Ice failure modes on a ship side (Varsta and Riska, 1977)

To take this effect in to account, the normal ice load has to be restricted by the hull-ice interaction force resulting from flexural ice failure as follow:

$$F_n \leq \frac{1.2\sigma_f {h_{ice}}^2}{\sin(\beta')} \tag{15}$$

And the final form factor expression can be modified to be:

$$fa = min\begin{cases} \dfrac{1.2CF_F}{sin(\beta')CF_c.M_{ship}^{0.64}} \\ \dfrac{\left(0.097 - 0{,}68\left(\frac{x}{L} - 0.15\right)^2\right)\alpha}{\sqrt{\beta'}} \\ 0.6 \end{cases} \tag{16}$$

Where $CF_F = \sigma_f {h_{ice}}^2$

4.3 Determination of design ice load patch

The design load patch is the average ice pressure distributed over a rectangular design area with height h and width W as configured by figure 5. This design area is considered as a simplification of the nominal contact area between the ship and the ice edge.

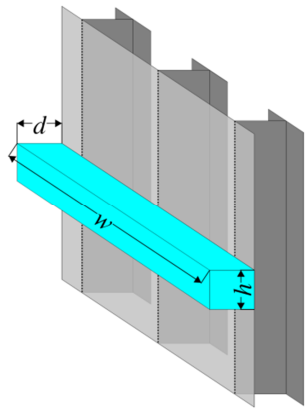

Figure 5: Ice patch load on ship side

According to the paper titled, "Conceptual Framework for an Ice Load Model"[8], prepared by Claude Daley and Kaj Riska, ice in contact with a wet steel structure does not crush as a pure continuum but as a combination of continuum damage and local shear cracking events as shown by figure 6. This edge spalling effect is accounted for in the IACS rules by reducing the design ice patch area and keep the design patch aspect ratio, AR, constant.

From equations (6) and (7), the aspect ratio is then obtained as follow:

$$AR = \frac{W}{H} = \frac{2Tan(\frac{\varphi}{2})}{\sin(\beta')} = \frac{7{,}46}{\sin(\beta')} \qquad (17)$$

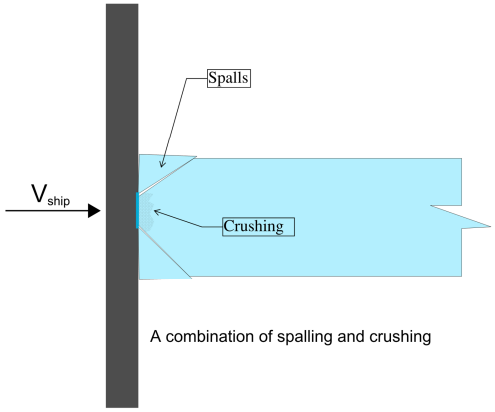

Figure 6: Ice failure model considering no flexural failure according to Claude Daley and Kaj Riska [20].

Considering equation (4), the nominal contact area of the ice patch becomes:

$$A_{nom} = h_{nom}.w_{nom} = \left(\frac{F_n}{Po}\right)^{\frac{1}{1+ex}} \tag{18}$$

Given that the aspect ratio AR is assumed to be constant, the nominal contact area yields:

$$A_{nom} = h_{nom}^2.AR \tag{19}$$

By combining equations (18) and (19), the ice patch height and width are obtained respectively as follow:

$$h_{nom} = \left(\frac{F_n}{Po.AR^{1+ex}}\right)^{\frac{1}{2+2ex}} \tag{20}$$

$$w_{nom} = \left(\frac{F_n}{Po.AR^{1+ex}}\right)^{\frac{1}{2+2ex}}.AR \tag{21}$$

The reduction in the area of the ice patch, as mentioned earlier, is then introduced in the rules by reducing the design ice patch width as follow:

$$w = w_{nom}^{wex} \qquad where\ wex = 0.7\ and\ ex = -0.1 \qquad (22)$$

Considering equations (20), (21) and (22), the final expression of the design load height and width in the bow area reads:

$$\begin{cases} w = F_n^{0.389} Po^{-0.389}.AR^{0.35} \\ h = F_n^{0.389} Po^{-0.389}.AR^{-0.65} \end{cases} \qquad (23)$$

Correspondingly the design line load and pressure in the bow area are obtained:

$$\begin{cases} Q = \dfrac{F_n}{w} = \dfrac{{F_n}^{0.61}.CF_D}{AR^{0.35}} \\ P = \dfrac{Q}{h} = {F_n}^{0.22}.CF_D^2.AR^{0.3} \end{cases} \qquad (24)$$

Where $CF_D = Po^{0.389}$

As we move from the stem toward the shoulders of the ship, the ice failure mode tends to move typically from bending/flexural to crushing. The Bending and crushing forces are strongly inter-linked when moving along the bow area and/or when varying the ice thickness, (fig. 7).

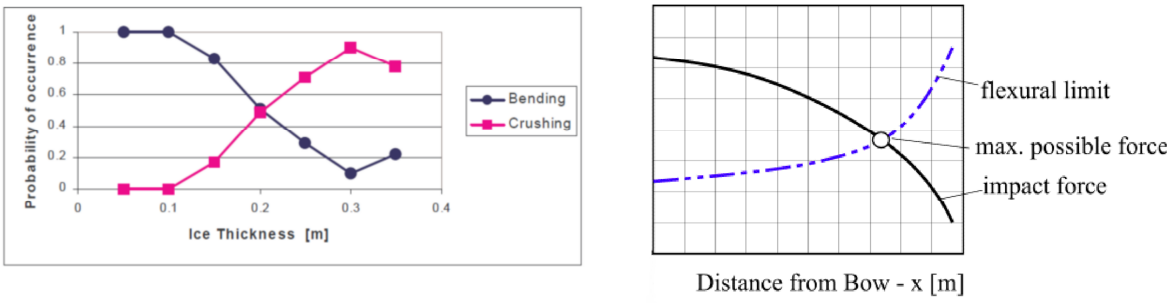

Figure 7: Crushing and bending of ice along the bow and probability of occurrence of crushing and bending versus ice thickness. (Claude Daley, 2000) (http://www.offshoremoorings.org/Moorings/2009/Group02_Prabhakar/OffshoreMoorings WEBSITE25sept2009/Bending.htm)

This fact makes the calculation of the normal ice load based on a single formula quite complicated, considering the variation of the hull shape along the bow. The ice proprieties and thickness in the IACS Polar rules are fortunately predefined by the assigned class notation. The remaining complication is then to find the maximum value along the bow of the minimum between the flexural and crushing normal force at several positions.

Practically, the normal ice force F_n and the corresponding design line load Q and pressure P in the bow area have to be calculated at least at fore different positions along the bow, as indicated by figure 8.

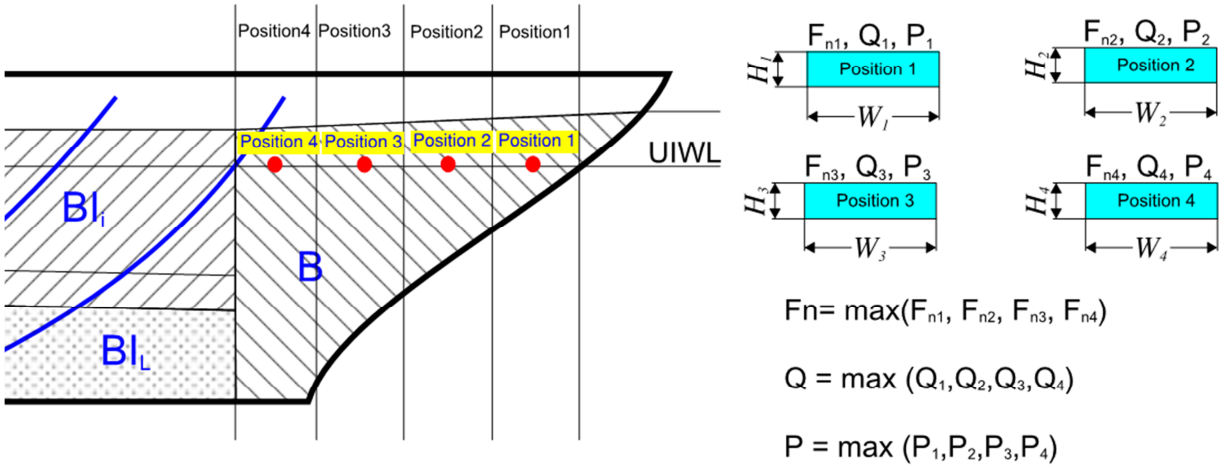

Figure 8: Calculation process the maximum normal ice force, line load and pressure along the bow region.

All the class dependant parameters such as ship speed, ice thickness and ice strength, are incorporated in the IACS Unified Requirements for Polar Ships by class factors as summarised by table 3.

Table 3: Ice parameters and the corresponding Class Factors according to IACS

	Po Ice strength [MPa]	V_{ship} [m.s^{-1}]	σ_f [MPa]	h_{ice} [m]	CF_c Crushing failure class factor	CF_F Flexural failure class factor	CF_D Load Patch Dimensions Class Factor	CF_{Dis} Displacement Class Factor
Formula					$Po^{0.36}.V_{ship}^{1.28}$	$\sigma_f h_{ice}{}^2$	$Po^{0.389}$	
PC1	6,00	5,70	1,40	7,0	17,7	68,6	2,008	250
PC2	4,20	4,40	1,30	6.0	11,2	46,8	1,748	210
PC3	3,20	3,50	1,20	5.0	7,6	30,0	1,572	180
PC4	2,45	2,75	1,10	4.0	5,0	17,6	1,417	130
PC5	2,00	2,25	1,00	3,0	3,6	9,0	1,309	70
PC6	1,4	2,25	0,70	2,8	3,2	5,5	1,140	40
PC7	1,25	1,75	0,65	2,5	2,2	4,1	1,091	22

The ice load on the other regions rather than the bow has not been studied analytically, but derived based on **scaling empirically** the bow normal ice load, eq.(13), along the ship. The scaling factors are sorted in the IACS Polar Rules *I2.3.2.2* by Table 3, "*Hull Area Factors (AF)*".

The form factor fa in the Non-Bow regions within the ice reinforced area is assumed to be constant as the hull angles α and β are quite constant within the flat side of the hull.

$$fa_{nonbow} = 3{,}6 \tag{25}$$

And the normal ice load in the non-bow areas, considering equation (13) and (25) becomes:

$$F_{NonBow} = 3{,}6.CF_c.DF \tag{26}$$

Where DF is a restrictive factor in the case of very large ice going vessels:

$$DF = \begin{cases} M_{ship}^{0.64} & if\ M_{ship} \le CF_{DIS} \\ CF_{DIS}{}^{0,64} + 0.1\left(M_{ship} - CF_{DIS}\right) & if\ M_{ship} > CF_{DIS} \end{cases} \tag{27}$$

CF_{DIS} is a class dependent factor.

From figure (9), we can see how load magnitude increases by increasing the ships displacement and the class in the same time. We see also that the DF factor restriction has no influence on ice load for polar classes PC4 and higher, the normal ice load within this range of class for Non-Bow regions could be simplified to be:

$$F_{NonBow,PC>PC4} = 3{,}6.\,CF_c.\,M_{ship}^{0.64} \tag{28}$$

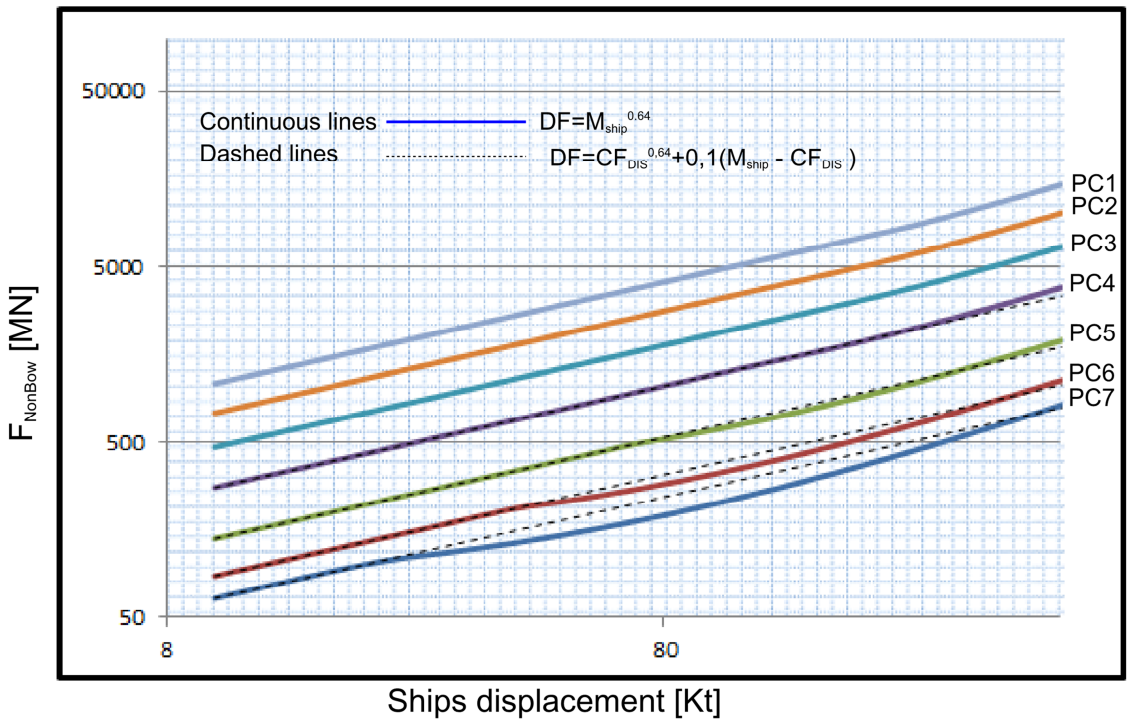

Figure 9: Plot of Non-Bow ice force versus ships displacement considering polar classes from PC7 to PC1

By considering an aspect ratio of $AR = 3{,}6$ in the non-bow regions, the ice patch width becomes:

$$W_{NonBow} = 3{,}6.\,b_{NonBow} \tag{29}$$

And from equation (24) and (29), the corresponding design line load in the non-bow area is obtained as:

$$Q_{NonBow} = 0{,}639.F_{NonBow}{}^{0{,}61}.CF_D \quad (30)$$

The normal ice forces together with the design ice patch dimensions for different hull regions are summarized by figure 10.

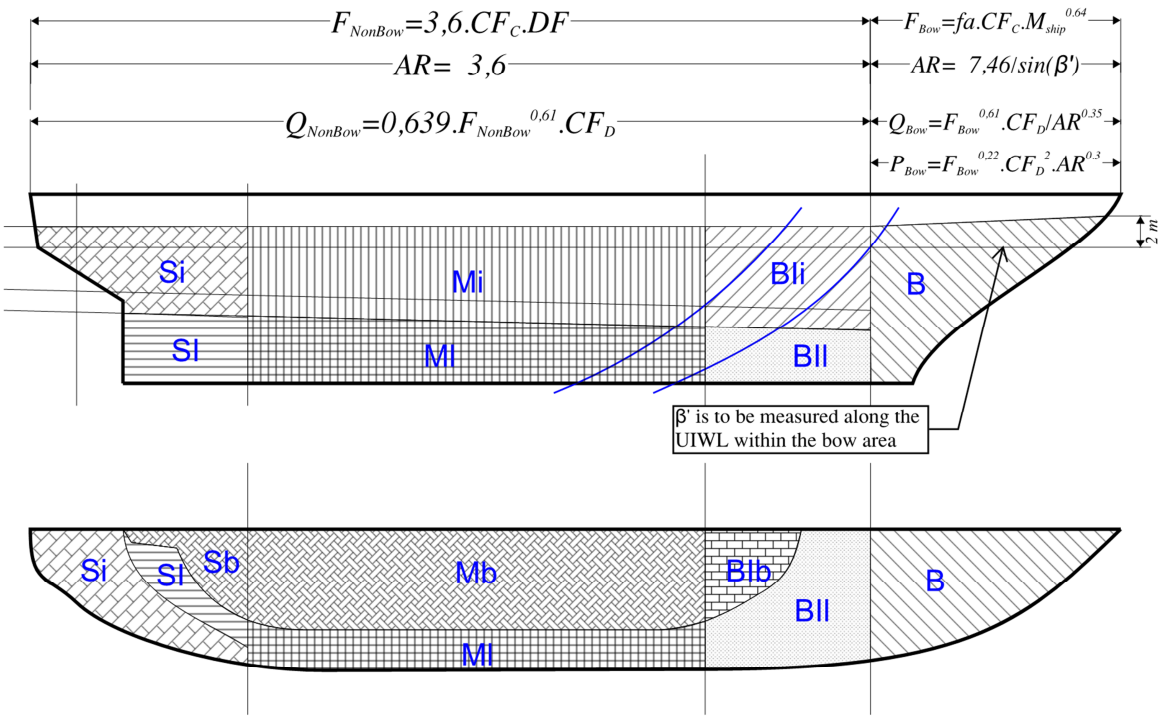

Figure 10: Normal ice force together with the corresponding line load and pressure for different hull regions.

The rationale behind the peak pressure factor, stated by table 2 in the IACS Unified Requirements for Polar Ships, is to take into account the fact that the design ice pressure increases for smaller areas. The smaller the contact area, the larger is the indentation pressure. This peak pressure factor is then to be multiplied with the average design ice pressure derived from the design ice patch.

This practice is actually a result of compromises made based on different opinions and discussions, and its legitimacy and correctness might be discussed and questioned.

Address:
NTNU
Department of Marine Technology
N-7491 Trondheim

Location
Marinteknisk Senter
O. Nielsens vei 10

Tel. +47 73 595501
Fax +47 73 595697

5. USFOS as a non-linear finite element analysis tool

USFOS as a non-linear finite element analysis tool has been used in this report to conduct plastic collapse and/or buckling analysis of both plate and frames subjected to ice load, considering different structural aspects, boundary conditions and ice patch widths.

The USFOS beam element is designed for being able to describe the behavior of the physical member with only one element, i.e. 2-nodes beam element with six degree of freedom at each node as shown by figure 11. This 2-nodes beam element provides for the geometric nonlinearity due to large lateral displacements and plasticity.

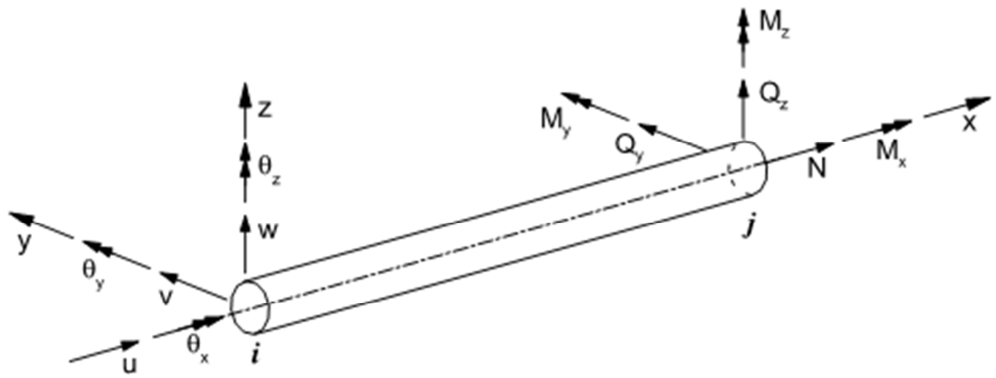

Figure 11: Three dimensional beam element (USFOS USER'S MANUAL, [30])

Generally, a beam is subjected to a combination of bending moment shear and axial force. The presence of shear and axial force reduce the plastic moment according to the plastic interaction equation between the three types of forces. This is accounted for in USFOS by introducing plastic hinges in the structural member when the interaction curve for stress is exceeded. Hinges may

then be introduced at both ends and at mid-span and their behavior is controlled by plastic flow theory, which yields an incremental relationship between Cauchy stresses σ_{ij} and true strains ε_{ij}, according to T. Moan and S. Sævik [20] et.al.

In an explicit way and in case of mid-span hinge, the plasticity in USFOS is accounted for as stated in the following quotation from USFOS USER'S MANUAL [19]:

> *"In case of a plastic hinge at midspan the element is divided into two new subelements. The plastic hinge at midspan is always attributed to the first subelement. The stiffness matrix for the two subelements is assembled. The internal node is eliminated by static condensation so as to maintain the conventional 2 node beam element in subsequent analysis. This is all performed at element level without involvement of the user."*

In the other hand, the USFOS Shell element is a fully nonlinear element where both material non linearity and nonlinear geometrical effects are automatically accounted for. This allows for describing the real physics of the member in concern by detecting several structural behaviors in the same time, i.e. the yielding, the buckling, the twisting etc.

USFOS follows an updated Lagrange formulation taking in consideration large displacement but restricted strain. Updated Lagrange approaches refers to the previous known configuration C^{n-1}, fig. 12, where the load is applied in steps, and the system stiffness equations are solved at every step. The force increment is obtained as follow $dR = (K_0 + K_\sigma)^{(n-1)} dr$

Where:

- K_0 is the elastic stiffness matrices.
- K_σ is the geometrical stiffness matrices.
- dr is the displacement increment.
- n is the step number.

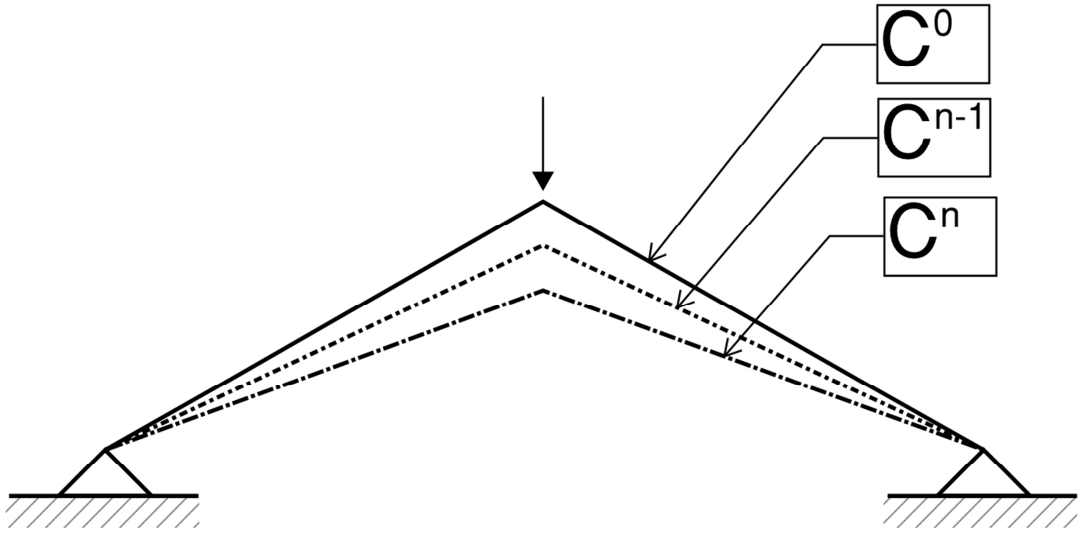

Figure 12: Loading steps with different configurations (T. Moan. Week 41.2012)

The geometric nonlinearity due to large nodal displacements is accounted for by updating the geometry after every displacement increment, according to the updated Lagrangian formulation. This is providing for a non-linear terms in the stiffness matrix and coupling between the axial and lateral displacement.

USFOS uses a combined incremental-iterative loading algorithm where the external load is applied in increments and in each increment equilibrium is achieved by iteration, as described by figure 13.

Address:
NTNU
Department of Marine Technology
N-7491 Trondheim

Location
Marinteknisk Senter
O. Nielsens vei 10

Tel. +47 73 595501
Fax +47 73 595697

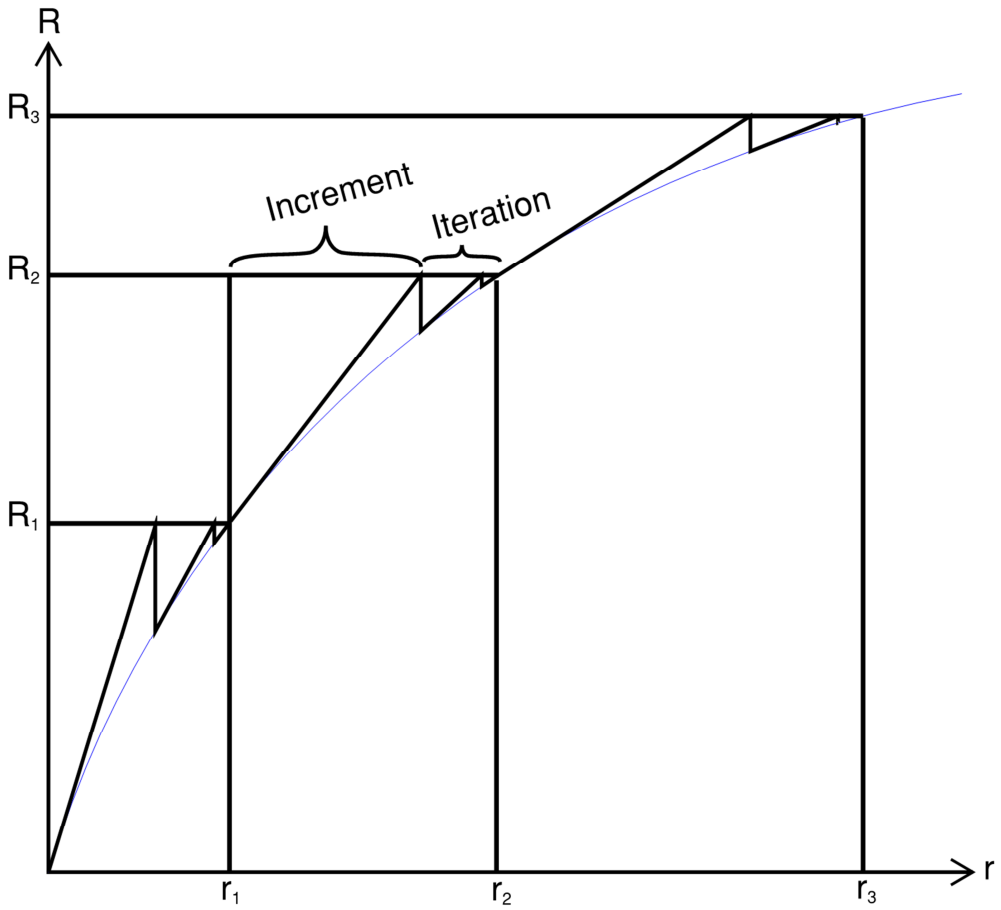

Figure 13: Combination of Euler-Cauchy incrimination and a modified Newton-Raphson iteration. (T. Moan and S. Sævik [20] et.al.)

Address:
NTNU
Department of Marine Technology
N-7491 Trondheim

Location
Marinteknisk Senter
O. Nielsens vei 10

Tel. +47 73 595501
Fax +47 73 595697

6. Plastic analysis method and background for the UR PC rules (UR I1)

6.1 Introduction

Ice load is assumed to occur arbitrary within a range of water level between the upper ice waterline (UIWL) and lower ice waterline (LIWL) with an extensive load magnitude, challenging the ship structural member's integrity. Hence, the structural members within an ice reinforced area have to be designed with sufficient safety against overloading caused by ice crushing and/or bending. In this purpose, the IACS Unified Requirements for Polar Ships has adopted nominal simplified plastic collapse mechanisms as design criteria for structural members, where the membrane and strain hardening effects are neglected. However and due to strength reserves from development of membrane stresses and strain hardening at the design load level, the structure tends to maintaining substantial strength reserve against the actual collapse or rupture.

Consider a plate strip with rectangular cross section bxh, as a part of a hull structure the plate will sustain membrane forces from neighboring members as illustrated by figure14.

It is seen from figure 14 that the capacity of the plate strip versus lateral deflection increases significantly when the membrane effect is considered.

The formulae in the rules are derived based on the assumption that a cross section is linearly elastic-perfectly plastic, fig.(15), where plastic deformations are assumed to be concentrated at the plastic hinge locations. However, the assumption of perfect plasticity, i.e. ignoring the effects of strain hardening, after reaching the yielding point, seems to be on the safe side.

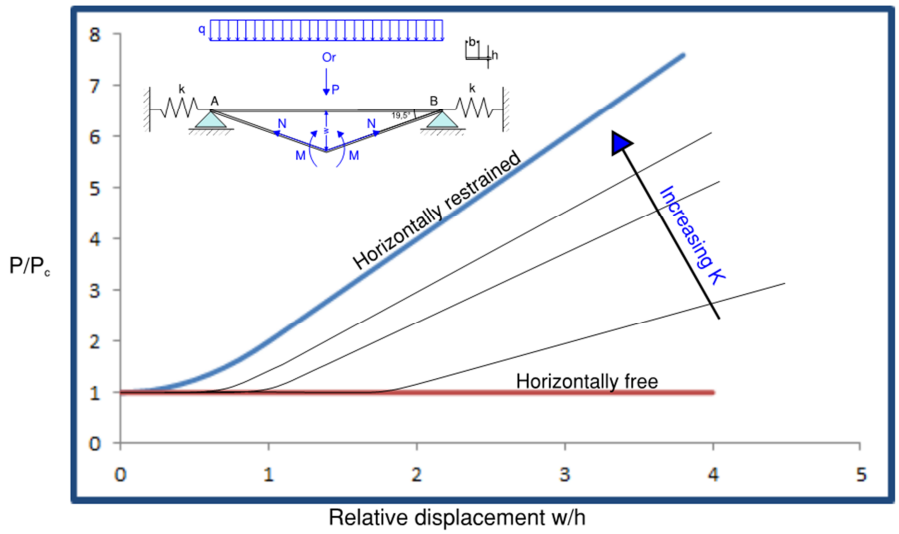

Figure 14: Load-deflection curves including membrane effect

(Tore H. Søreide, Ultimate Load Analysis Of Marine Structures, 1985)

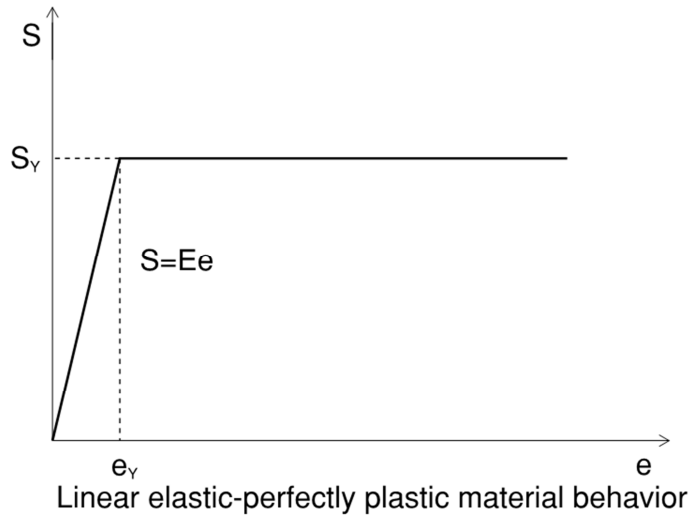

Figure 15: (Jørgen Amdahl, MTS 2007-01-10)

6.2 Framing

6.2.1 Development of plastic collapse mechanism for a beam

As explained by Tore H. Søreide (1985) and Amdahl (MTS 2007-01-10) et al., the plastic mechanism for a clamped frame subjected to an uniform load develops through the following three stages. Fig. 17:

- At the 1st stage the beam continues to deform elastically until yield occurs at the outer fibre of the frame section at the clamped ends. At this stage the bending moment at the ends is :

  $$\frac{q_1 l^2}{12} = \sigma_y Z_y \qquad (31)$$

  Where σ_y the yield is stress and Z_y is the elastic section modulus.

  Considering a linear elastic-perfectly plastic material behavior as shown by figure 15, the stress distribution along the cross section for different stages of the loading is as illustrated by figure 16.

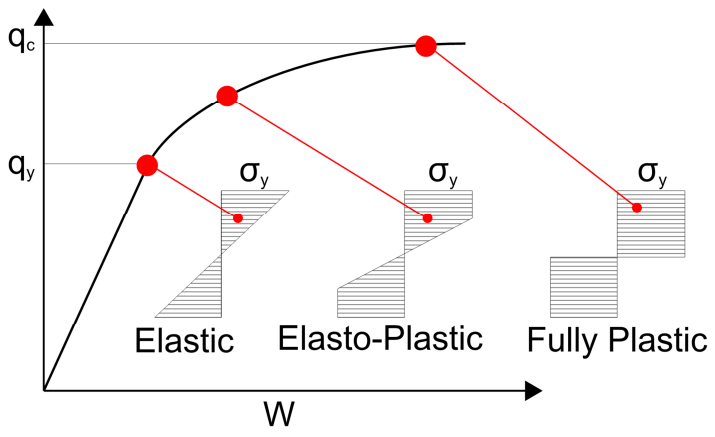

Figure 16: Capacity-displacement curve and plasticity development in the cross section.

- At The 2nd stage the load keeps increasing to reach:

$$q_2 = \frac{12M_p}{l^2} \quad (32)$$

Where full plastification of the cross section takes place at the supports. The bending moment at the supports has then reached its maximum value M_p and the frame at the clamped ends can take **no more moment**. From this point, the frame acts as it is **simply supported**.

- The 3th stage is that the load continues to increase to:

$$q_c = q_2 + q_3 \quad (33)$$

until a hinge develops at the centre of the frame with full plastification. The frame acts then as a mechanism and collapses. The bending moment at the middle at this point is:

$$M_p = \frac{q_2 l^2}{24} + \frac{q_3 l^2}{8} \quad (34)$$

Combining equations (32) and (34), the additional load at stage three becomes:

$$q_3 = \frac{4M_p}{l^2} \quad (35)$$

And the total capacity of the frame reads:

$$q_c = q_2 + q_3 \rightarrow q_c = \frac{16M_p}{l^2} \quad (36)$$

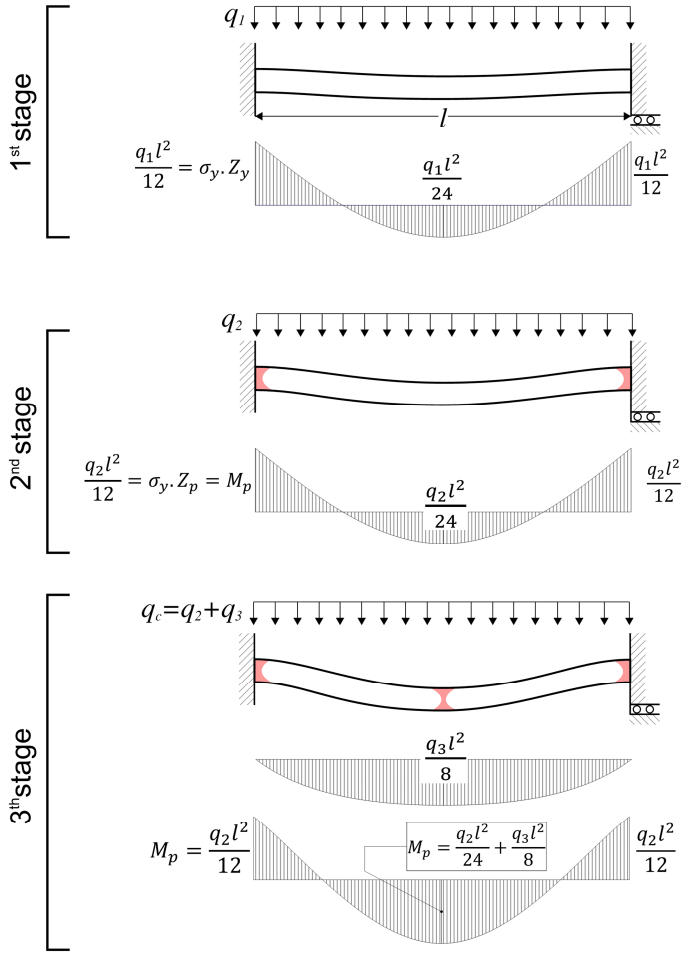

Figure 17: loading stages for an uniformaly loaded frame with clamped ends

The plastic capacity of a frame subjected to an uniform load, regardless of the frame span, the load and the boundary conditions, is totally depending on the shape factor α defined as the ratio of the plastic section modulus to the elastic one.

The shape factor α describes the ability of the frame to withstand bending moment beyond the elasticity limit, i.e. first yield. Figure (18) shows how the collapse capacity changes with different shape factors

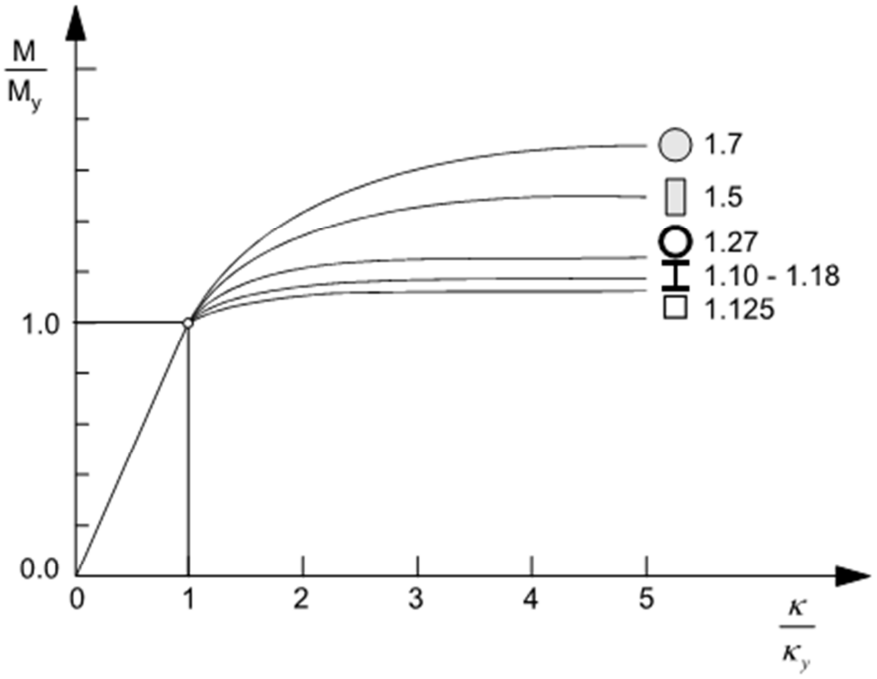

Figure 18: Bending moment versus curvature (Jørgen Amdahl [6])

6.2.2 IACS Polar class requirement for transverse framing

The calculation of framing capacity in the IACS Unified Requirements rules for framing are generally based on the energy principles implying that external work is to be balanced by the internal one. To simplify the process, the elastic energy prior to collapse has been neglected and small deflection has been assumed.

In this regard, three different energy absorbing mechanisms have been considered, where the energy is assumed to be mainly dissipated at the hinges. These mechanisms are:

- 3 hinges collapse mechanism considering a centrally patch loaded frame, with either fixed-fixed or fixed-simply supported ends. The fixed-simply supported case is

considered here to include the case when one end is located outside the ice-strengthened area. Figure 23.

- Combination of shear and bending hinge with clamped ends. The fixed boundary conditions force the ends to undergo substantial shear stresses, depending on the shape factor of the cross section. As a result, the plastic capacity of the ends will be reduced to M_{pr}. This fact is due to the bending-shear interaction represented by equation (37).

$$\left(\frac{M}{M_{ult}}\right)^2 + \left(\frac{T}{\alpha T_{ult}}\right)^2 = 1 \qquad (37)$$

Where α is the shape factor.

By increasing the shear force, the web contribution to the total plastic capacity decreases until it reaches yield shear stress $\tau_y = \frac{\sigma_y}{\sqrt{3}}$ and the remaining plastic capacity of the frame becomes Z_f, which is the contribution of the flange to the plastic section modulus. Figure 19 illustrates how the shear interacts with the bending moment for both a flanged and un-flanged cross section.

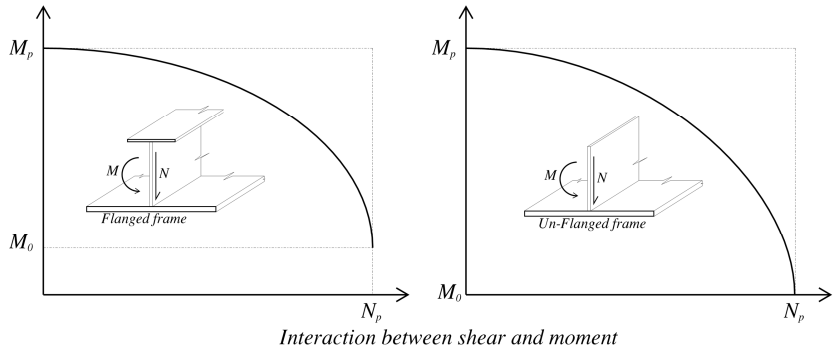

Figure 19: Interaction plot for moment and shear (C.G .Daley [9])

- The third collapse mechanism is the shear hinge mechanism, considering an off-center (asymmetrical) patch load, fig. 26. In this case the frame is considered to be built on both ends to be able to transfer the plastic moment to the neighboring structure. The boundary condition is than fixed-fixed.

6.2.2.1 *Centrally patch loaded frame:*

Due to the fact that the cross-sectional area of the attached plate flange is much larger than the cross-sectional area of the local frame, it is assumed by C.G.Daley et.al [9] that the neutral axis is situated at the intersection point between the plate and the web, fig. (20). This assumption is made mainly to simplify the standard plastic bending model, and the derivation of the rule requirement. This assumption implies to a certain extent that the stress in the plate will balance the forces in the web and the flange without averagely exceeds the yield stress, fig. (20).

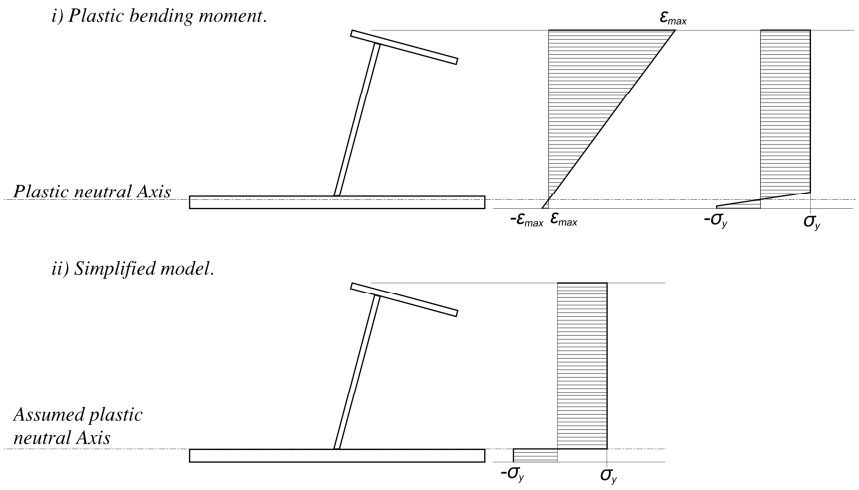

Figure 20: Simplified plastic modulus concept (C.G .Daley [9])

Consequently, the approximated plastic section modulus used in the derivation of the IACS frame requirement, for $\varphi_w = 90^o$ is as follow:

$$Z_p = A_w\left(\frac{h_w}{2} + \frac{t_p}{2}\right) + A_f\left(h_{fc} + \frac{t_p}{2}\right) \tag{38}$$

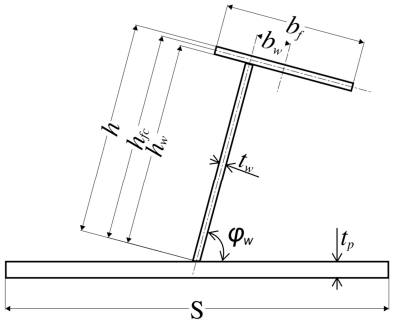

Figure 21: Cross section dimensions as defined by IACS Polar rules.

In the case where the plastic neutral axis is situated above the intersection point between the plate and the web, the neutral axis position above the plate for $\varphi_w = 90^o$ is obtained as follow:

$$z_{na} = \frac{A_f + h_w t_w - t_p.s}{2t_w} \tag{39}$$

And the corresponding exact plastic section modulus becomes:

$$Z_{p,exact} = t_p.s.\left(z_{na} + \frac{t_p}{2}\right) + \frac{((h_w - z_{na})^2 + z_{na}^2)t_w}{2} + A_f\left(h_{fc} - z_{na}\right) \tag{40}$$

Where:

A_f = net cross-sectional area of the local frame flange.

A_w= net cross-sectional area of the local frame web = $h_w.t_w$

h_{fc} = As defined by figure 21

The accuracy of this assumption is assessed in this report by plotting the plastic section modulus for cross sections versus increasing z_{na} considering both the approximated, eq.38, and the exact section plastic modulus, eq.(40)

The cross sections considered in the plot, fig.22, are based on the following cross sectional scantlings:

- Increasing t_f and t_w with $t_f = t_w$
- $h_w = 200\ mm$
- $b_f = 200\ mm$
- $s = 400\ mm$
- $t_p = 21\ mm$

From figure 22, it is shown that the difference between the approximated section modulus adopted in the derivation of IACS framing requirement and the exact plastic section modulus tends to increase dramatically as the plastic neutral axis rises above the attached shell plate.

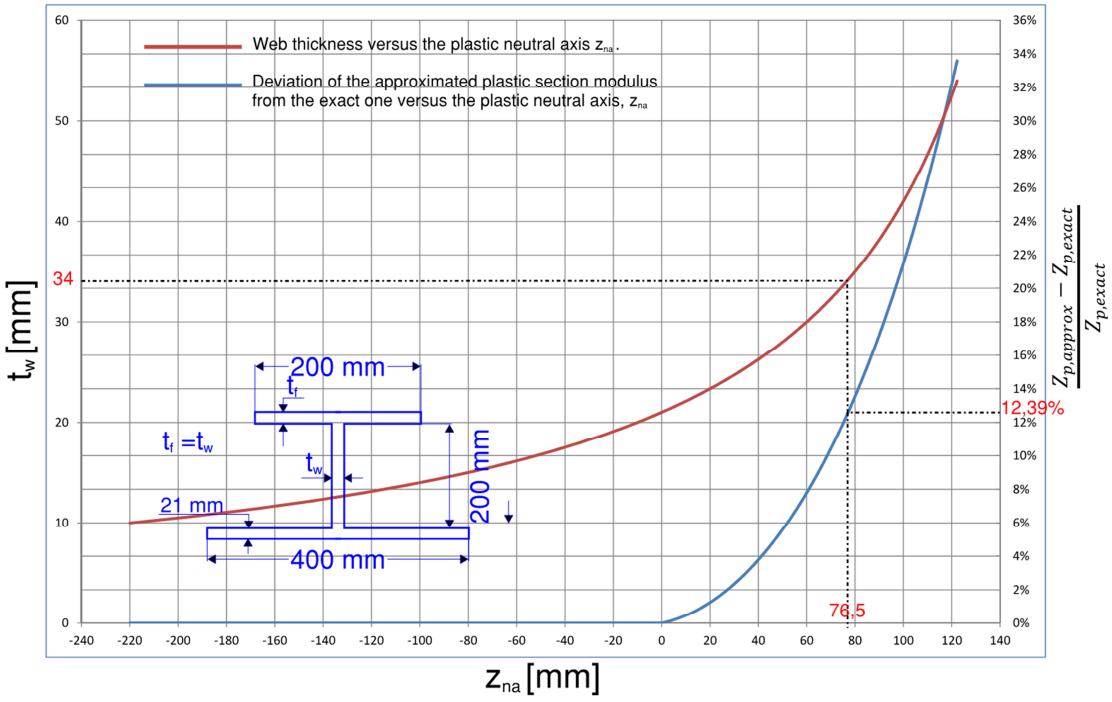

Figure 22: Deviation of the approximated section modulus, Zp, from the exact one as a result of increasing the position of the plastic neutral axis Z_{na}.

The consequences of this resulting difference in the plastic section modulus will be discussed thoroughly later in this report.

From figure 23, the external work due to the patch load and the corresponding internal work are obtained respectively as follow:

$$\delta w_e = 2\int_{\frac{b}{2}}^{0} P.S.\frac{2w}{L}.\left(x-\frac{L}{2}\right)dx = P.b.S.w\left(1-\frac{b}{2L}\right) \quad (41)$$

$$w_i = M_p\frac{4w}{L} + M_{pr}\frac{j2w}{L} \quad (42)$$

Where:

P= the patch pressure

S= frame spacing

$M_p = Z_p\sigma_y$

$M_{pr} = Z_{pr}\sigma_y$

σ_y= yield stress

Z_{pr}= the reduced plastic section modulus = $Z_p.A$

$$A = \left[1-k_w+k_w\sqrt{1-\left(\frac{A_0}{A_w}\right)^2}\right]$$

$$k_w = \frac{Z_w}{Z_p} \approx \frac{1}{1+\frac{2A_f}{A_w}}$$

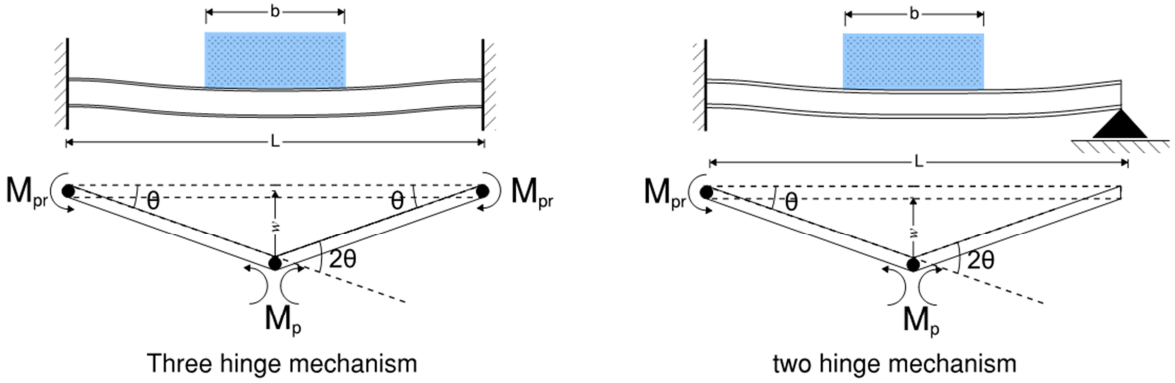

Figure 23: Collapse mechanisms for centrally patch loaded frame with fixed-fixed and fixed free ends.

By balancing the external work with the internal one, the plastic modulus section requirement for a centrally patch loaded transverse frame is obtained:

$$\begin{cases} Z_{p,req} = P.b.S\left(1-\frac{b}{2L}\right)\frac{L}{4\sigma_y}A_1 \\ Where\ A_1 = \dfrac{1}{\left[1+\frac{j}{2}-\frac{j}{2}k_w\left(1-\sqrt{1-\left(\frac{A_0}{A_w}\right)^2}\right)\right]} \end{cases} \quad (41)$$

Where:

j = 1 for framing with one simple support outside the ice-strengthened areas

= 2 for framing without any simple supports

$A_0 = \frac{PbS\sqrt{3}}{2\sigma_y}$

A_w= net web cross-sectional area = $h_w.t_w$

The corresponding pressure capacity is obtained according to following capacity equations derived by C.G.Daley [9]:

$$P_{Cenrally} = \frac{(2-k_w)+k_w\sqrt{1-48Z_{pns}(1-k_w)}}{12Z_{pns}k_w^2+1}\left(\frac{Z_p\sigma_y 4}{SbL\left(1-\frac{b}{2L}\right)}\right) \leq 2\frac{A_w\sigma_y}{\sqrt{3}Sb} \qquad (42)$$

Where:

$$Z_{pns} = \left(\frac{Z_p}{A_wL\left(1-\frac{b}{2L}\right)}\right)^2$$

Detailed calculations for IACS the requirement of the plastic section modulus for transverse frames and the corresponding pressure capacity can be found in reference [9].

In a similar way as it is done earlier in section 6.2.1 “Development of plastic collapse mechanism for a beam”, the plastic mechanism of a clamped frame subjected to a centrally patch load with breadth “b” develops also trough the same three stages as described by figure 17, with different moment magnitudes as shown by figure 24.

For detailed calculations of the bending moment distributions shown in figure 24, see the enclosed Matlab script in appendix A.

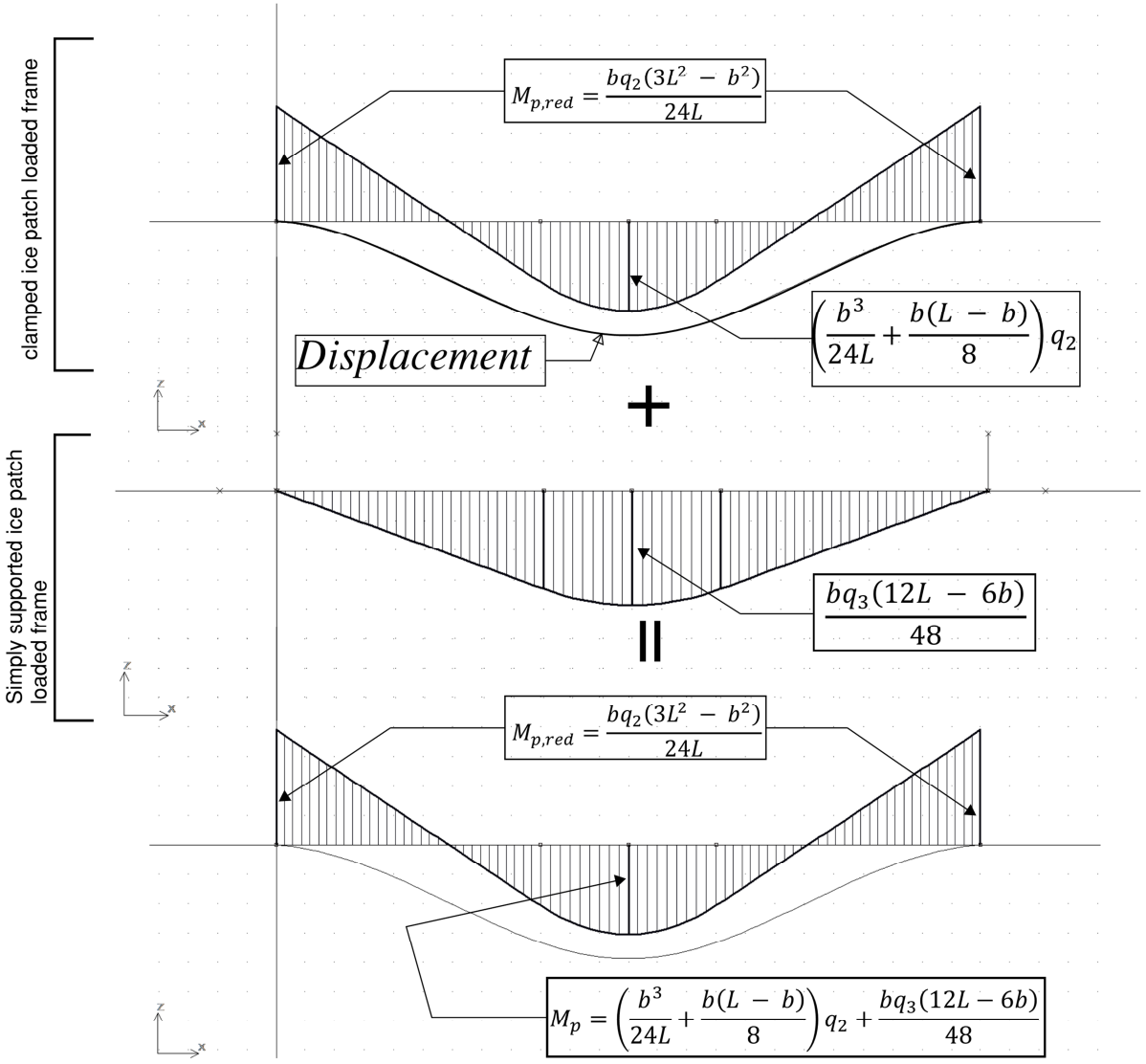

Figure 24: loading stages for a patch loaded frame with clamped ends

- At The 2nd stage described by figure 24, the load increases to q_2 to attain full plasticity at the ends due to both bending and shear:

$$q_2 = \frac{M_{p,red} 24L}{b\left(3L^2 - b^2\right)} \tag{43}$$

Where:

$$M_{p,red} = \sigma_y . Z_p . A \text{ and } A = \left[1 - k_w + k_w \sqrt{1 - \left(\frac{A_0}{A_w}\right)^2}\right]$$

- The 3th stage is when a hinge develops at the centre of the frame with full plastification, and the plastic bending moment at this point can be obtained by summing the values of the bending moment at the centre point of the frame for both clamped and simply supported cases:

$$M_p = \left(\frac{b^3}{24L} + \frac{b(L - b)}{8}\right) q_2 + \frac{b q_3 (12L - 6b)}{48} \tag{44}$$

Where:

$$M_p = \sigma_y . Z_p$$

By combining (43) and (44), the additional load q_3 to q_2 to reach full plastification at the midpoint hinge is found:

$$q_3 = -\frac{8\left(\frac{A\left(6L^2 b - 6Lb^2 + 2b^3\right)}{2b\left(3L^2 - b^2\right)} - 1\right)}{b(2L - b)} \sigma_y . Z_p \tag{45}$$

The critical patch line load is then obtained by the sum of the line loads q_2 and q_3, i.e. $q_c = q_2 + q_3$ and the frame line load plastic capacity yields:

$$q_c = \frac{8(A + 1)}{b(2L - b)} \sigma_y . Z_p \tag{46}$$

Rearranging equation (46) and substituting $\frac{1}{A+1}$ with A_1 and q_c with $P_c . S$ where S is the frame spacing and P_c is the critical patch pressure, the required plastic section modulus yields exactly the IACS capacity for a centrally patch loaded frame with clamped ends:

$$\begin{cases} Z_{p,req} = P_c . b . S \left(1 - \frac{b}{2L}\right) \frac{L}{4\sigma_y} A_1 \\ Where\ A_1 = \frac{1}{\left[2 - k_w \left(1 - \sqrt{1 - \left(\frac{A_0}{A_w}\right)^2}\right)\right]} \end{cases} \text{ for clamped ends} \quad (47)$$

By considering the capacity equation (42), the total reserve resistance can be obtained as follow:

$$\frac{q_c}{q_y} = \left[\frac{(2 - k_w) + k_w\sqrt{1 - 48Z_{pns}(1 - k_w)}}{12Z_{pns}k_w^2 + 1}\left(\frac{(3L^2 - b^2)}{3L(2L - b)}\right)\right]\alpha \quad (48)$$

Where:

- $\alpha = \frac{M_p}{M_y}$ is the shape factor
- $Z_{pns} = \left(\frac{Z_p}{A_w L\left(1 - \frac{b}{2L}\right)}\right)^2$
- And $q_y = \frac{M_y 24L}{b(3L^2 - b^2)}$ is the elastic capacity of the frame

It is observed from equation (48) that the reserve resistance of a frame subjected to a centrally ice patch load is depending on the following factors:

- The shape factor α
- The span of the frame
- The patch load breadth
- The capability of the frame of carrying shear at the ends.
- And the boundary conditions.

From equation 42 it is stated that the line load capacity is to be limited by $q_{c,lim} = 2\frac{A_w\sigma_y}{\sqrt{3}Sb}$.

In other words:

$$Z_{pns} = \frac{1}{48(1-k_w)} \rightarrow Z_p = Z_{p,max} = \frac{A_w L}{\sqrt{48(1-k_w)}}\left(1 - \frac{b}{2L}\right) \quad (49)$$

For a given cross section, eq.(49) means that the patch breadth ratio to span is to be as follow:

$$\left(\frac{b}{L}\right)_{lim} = 2\left(1 - \frac{Z_p\sqrt{48(1-k_w)}}{A_w L}\right) \quad (50)$$

For $\frac{b}{L}$ above the limit expressed in eq. (50) the centrally patch loaded frame will first fail by shear at both supports and the capacity becomes $q_{c,lim} = 2\frac{A_w \sigma_y}{\sqrt{3}Sb}$.

To study how the total reserve resistance changes with b, the derivative of equation (48) with respect to b , $\frac{d\left(\frac{q_c}{q_y \alpha}\right)}{db}$, has been studied numerically for different cross sections and different frame spans, see appendix B.

Figure (25) shows plots of the ratios $\frac{q_c}{q_y \alpha}$, $\frac{q_{c,lim}}{q_y \alpha}$ and $\frac{d\left(\frac{q_c}{q_y \alpha}\right)}{db}$ versus the $\frac{b}{L}$ ratio for the selected cross section and span, as specified in the same figure.

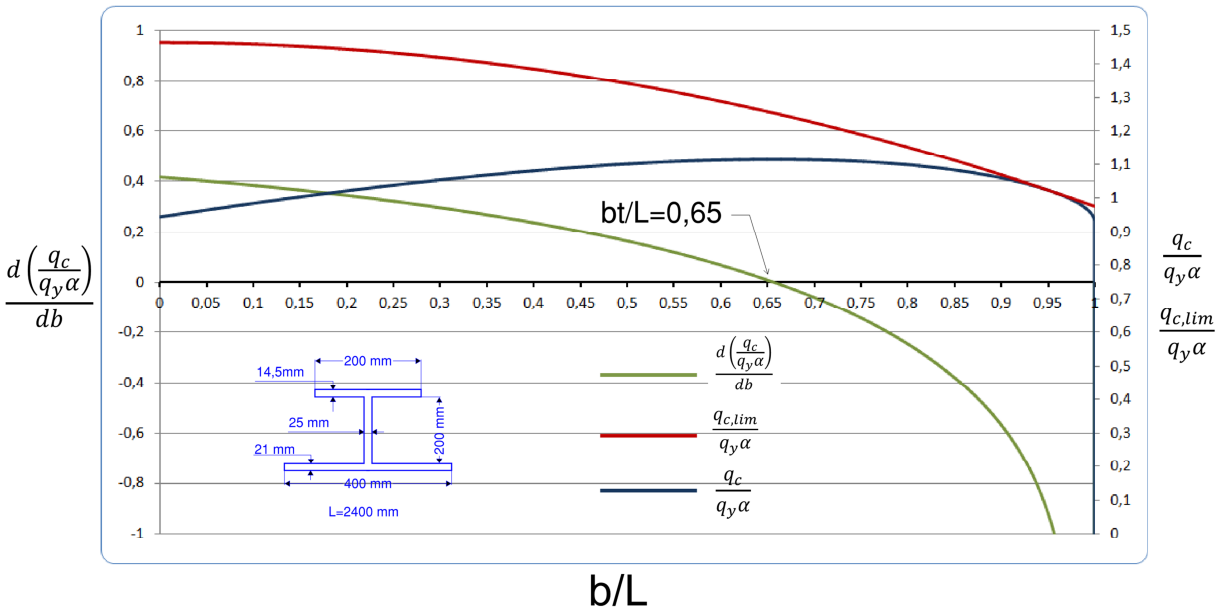

Figure 25: Plot of the ratios $\frac{q_c}{q_y\alpha}$, $\frac{q_{c,lim}}{q_y\alpha}$ and $\frac{d\left(\frac{q_c}{q_y\alpha}\right)}{db}$ versus $\frac{b}{L}$ for the cross section and the span indicated in the figure.

It is noticed from figure (25) and similar figures in appendix (B) for different cross sections and spans that the total reserve resistance is not a monotonic function with respect to $\frac{b}{L}$ and has a top value at $b = b_t$ varying with the ratio of the web modulus $k_w = \frac{Z_w}{Z_p}$ and span L.

By plotting the ratios of the ice patch breadth b_t to the span L, where the total reserve resistance is maximum, i.e. $\frac{b_t}{L}$, versus k_w for different cross sections and spans, it is observed from appendix (B), fig.(B.6), that the ratio $\frac{b_t}{L}$ may be approximated by a product of a polynomial of $k_w$and $\left(\frac{b}{L}\right)_{lim}$, i.e. $\frac{b_t}{L} = P(k_w).\left(\frac{b}{L}\right)_{lim}$

By a polynomial regression from figure (77) appendix B, $P(k_w)$ may be approximated as follow:

$$P(k_w) = -1{,}36k_w^3 + 1{,}36k_w^2 - 1{,}0633k_w + 0{,}986 \qquad (51)$$

And the ratio $\frac{b_t}{L}$ may be expressed as:

$$\frac{b_t}{L} = 2.(-1{,}36k_w^3 + 1{,}36k_w^2 - 1{,}0633k_w + 0{,}986)\left(1 - \frac{Z_p\sqrt{48(1-k_w)}}{A_w L}\right) \quad (52)$$

For the case indicated by figure (25), we have that $\left(\frac{b}{L}\right)_{lim} = 1$ and the corresponding $\frac{b_t}{L}$ ratio becomes: $\frac{b_t}{L} = (-1{,}36k_w^3 + 1{,}36k_w^2 - 1{,}0633k_w + 0{,}986) = 0{,}65$

For $\frac{b}{L} < \frac{b_t}{L}$ the total reserve resistance increases by increasing b and vice versa.

6.2.2.2 *Off-center (asymmetrical) patch load*

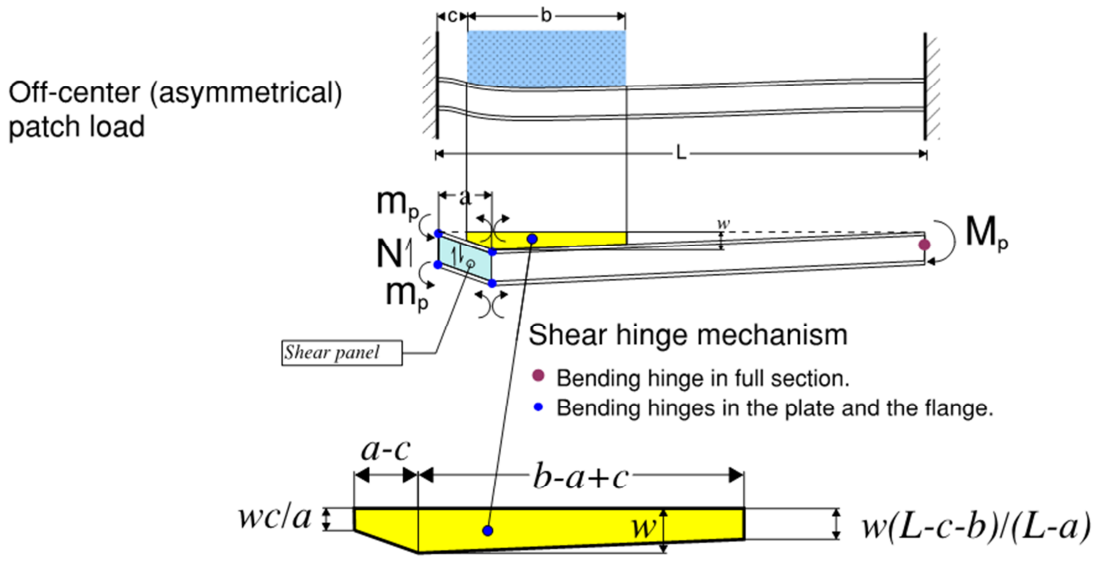

Figure 26: Off-center (asymmetrical) patch loaded transverse frame (C.G .Daley [9])

Considering figure 26, it is seen that the external work can obtained as:

$$\delta w_e = P.S.\left(\frac{\left(\frac{w(L-c-b)}{L-a}+w\right)(b-a+c)}{2}+\frac{\left(\frac{wc}{a}+w\right)(a-c)}{2}\right) \quad (53)$$

From equation (53) the corresponding maximum external work is found as follow by differentiating δw_e with respect to c:

$$\delta w_{e,max} = PbSw\left(1-\frac{b}{2L}\right) \quad (54)$$

The total internal work done by the resulting shear force N, the plastic bending moment at the flange, m_p, and the plastic bending in the full cross section at the opposite end reads:

$$w_i = w\sigma_y\left(\frac{A_w}{\sqrt{3}}+Z_p\left(\frac{1}{l-a}+k_z\left(\frac{2}{a}-\frac{1}{L-a}\right)\right)\right) \quad (55)$$

Where:

A_w= net web cross-sectional area = $h_w.t_w$

$k_z = z_p/Z_p$

$z_p = z_{p,flange} + z_{p,plate}$

From equation (55) the corresponding minimum internal work is obtained by differentiating w_i with respect to a as follow:

$$w_{i,min} = w\sigma_y\left[\frac{A_w}{\sqrt{3}}+\frac{Z_p}{L}(1.1+5.7k_z^{0.7})\right] \quad (56)$$

By balancing the maximum external work with the minimum internal work, the plastic section modulus requirement for an off-center patch loaded frame yields:

$$\begin{cases} Z_{p,req} = \frac{PbSL}{\sigma_y 4}\left(1-\frac{b}{2L}\right).A_2 \\ A_2 = \frac{1}{(0.275+1.425k_z^{0.7})}\left[1-\frac{A_w}{2A_0\left(1-\frac{b}{2L}\right)}\right] \end{cases} \quad (57)$$

And the corresponding pressure capacity is obtained:

$$P_{Off-center} = \frac{\sigma_y}{Sb\left(1-\frac{b}{2L}\right)}\left[\frac{A_w}{\sqrt{3}}+\frac{Z_p}{L}\left(1.1+5.75{k_z}^{0.7}\right)\right] \quad (58)$$

General requirement for a transverse frame considering both the centrally and the off-center patch loaded frame, i.e. equation (47) and (57), can be summarized as follow:

$$\begin{cases} A_w > A_0 \\ Z_p \geq \frac{PbSL}{\sigma_y 4}\left(1-\frac{b}{2L}\right).A \\ A = \max(A_1, A_2) \end{cases} \quad (59)$$

6.2.3 IACS Polar class requirement for longitudinal framing

For the case of longitudinally stiffened shell, the ice patch is considered to have the same length as the longitudinal frame, i.e. b=L. Considering the interaction plot for shear collapse mechanism, fig. (27), and the case of b=L, it is seen that the shear mechanism curve is laying under the 3 hinge mechanism curve, implying that the latter is the governing mechanism, i.e. the factor A_2 in equation (59) is irrelevant.

As longitudinal frames are for the most of the cases continuous, i.e. j=2, and b=L, equation (59) becomes:

$$\begin{cases} A_w > A_0 \\ Z_p \geq P.S\dfrac{L^2}{8\sigma_y}A_3 \\ Where\ A_3 = \dfrac{1}{\left[2 - k_w\left(1 - \sqrt{1 - \left(\dfrac{A_0}{A_w}\right)^2}\right)\right]} \end{cases} \quad (60)$$

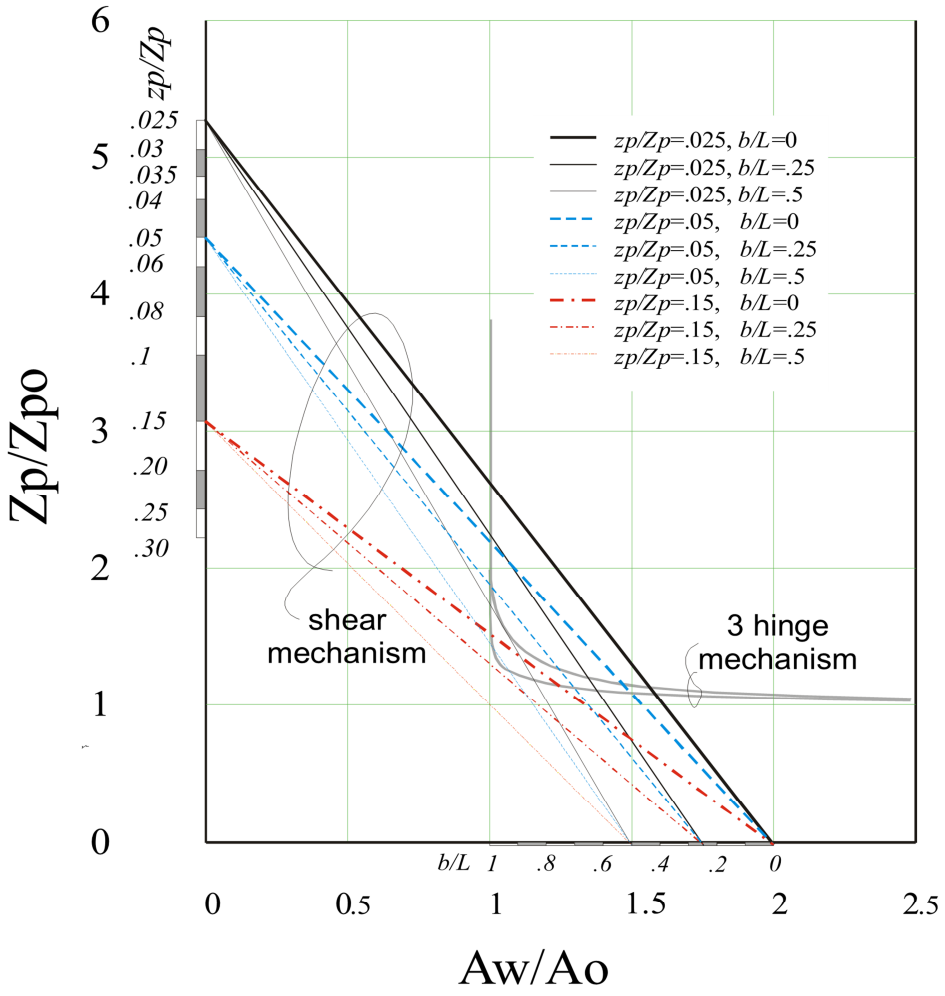

Figure 27: Interaction plot for off-center shear and 3 hinges collapse mechanisms.

(A. Kendrick, AMARK Inc, C. Daley, Daley R&E, 2000)

6.2.4 Framing – Structural stability

6.2.4.1 Introduction and background

For the IACS plastic section modulus to be valid the frame must acquire a high rotational resistance and/or lower slenderness to make sure that the frame attains its fully plastic bending. A slender frame or a frame with low rotational capacity may rotate and /or buckle locally causing a drop-off in load carrying capacity. Consequently, the member may collapse with a maximum bending moment no more than the yield moment or even less.

According to DNV-OS-C101 [18], a frame cross section is classified as summarized in table A1 and figure 1, reproduced in this report in table 4 and figure28.

Table 4: cross section classifications

Cross sectional types	
I	Cross sections that can form a plastic hinge with the rotation capacity required for plastic analysis
II	Cross sections that can develop their plastic moment resistance, but have limited rotation capacity
III	Cross sections where the calculated stress in the extreme compression fiber of the steel member can reach its yield strength, but local buckling is liable to prevent development of the plastic moment resistance
IV	Cross sections where it is necessary to make explicit allowances for the effects of local buckling when determining their moment resistance or compression resistance

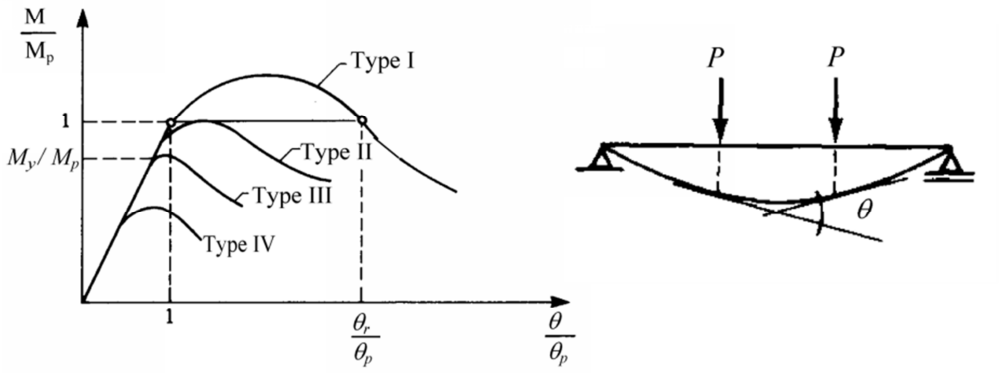

Figure 28: Relation between moment M and plastic moment resistance Mp, and rotation θ for cross sectional types. My is elastic moment resistance (DNV-OS-C101 [18])

The classification of a specific cross-section depends on the width-to-thickness ratio, b/t, of each of its compression elements.

The elastic critical buckling stress (Euler buckling stress) for a plate element with an aspect ratio, a/b (length-to-width), greater than about 0,8 is given by the following expression:

$$\sigma_{cr} = k_\sigma \frac{\pi^2 E}{12(1-\upsilon^2)}\left(\frac{t}{b}\right)^2 \qquad (61)$$

Where:

- υ is Poisson's coefficient
- E Young's modulus
- t: plate thickness
- b: plate width
- k_σ is the plate buckling factor, depending on edge support conditions, on type of stress and on the ratio of length to width (a/b), aspect ratio of the plated field.

From equation (61) it is seen that the critical buckling stress, is inversely proportional to $\left(\frac{b}{t}\right)^2$, playing the same role as the reduced slenderness given according to Eurocode 3 et al. [17] for cross section type I, II and III by:

$$\bar{\lambda} = \sqrt{\frac{f_y}{\sigma_{cr}}} \tag{62}$$

In the Eurocode 3[17] the cross-section requirements for plastic analysis is that elsewhere in the member the compression flange should be class I or class II and the web should be class I, class II or class III.

Apparently, the same intention as in Eurocode 3 is adopted by the IACS frame structural stability rules. Cross sections of class I, II and III are provided for in the IACS rules by requiring a $\frac{b}{t}$ ratio to be small enough to ensure that σ_{cr} exceeds the material yield strength f_y, so that yielding occurs before the plate element undergoes any substantial buckling, i.e. $\bar{\lambda} < 1$.

By considering equation (61) and (62) and taking $\upsilon = 0.3$, the reduced slenderness $\bar{\lambda}$ can be expressed as follow:

$$\bar{\lambda} = 1{,}05\frac{b}{t}\sqrt{\frac{f_y}{E.k_\sigma}} \tag{63}$$

The reduced slenderness limit of 1 is adjusted to be even smaller then 1 to take in to account the effect of the possible plate imperfections, including, inter alia, residual stresses and geometrical imperfections such as lack of verticality, straightness and/or flatness.

As illustrated by figure 29, due to imperfection the plate starts buckling at the onset of the axial load, not at Euler buckling load, eq. (61). In Eurocode 3 [17] the reduced slenderness limit adopted is $\bar{\lambda} < 0{,}74$ for class III compression elements.

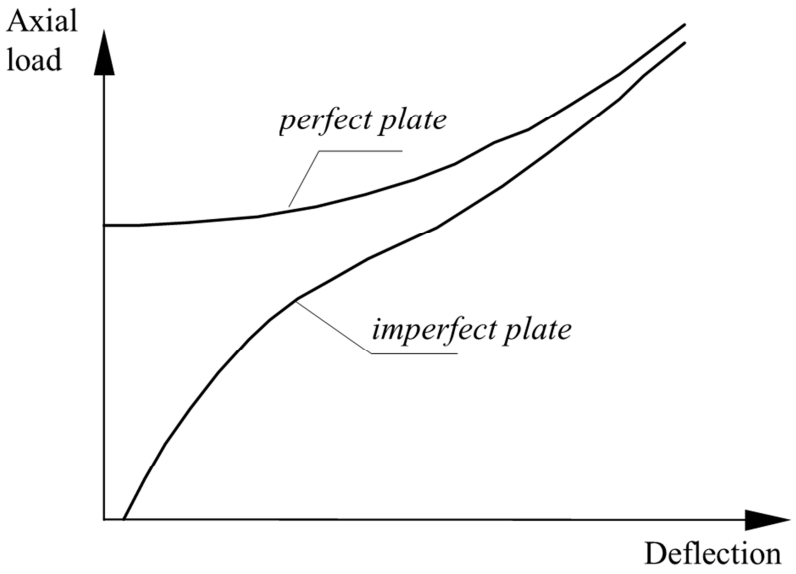

Figure 29: Load-deflection behavior of plate element (Jørgen Amdahl et al., MTS-2009.05.18)

Equation (63) in combination with the slenderness limit to compensate for the plate imperfection are apparently the background for the IACS framing – Structural stability.

6.2.4.2 Comparison of IACS rules for structural stability with FE analysis results

Web and flange local buckling is prevented in the IACS unified rules by requiring that the cross section is fulfilling the following:

- For flat bar section: $\frac{h_w}{t_w} \leq \frac{282}{{\sigma_F}^{0,5}}$ (64)
- For bulb, tee and angle section: $\frac{h_w}{t_w} \leq \frac{805}{{\sigma_F}^{0,5}}$ (65)
- In addition, the following shall be satisfied: $t_w \geq 0{,}35.\, t_p.\left(\frac{\sigma_F}{235}\right)^{0,5}$ (66)
- To prevent local flange buckling of welded profiles, the following shall be satisfied:

$$\frac{b_{out}}{t_f} \leq \frac{155}{{\sigma_F}^{0,5}} \tag{67}$$

To emphasize the effect of structural stability requirements for webs, deep girders with three different web thicknesses as described by figure 32 are subjected to centrally progressive patch load in USFOS with an ice patch breath b=1200 mm. The material selected is with a yield stress of 400 MPa.

The boundary conditions selected for this purpose are clamped ends. Due to symmetry, the plate is restrained to rotate around x- and z-axis and to move horizontally along y-axis as shown by figure 30.

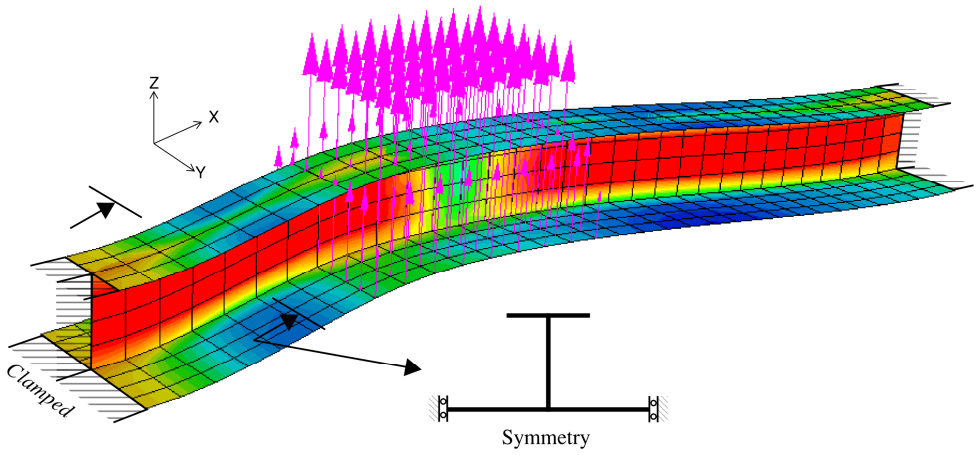

Figure 30: Boundary conditions for frame modeled with shell element in USFOS

The web thickness suggested in figure 32, cross section A, may not be realistic for a member within an ice reinforced area. However, as mentioned earlier this choice is maid just to emphasize the instability requirement legitimacy.

Cross section A and B do not satisfy respectively the requirements in equation (66) and (65). From figure 32, it is observed, for cross section A, that the web buckles centrally and from figure 31 it is observed that the frame collapses immediately, without any strength reserve, after buckling.

For cross section B the web plate buckles in area closer to the ends of the girder, fig.32, before reaching its IACS collapse capacity, however from figure 31, it is seen that the load keeps increasing until a total collapse of the frame occurs right at the IACS collapse pressure capacity. In these two cases, cross sections A and B may be regarded as type IV.

For the case of cross section C, fig.32, the requirement stated by equation (65) is barely satisfied. One can see from figure 31 and 32 that the web starts buckling slightly before reaching the IACS collapse capacity with enough strength reserve to reach P_{IACS}. In this case, cross section C may be regarded as of type III.

The web plate for cross section D, fig 32, is stocky enough to develop the 3 hinges collapse mechanism as anticipated by IACS rules, fig 31. Cross section D may be regarded of type I or II.

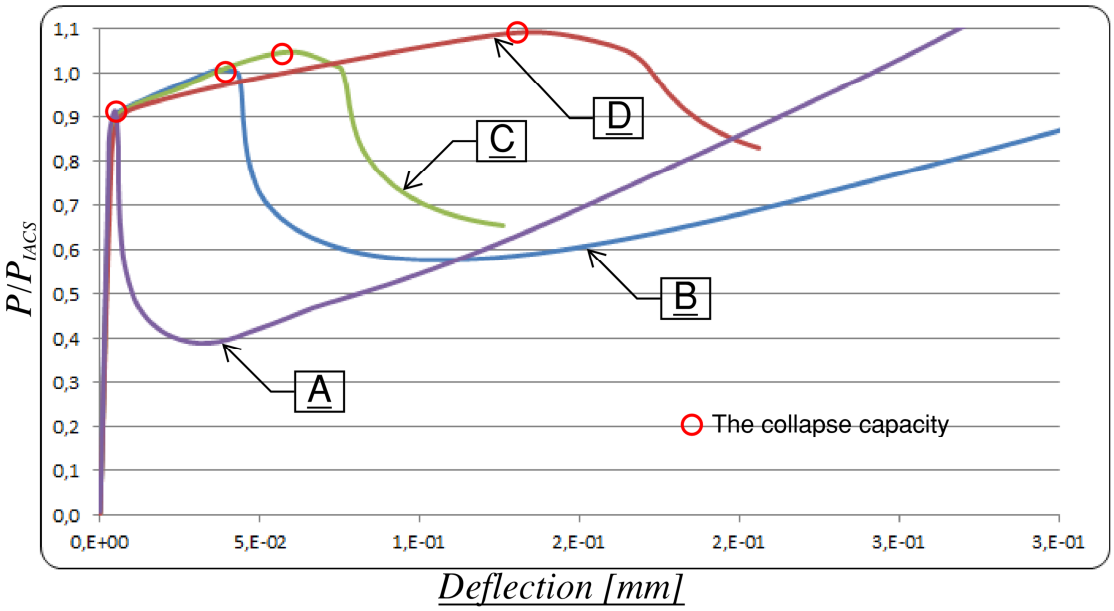

Figure 31: USFOS resistance predictions for centrally patch loaded girders with clamped ends. Cross sections A, B, C and D and deformation patterns are given in figure 32.

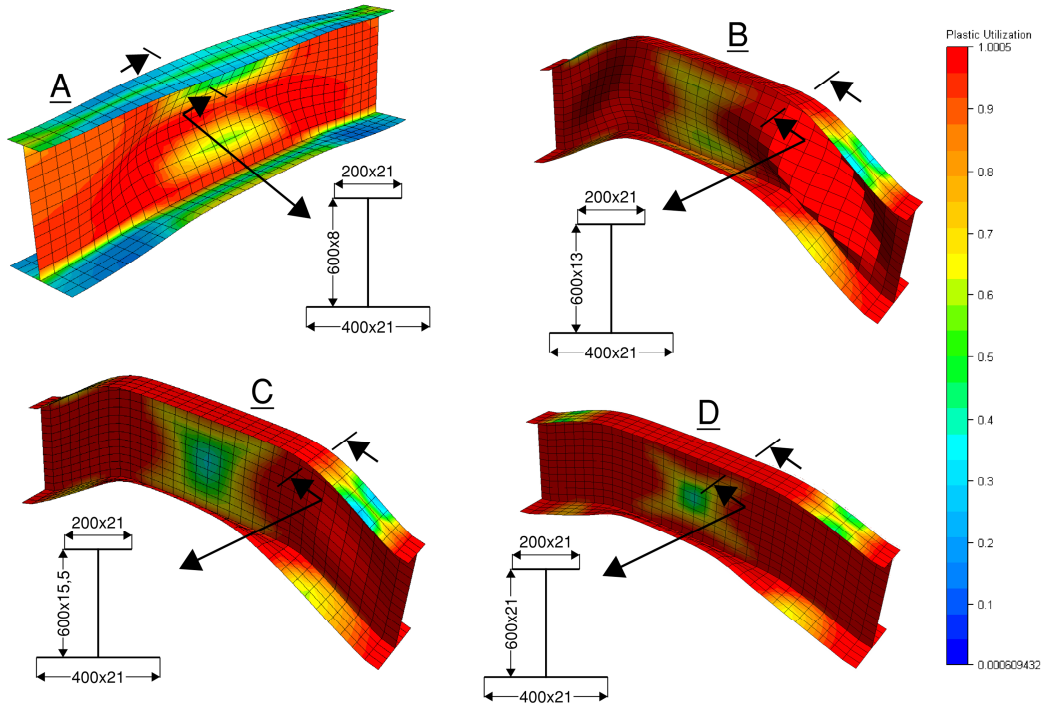

Figure 32: Corss sections and the coresponding deformatin pattern at collapse load.

According to DNV rules Pt.5 Ch.1 Sec.8 C206, load-carrying stringers and web frames are generally to be of symmetrical cross-sections. When the flange is arranged to be unsymmetrical, an effective tripping support shall be provided at the middle of each span length. To illustrate the significance of this requirement, a USFOS progressive collapse analysis is conducted for a centrally patch loaded web frame with an L-profile and an ice patch breath of b=1200 mm. The scantlings are included in figure 33. The material selected is with a yield stress of 400 MPa.

It is seen from figure 33 that the frame web trips and starts loosing stiffness straightaway after reaching a pressure capacity 10% lower than the IACS collapse capacity.

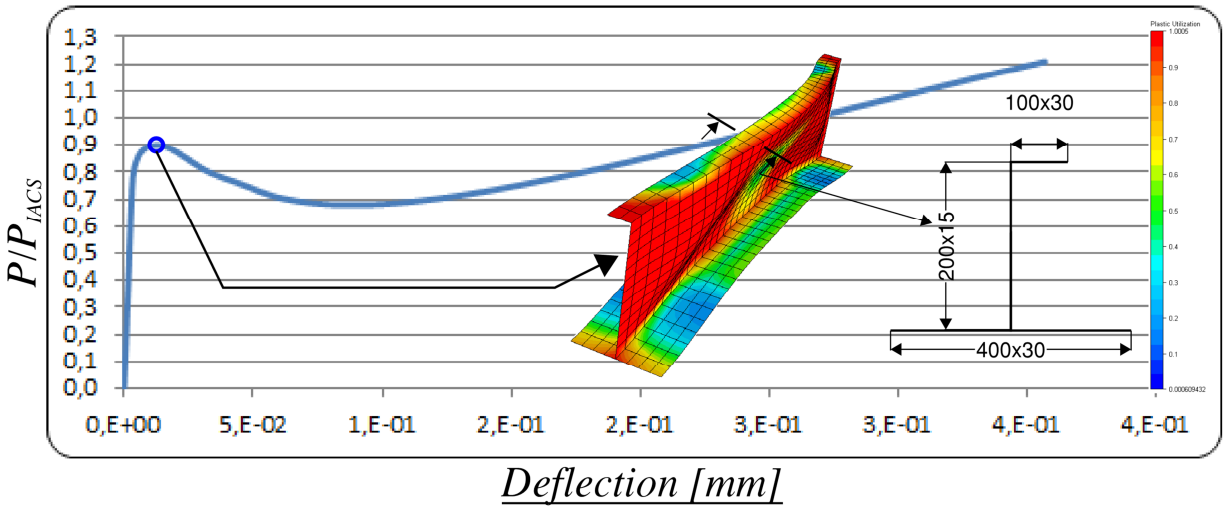

Figure 33: USFOS resistance prediction for centrally patch loaded girder with clamped ends and unsymmetrical cross section.

A perforated deep girder is a common structural member in a ship, especially in side tanks as shown in figure 34. The instability of the girder due to this weakness can also be regarded as a buckling failure of fictitious web plate within the cut-out with zero thickness and infinite slenderness.

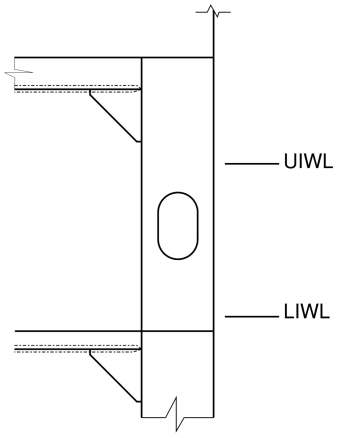

Figure 34: Perforated deep girder in a ship side

Address:
NTNU
Department of Marine Technology
N-7491 Trondheim

Location
Marinteknisk Senter
O. Nielsens vei 10

Tel. +47 73 595501
Fax +47 73 595697

The collapse capacity of such a frame, subjected to an ice patch load, drops significantly by introducing a cut out in the middle of the web, fig. 35 and 36. A common practice among designers is to place the cut-out in the middle of the web girder to avoid the concentrated shear forces occurring at the ends. From figures 35 and 36 it is seen, for the girder without cut-out, that the area where the cut-out is supposed to be is the less stressed area in the web.

The loss of the capacity of a perforated girder is partly due to the loss of the plastic section modulus in the midpoint and partly due to the occurrence of secondary bending and/or local collapse of the frame in way of the cut-out.

Figures 35 and 36 show the drop of the collapse pressure capacity of a 600x20+200x10 deep girder with a cut-out in the middle of the frame, the size of the cut-out is 600x400.

The girder is clamped on both ends and loaded centrally with a patch load of breadth b=1200. For the off-center case the frame is loaded with an ice patch with breadth b=600. The material selected for both cases is with a yield stress of 235 MPa.

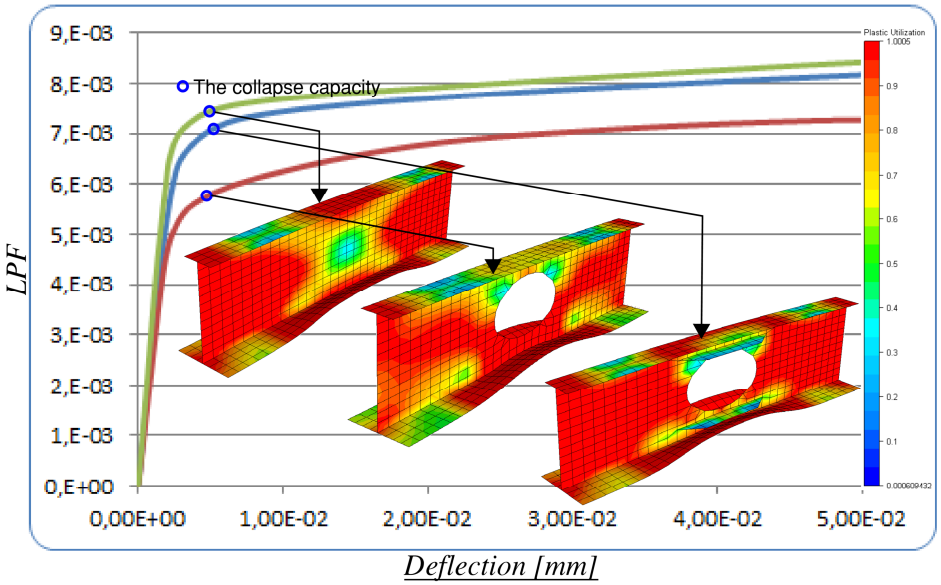

Figure 35: USFOS resistance predictions for centrally patch loaded girders with clamped ends and perforated web.

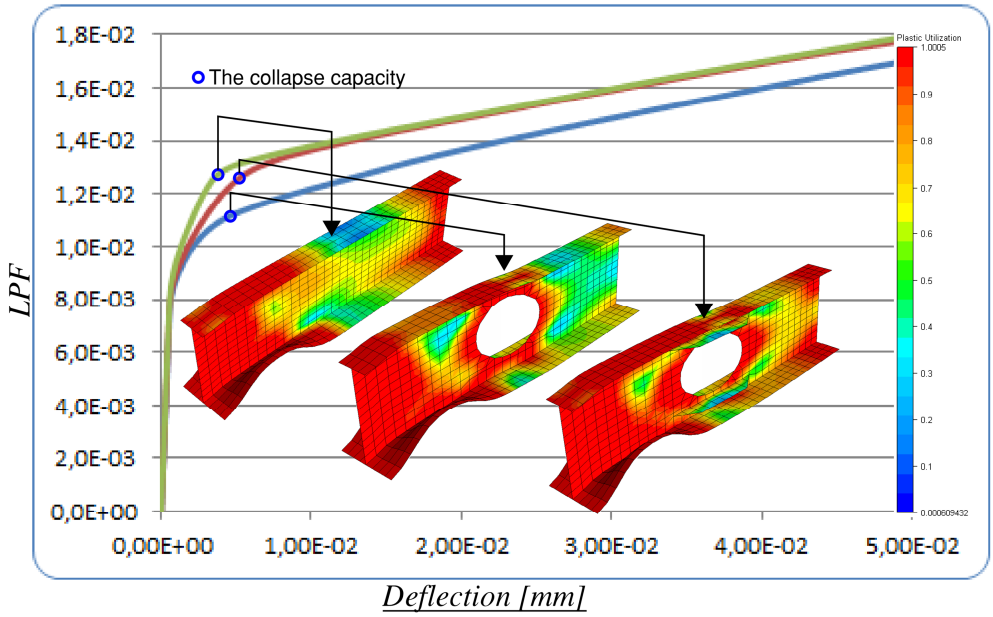

Figure 36: USFOS resistance predictions for off-center patch loaded girders with clamped ends and perforated web.

It is noticed form figure 35 that the web girder collapses locally at the sub-frame under the cut-out before reaching its original maximum collapse capacity.

From figure 36 where the girder is subjected to an off-center ice patch load, it is observed that the shear mechanism, as defined by figure 26, does not develop fully along the web girder to reach the point where the far web frame end collapses in bending. This is of course due to the existence of the weak link in the middle presented by the cut-out.

For the IACS 3 hinge and shear collapse mechanism to be valid in the case of a perforated girder, the girder is to be reinforced to compensate for the loss of the plastic section modulus resulting from the introduction of the cut-out. This can be achieved by either increasing the web thickness locally in way of the cut-out and/or fitting stiffeners acting as local flanges along the opening, fig. 37. The reinforcement has to be good enough to provide for web shear areal more than the

minimum required value, i.e.$A_0 = \frac{PbS\sqrt{3}}{2\sigma_y}$ where b in this case is the minimum of the ice patch breadth and the cut-out wide.

The reinforcement should also be in such a way to prevent development of a local 3 hinge collapse mechanism in way of the cut-out. Figures 35and 36 show that the web frame collapse capacity in both load cases is well restored after fitting a flat-bar of 100x32 along the cut-out and increasing the web thickness locally in way of the cut-out from 20 mm to 32 mm, fig. (37).

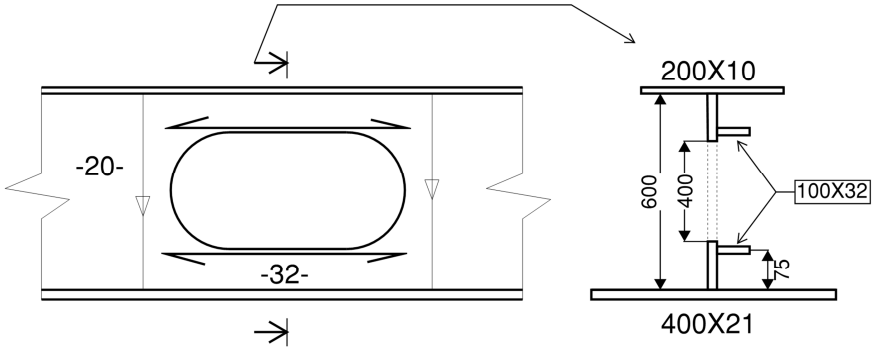

Figure 37: Proposal reinforcement of a perforated girder within the ice reinforced area.

6.2.5 Discussion of the adopted IACS collapse mechanism for frames

In this study, it is decided to use the progressive collapse analysis software USFOS [11] to discuss the capacity of centrally and off-center patch loaded frame. The elements selected for this purpose is a **4 node quadrilateral shell** element.

The boundary conditions considered in this analysis are as described earlier by figure 30.

To include both the 3 hinge and the shear hinge collapse mechanism in this discussion, the scantlings of the cross sections selected in this discussion are determined to fulfill the following criteria in connection with the factors A_1 and A_2 as stated by respectively equation (47) and (57):

- For the case of a centrally patch loaded frame, the cross section and the span are selected to ensure that $A_1 > A_2$ i.e. 3 hinge collapse mechanism.
- For the case of an off-center patch loaded frame, the cross section and the span are selected to ensure that $A_2 > A_1$ i.e. shear hinge collapse mechanism.

For the off-center loaded frame, the ice patch is placed on the frame considering the position that gives the maximum external work and the minimum internal work. The corresponding distance "c" considered in this discussion, as shown in figure 26, is calculated in details in the "*Derivation of plastic framing requirements for polar ships*", by C.G.Daley [9] and obtained as follow:

$$c = a\left(1 - \frac{b}{L}\right) \text{ where } \frac{a}{L} \approx 0.64 k_z^{0.3333}$$

The fact that the 3 hinge collapse mechanism, compared with the 4 hinge collapse mechanism, for a centrally patch loaded frame is the governing or the worst mechanism giving the minimum possible capacity, is not always true. The prevailing mechanism is actually depending both on the ratio of the ice patch breadth, b, to the frame span and the cross section in consideration. By increasing the ice patch breadth b for a particular cross section, the governing collapse

mechanism tends to change from being 3 hinges to become 4 hinges collapse mechanism, fig. 38, as demonstrated in appendix C, fig C.2, C.3 and C.4.

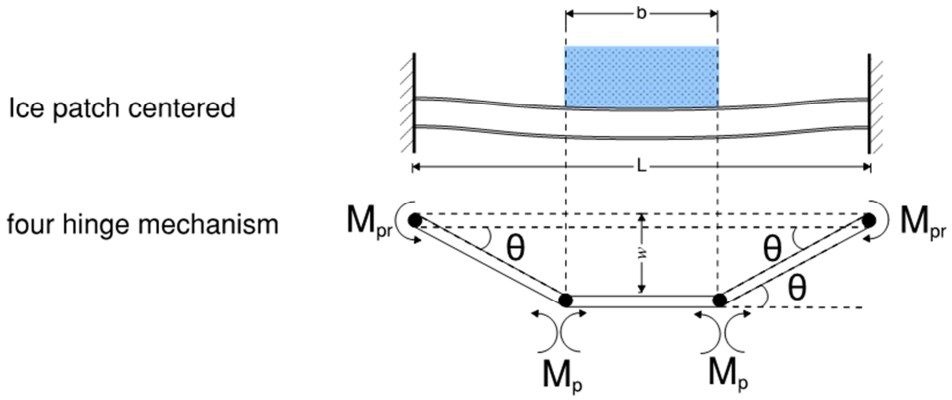

Figure 38: Four hinges Collapse mechanisms for centrally patch loaded frame with fixed ends

The 4 hinges mechanism pressure capacity is obtained as follow:

$$P_{Cenrally,4h} = \frac{(2-k_w)+k_w\sqrt{1-48Z_{pns}(1-k_w)}}{12Z_{pns}k_w^2+1}\left(\frac{Z_p\sigma_y 4}{SbL\left(1-\frac{b}{L}\right)}\right) \leq 2\frac{A_w\sigma_y}{\sqrt{3}Sb} \qquad (68)$$

Where:

$$Z_{pns} = \left(\frac{Z_p}{A_wL\left(1-\frac{b}{L}\right)}\right)^2$$

Detailed calculations for the 4 hinges pressure capacity together with plots of the capacity ratio $\frac{P_{Cenrally,4h}}{P_{Cenrally,3h}}$ versus $\frac{b}{L}$ are included in appendix C.

For a frame with span L=2400mm and a flat bar cross section with web height h_w=600 mm and plate thickness t_p=21 mm the ratio $\frac{P_{Cenrally,4h}}{P_{Cenrally,3h}}$ versus $\frac{b}{L}$ is plotted in figure 39.

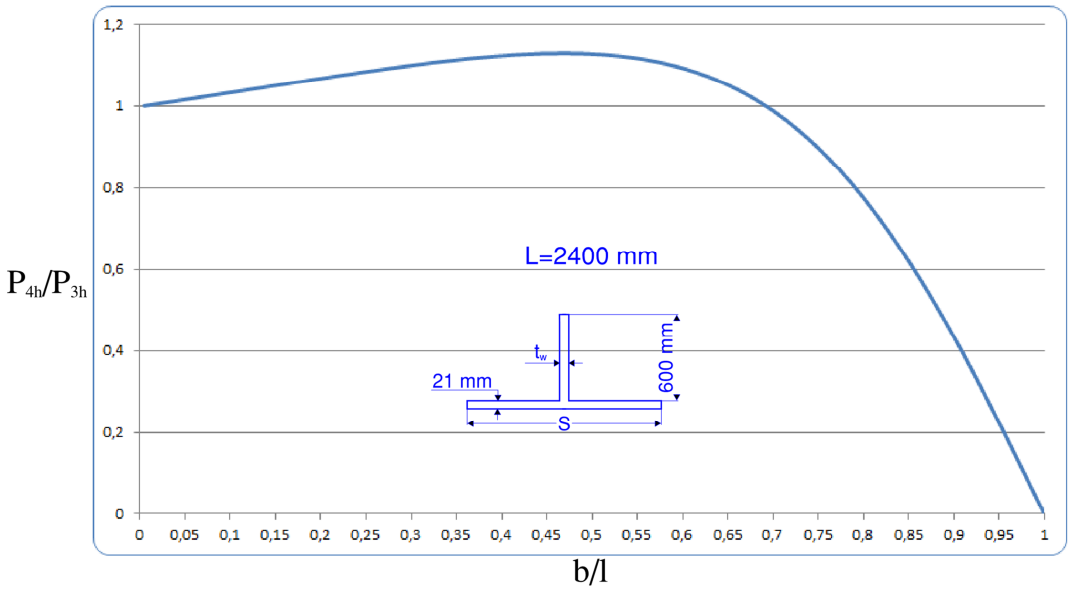

Figure 39: the ration $\frac{P_{Cenrally,4h}}{P_{Cenrally,3h}}$ versus $\frac{b}{L}$ for a flat bar cross section

From figure 39 it is observed, regardless of the web thickness and the spacing S, that the 4 hinges collapse mechanism becomes the governing mechanism for b/L>0,7.

The accuracy of pressure capacity for a centrally patch loaded frame is also depending on the relevancy of the assumption that the plastic neutral axis is situated at the intersection between the web and the plate.

Referring to figure 22 reproduced here as figure 40. The frame considered in this figure is with a span of L=2400mm and a flat bar cross section with web height of 600 mm , connected plate of 400x21 and a varying web thickness, fig 40. The pressure capacity deviation in present that corresponds to the difference between the exact and the approximated plastic section modulus, respectively eq.(38) and eq.(40), versus Z_{na} for different patch breadths are also included in figure 40.

It is seen that the discrepancy between $P_{3h,approx}$ and $P_{3h,exact}$ increases as the plastic neutral axis get raised above the plate, and decreases with increasing ice patch breadth.

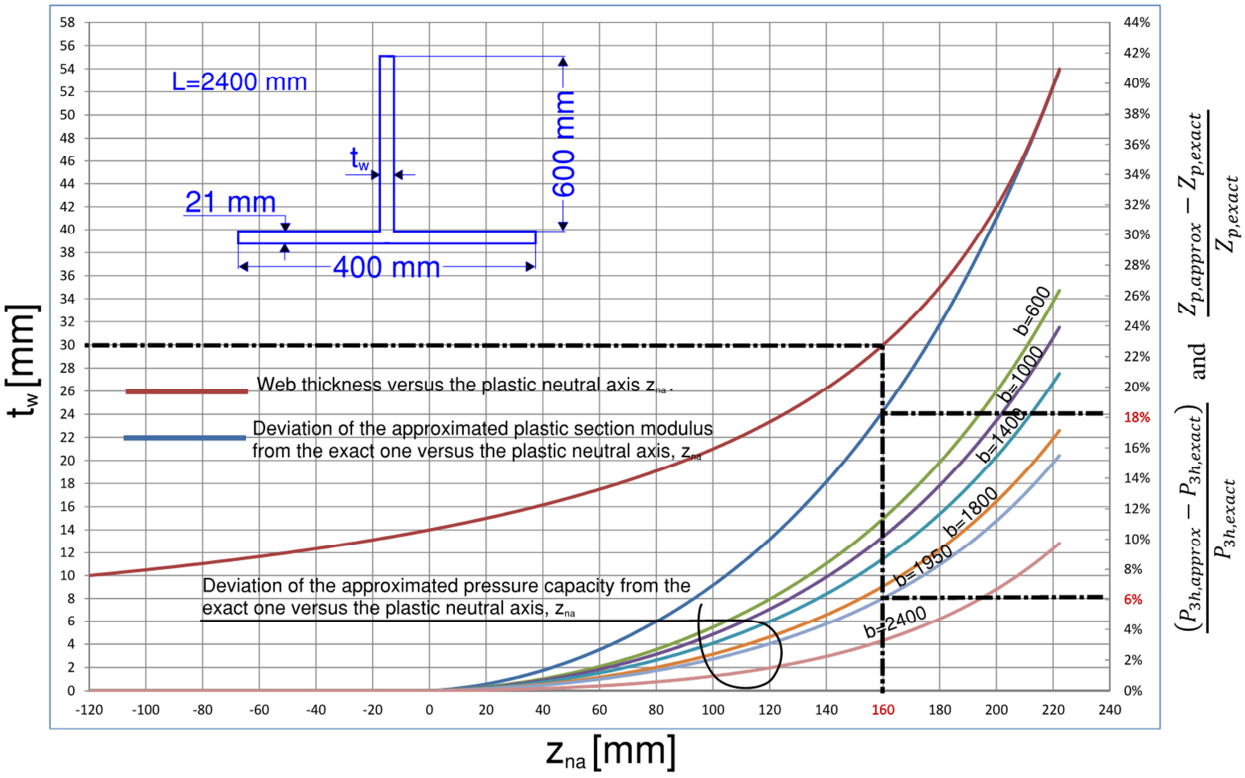

Figure 40: Deviation of the approximated plastic section modulus from the exact one together with deviation of the resulting approximated capacity from the exact one as a result of increasing the position of the plastic neutral axis considering different ice patch breadths.

By considering a centrally patch loaded frame with a flat bar cross section and the following scantlings:

- L=2400 mm
- h_w=600
- t_w=30 mm
- S=400 mm
- t_p=21 mm
- σ_f=235 MPa

- b/L=0,813

It is notice from figure (39) that the governing mechanism will be a 4 hinge collapse mechanism, where $\frac{P_{Cenrally,4h}}{P_{Cenrally,3h}} = 0{,}75$ and from figure (40) it is seen that the IACS approximated frame capacity is 6% higher than the exact one. The actual capacity of the frame will then become:

$$P_{Cenrally,4h} = P_{IACS} \cdot \frac{0{,}75}{1{,}06} \tag{69}$$

By plotting the ratio of USFOS capacity to the IACS capacity for the above mentioned frame, fig (41), considering an ice patch breadth ratio to span of b/L=0,813, it is seen that the IACS frame capacity is overestimated as a result of both the assumed position of the plastic neutral axis and the 3 hinge collapse mechanism. By implementing the correction stated in equation (69), it is noticed from figure (41) that the capacity of the frame tends to be more reasonable.

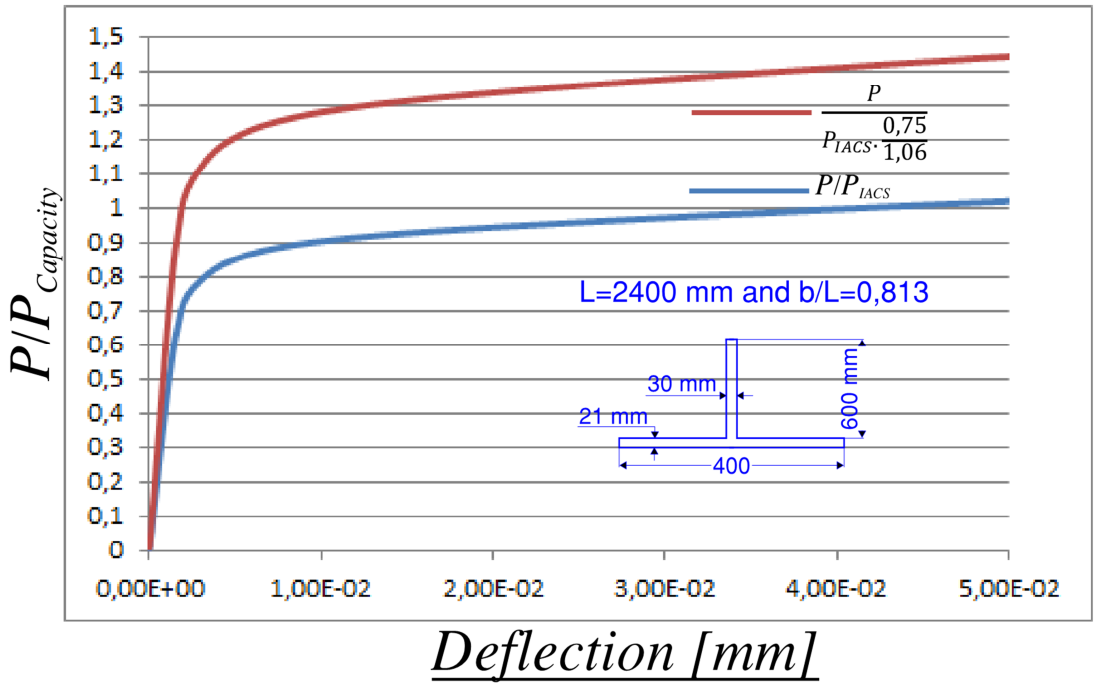

Figure 41: Comparison of USFOS capacity for a centrally patch loaded frame with the approximated 3 hinge IACS capacity and the exact 4 hinge pressure capacity.

For the case where the shear mechanism is the governing one, the only factor that may influence the accuracy of the IACS frame capacity is the assumption concerning the plastic neutral axis position.

Considering a frame with L=2400 mm and a cross section with varying web and flange thickness as shown in figure 42, the deviation between the exact and the approximated plastic section modulus, respectively eq.(38) and eq.(40), and the corresponding pressure capacity deviation considering equation (58) versus Z_{na} are shown in figure42.

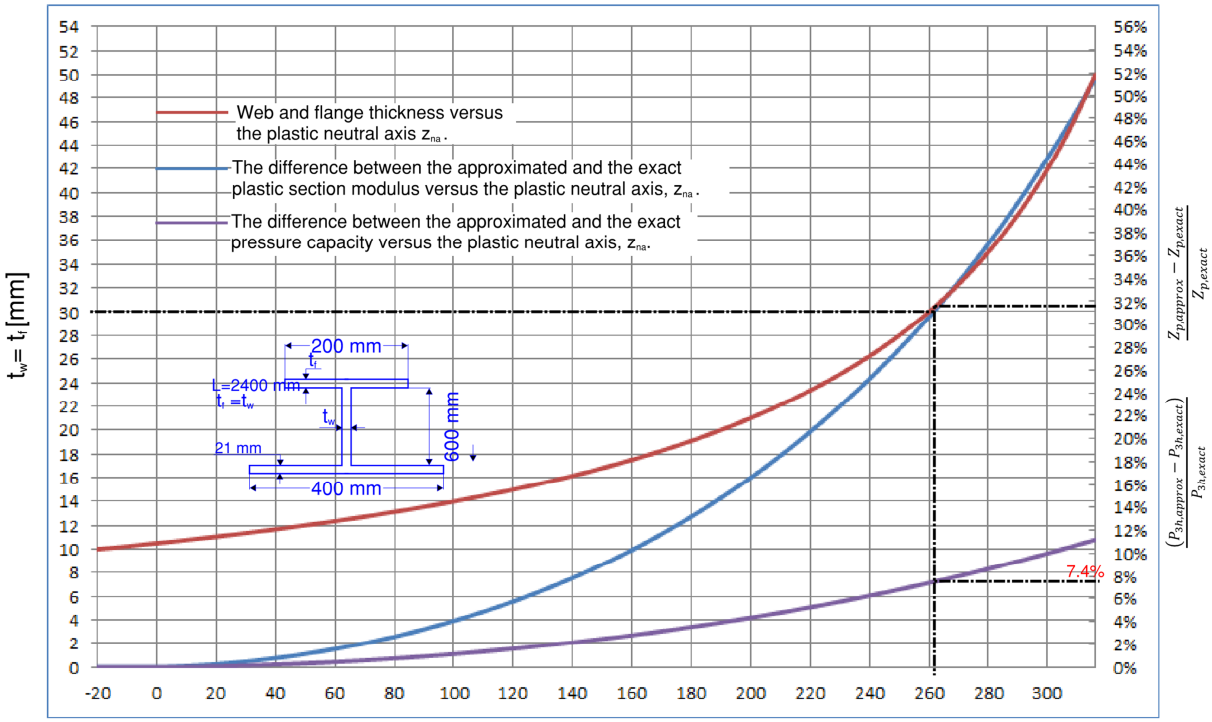

Figure 42: Deviation of the approximated plastic section modulus from the exact one as a result of increasing the position of the plastic neutral axis.

To emphasize the effect the plastic neutral axis assumption adopted by IACS, an off-center patch loaded frame with two different cross sections, where $z_{na} = 0$ and $z_{na} > 0$, are considered in the following USFOS analysis, fig. (43).

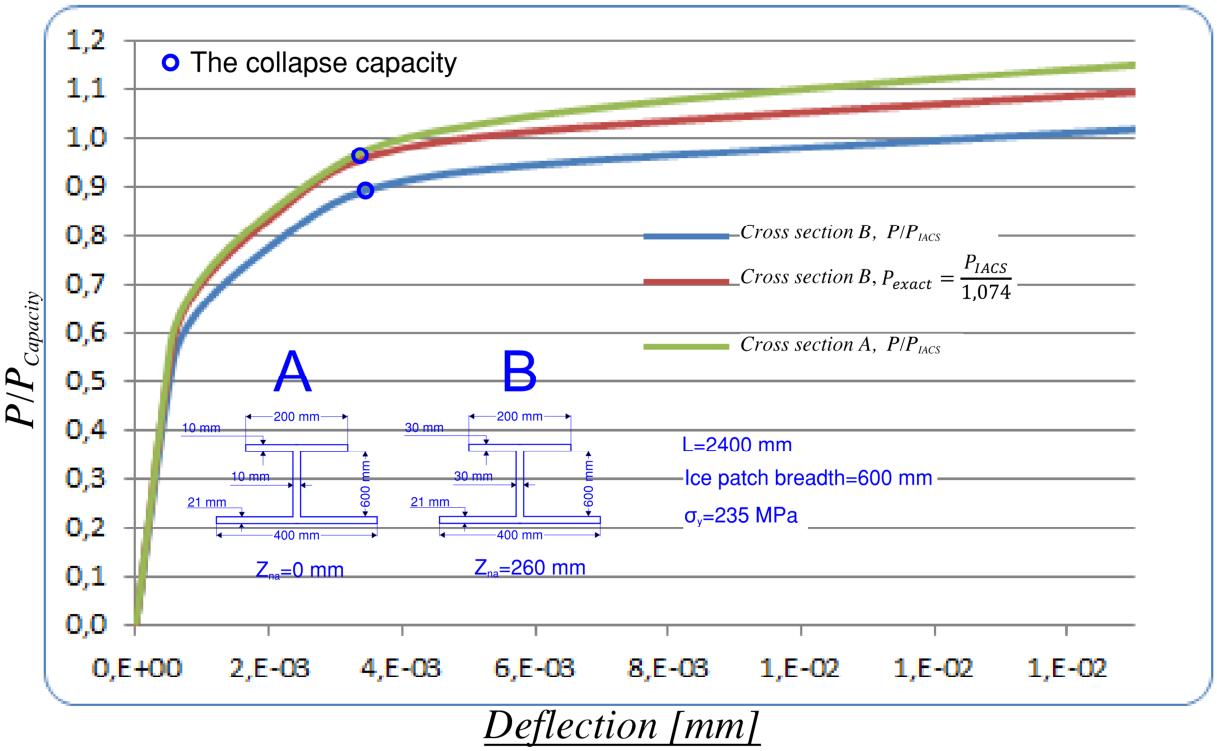

Figure 43: Comparison of USFOS pressure capacity for an off-center patch loaded frame with the IACS approximated pressure capacity and the exact one, considering both a cross section with Z_{na} at and above the intersection of the web and the attached plate.

It is seen from figure 43, for the case where Z_{na}=0, cross section A, the USFOS pressure capacity for an off-center patch loaded frame yields exactly the corresponding IACS capacity. However for the case where Z_{na}=260 mm, cross section B, it is seen that the IACS pressure capacity is overestimated as a result of assuming the position of the plastic neutral axis at the intersection of the web and the attached plate. By implementing the correction factor derived from figure42, $P_{exact} = \frac{P_{IACS}}{1,074}$, it is observed that the corrected IACS pressure capacity yield exactly the USFOS collapse pressure capacity.

The fact that frames are normally members of a complex panel system may fortunately hinder the frame from bearing the brunt of the total ice patch load, depending on the size of the panel, the supporting structure around the edge of the panel and the position of the stiffener within the panel.

To conduct a FE collapse capacity comparison of a frame with end brackets within a panel with the IACS frame capacity, a panel of size 4800x2400, fig.44, with the following scantlings has been modeled in USFOS:

- S=400
- Plate thickness t=21 mm
- Web height h=200 mm
- Web thickness t_w=25
- Flange breadth b_f=200
- Flange thickness t_f=15
- Bracket 200x200x25
- Yield stress σ_f=235 MPa

The panel is clamped in the transverse direction. The actual panel modeled in USFOS is with dimensions 2200x2400; however, in the longitudinal direction the plate is clamped in one end and restricted with symmetry boundary conditions in the other end to simulate the 4400x2400 panel. The load case considered in this comparison is a centrally patch loaded panel, fig .44. The plate and the frames are modeled with 4 nodes quadratic shell element and for the sake of simple modeling the bracket is modeled with triangular shell elements. The ice patch height considered in this analysis is with a breadth of b=600 mm.

Address:
NTNU
Department of Marine Technology
N-7491 Trondheim

Location
Marinteknisk Senter
O. Nielsens vei 10

Tel. +47 73 595501
Fax +47 73 595697

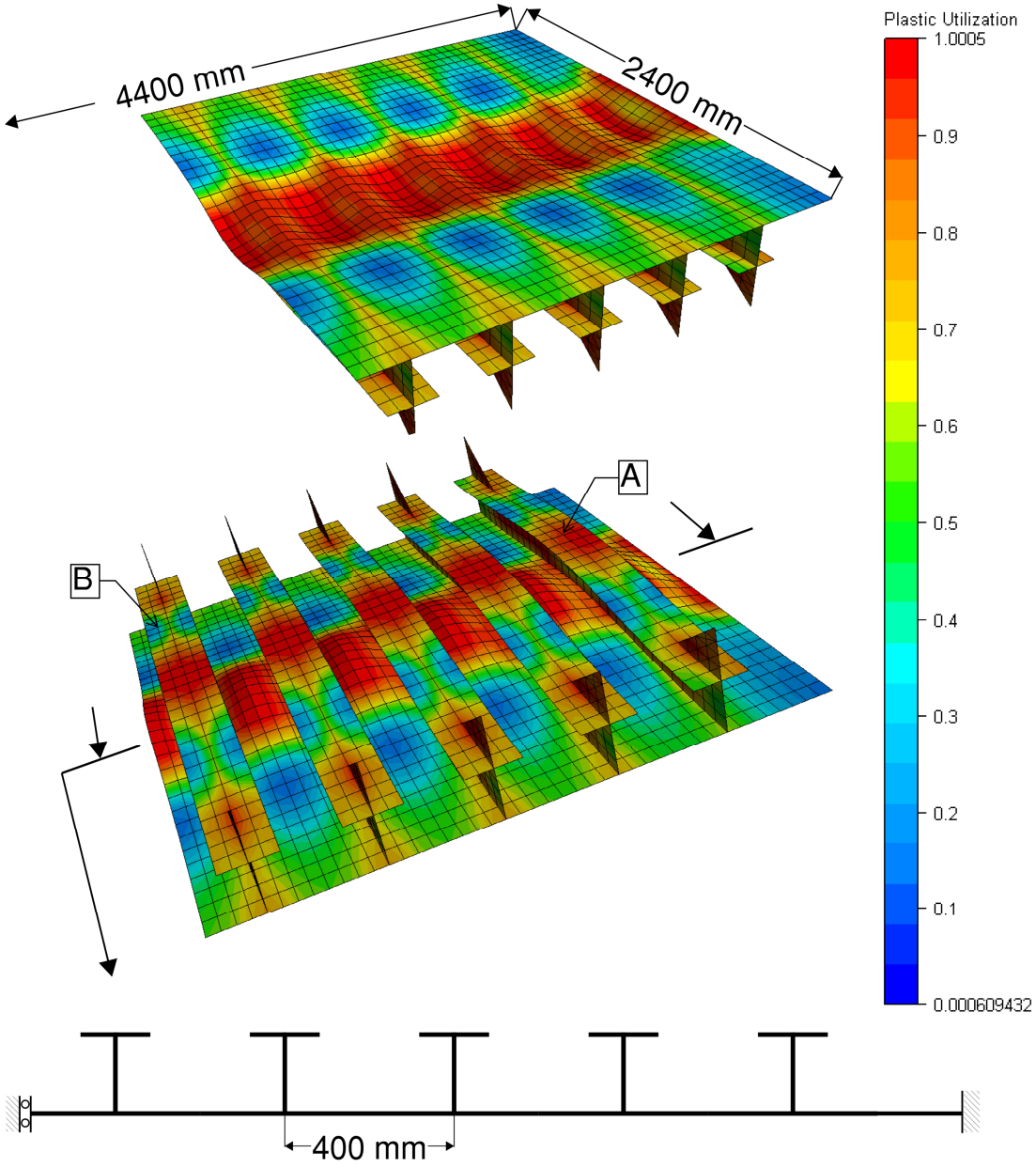

Figure 44: A centrally patch loaded panel

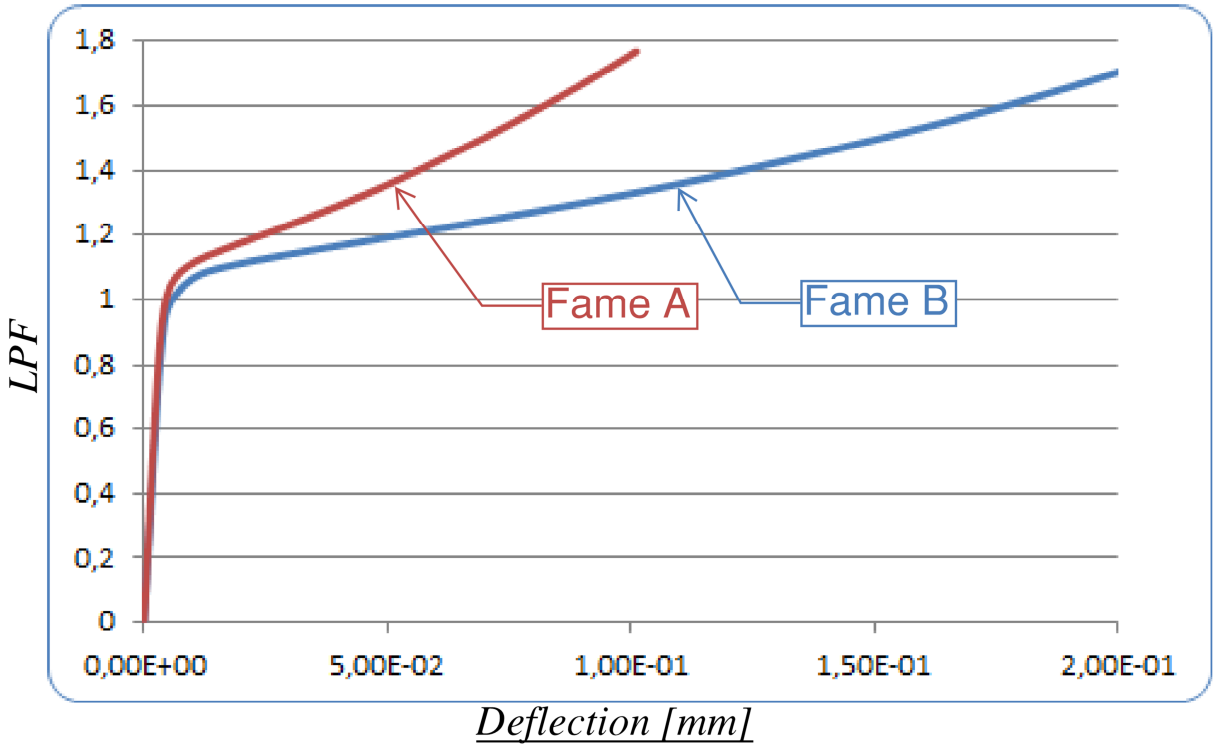

Figure 45: USFOS resistance predictions for frames within a centrally patch loaded panel, as illustrated by figure 44.

From figure 44 and 45, it is observed that frame A has a slightly higher capacity than frame B at the development of the middle hinge, but significantly higher reserve strength afterwards.

As expected, this is due to the fact that frame A benefits more from the adjacent hull structures which could be a bulkhead or a deep web girder.

Conclusion:

From this above discussion, it is concluded that the IACS 3 hinge collapse mechanism together with the assumptions made, may overestimate the pressure capacity for an ice patch loaded frame, depending on the cross section and the ratio $\frac{b}{L}$ considered.

6.3 Plate thickness requirement

6.3.1 Introduction

The IACS polar class requirement for plating is based on deriving the net thickness that corresponds to the ultimate strength of a plate filed. In this purpose, the kinematic method of the ultimate balance theory has been applied on a simplified collapse mechanism, by assuming rectilinear edge hinges to define a collapse mechanism envelope as close as possible to the real collapse mechanism.

6.3.2 Background

For the sake of simplifying the analysis and net thickness requirement derivation, it is assumed that the boundaries of the plate are horizontally free, which eliminates the contribution of the membrane effect from the adjacent structure. This assumption appears to make the IACS net thickness requirement conservative. Making such an assumption could be regarded to a certain level as a safety factor in terms of avoiding permanent deformation of shell plating within the ice reinforced area.

From figure 46 and due to symmetry, the analysis has been reduced to focus only on the sector ABCD. The internal works per unit length within the ABCD zone are obtained as follow:

$$w_i{}^{AB} = m_p.\frac{\theta_{AB} b}{2} \tag{70}$$

$$w_i{}^{AD} = m_p.\frac{\theta_{AD} S}{2} \tag{71}$$

$$w_i{}^{OC} = m_p.\frac{2\theta_{AB}(b-2n)}{2} \tag{72}$$

$$w_i{}^{AO} = m_p.\theta_{AO}\sqrt{\frac{S^2}{4}+n^2} \tag{73}$$

Where: $m_p = \frac{\sigma_y t^2}{4}$, $\theta_{AB} = \frac{2\delta}{S}$ and $\theta_{AD} = \frac{\delta}{n}$

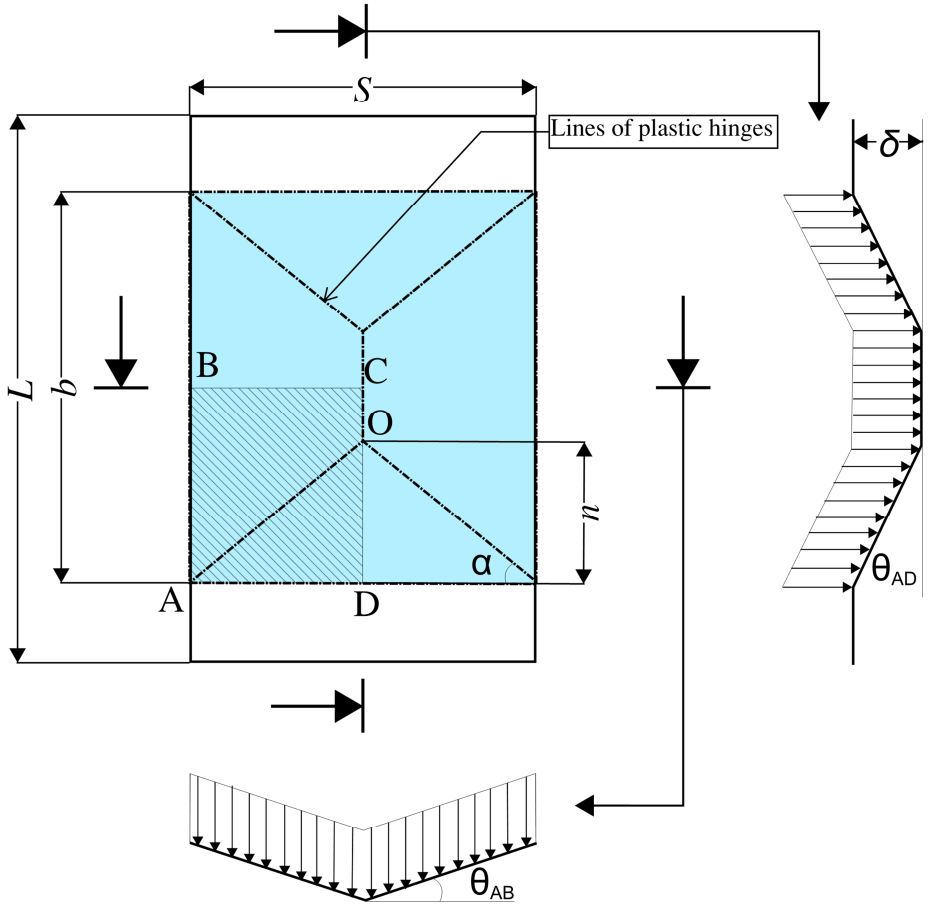

Figure 46: Roof-top collapse mechanism. (Tore H. Søreide et. al. [1])

The relative angle between the planes AOB and AOD is defined, according to Tore H. Søreide [1] et al., by decomposing θ_{AB} and θ_{AD} along the line AO, fig. (47) as follow:

$$\theta_{AO} = \theta_{AD}\cos(\alpha) + \theta_{AB}\sin(\alpha)$$

Where $\cos(\alpha) = \frac{S}{2\sqrt{\frac{S^2}{4}+n^2}}$ and $\sin(\alpha) = \frac{n}{\sqrt{\frac{S^2}{4}+n^2}}$

And the plate angle along AO reads:

$$\theta_{AO} = \frac{\delta}{\sqrt{\frac{S^2}{4}+n^2}}\left(\frac{S}{2n}+\frac{2n}{S}\right) \tag{74}$$

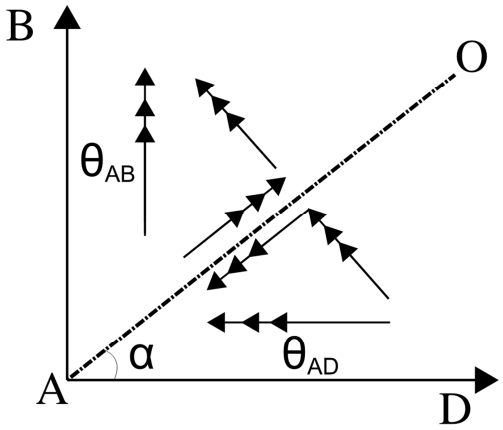

Figure 47: Decomposition of rotation (Tore H. Søreide et. al. [1])

Considering equations (70), (71), (72), (73) and (74), the total internal work is obtained as follow, considering the whole ice patch and the lines of plastic hinges described by figure 46:

$$w_i{}^{Tot} = 4w_i{}^{AB} + 4w_i{}^{AD} + 2w_i{}^{OC} + 4w_i{}^{AO} = \frac{2}{\sqrt{3}}\sigma_y t^2 \delta\left(2\frac{b}{S}+\frac{S}{n}\right) \tag{75}$$

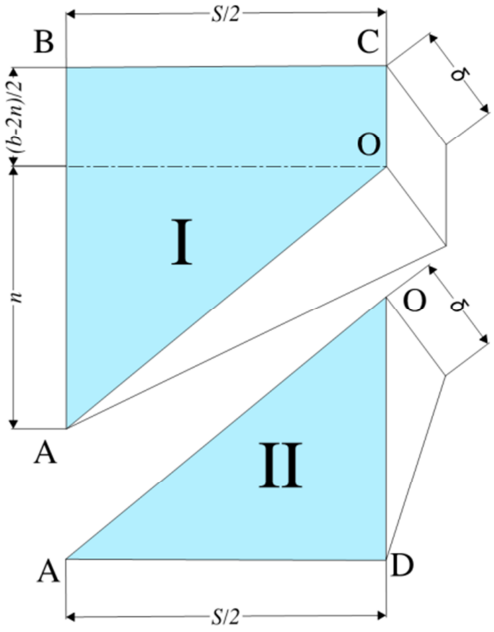

Figure 48: Volums considered in external work calculations

The external work from the ice patch pressure on zone ABCD is:

$$W_{ex}{}^{ABCD} = P_U(V_I + V_{II})$$

Where:

$$V_I is\ the\ volume\ of\ body\ I, fig.43, V_I = \frac{\delta S(b-2n)}{8} + \frac{\delta S n}{12}$$

$$V_{II} is\ the\ volume\ of\ body\ II, fig.43, V_{II} = \frac{\delta S n}{12}$$

$$P_U\ is\ the\ ultimate\ ice\ pressure.$$

And the corresponding total external work is obtained as follow:

$$W_{ex}{}^{Tot} = P_U \delta S \left(\frac{b}{2} - \frac{n}{3}\right) \tag{76}$$

The unknown parameters in the expresions of work, n and P_U , can be found, according to Evgeny Appolonov[3], by means of the kinematic method, enforcing the following conditions:

$$\begin{cases} \dfrac{\partial({W_{ex}}^{Tot} - {w_i}^{Tot})}{\partial n} = 0 \\ \dfrac{\partial({W_{ex}}^{Tot} - {w_i}^{Tot})}{\partial \delta} = 0 \end{cases} ==> \begin{cases} \left(\bar{b} + \dfrac{1}{n}\right) - \dfrac{\bar{P}}{4}(\bar{b} - \dfrac{\bar{n}}{3}) = 0 \\ -\dfrac{1}{\bar{n}^2} + \dfrac{\bar{P}}{12} = 0 \end{cases} \tag{77}$$

$$where\ \bar{b} = \frac{b}{S}\ ; \bar{n} = \frac{2n}{S}\ ; \bar{P} = \frac{P_u S^2}{\sigma_y t^2}$$

By solving equation system (77), the unknown parametrs n and P_U are found as follow:

$$\begin{cases} P_u = \dfrac{8}{\sqrt{3}} \dfrac{\sigma_y t^2}{S^2} \left(\dfrac{1}{\sqrt{3}\bar{b}} + \sqrt{\dfrac{1}{3\bar{b}^2} + 1} \right)^2 \\ \bar{n} = \sqrt{\dfrac{12}{\bar{P}}} \end{cases} \tag{78}$$

And by considering the fact that for an ice going vessel we have for the most of the cases that $\frac{1}{3\bar{b}^2} \ll 1$, the normalised collapse pressure from equation (78) is simplified to be:

$$\bar{P} = \frac{8}{\sqrt{3}} \left(\frac{1}{\sqrt{3}\bar{b}} + 1 \right)^2 \approx 4 \left(\frac{0.5S}{b} + 1 \right)^2 \tag{79}$$

The final IACS net thickness requirement for a transversaly stiffened plate field is derived from equation (79) as follow:

$$t_{net} = \frac{S}{2} \sqrt{\frac{P_u}{\sigma_y}} \cdot \frac{1}{\dfrac{0.5S}{b} + 1} \tag{80}$$

For a longitudinaly stifenned shell plate, the t_{net} requirement yields:

$$t_{net} = \frac{S}{2} OF \sqrt{\frac{P_u}{\sigma_y}} \cdot \frac{1}{\frac{0.5S}{l} + 1} \tag{81}$$

where OF is an orientation factor.

More thourough calculations for the IACS plate thickness requirement derivation are included in the background Notes to shell plating thickness, by Evgeny Appolonov Krylov [3].

6.3.3 Discussion of the adopted IACS collapse mechanism for plates.

6.3.3.1 Correlation between the ice patch breadth "b" and the adopted roof top collapse mechanism hinge lines

The assumption made by Evgeny Appolonov [3], stating that the line yield hinge in way of the unsupported patch edge coincides with the unsupported ice patch edges, is mainly made to simplify the process of calculating the net thickness requirement. A numerical solution of the energy equation, carried out by Evgeny Appolonov [3], considering the roof top mechanism and rejecting the above assumption, has proven that the line yield hinge tends to coincide with the ice patch edge as the ice patch height b increases. This tendency is seen clearly from results of the non-linear finite element analysis carried out by USFOS, fig.49. In this analysis, a plate filed with scantlings of 2400x800x12 and boundary conditions transversally fixed, horizontally free and rotationally clamped, has been subjected to several ice patch loads with increasing height “b”.

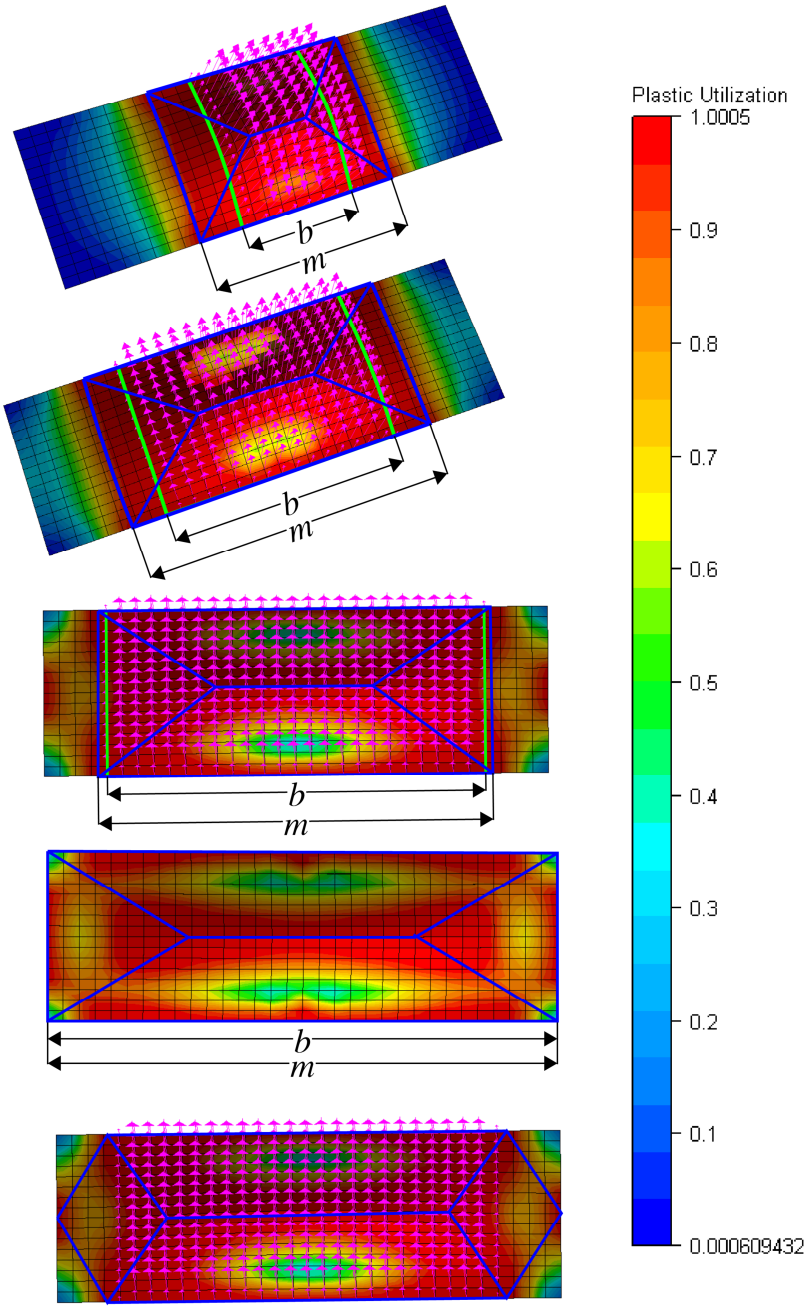

Figure 49: Plate collapse patterns and their consistency with the roof-top collapse mechanism.

Address:
NTNU
Department of Marine Technology
N-7491 Trondheim

Location
Marinteknisk Senter
O. Nielsens vei 10

Tel. +47 73 595501
Fax +47 73 595697

It is seen form figure 49 that the gap between the yield line in way of the unsupported ice patch edge is quite significant for smaller b. this means that the capacity of the plate using the roof-top collapse mechanism is deviating from the real plate capacity as the patch breadth gets smaller. The remaining question is whether the roof-top collapse mechanism gives a conservative result or not.

To answer the above question, the IACS plate field capacity is compared with a non-linear FE-analysis for a 2400x800x35 plate field, using the progressive collapse analysis software USFOS [11], and considering four ice patch heights, 600, 900, 1200, 1800 and 2400, fig. (50). The material is assumed to be rigid-perfectly plastic, with yield strength σ_y =400 MPa and boundary conditions are chosen to be transversally fixed, horizontally free and rotationally clamped.

The normalized pressure capacities in proportion to the corresponding IACS capacity are plotted in figure 50.

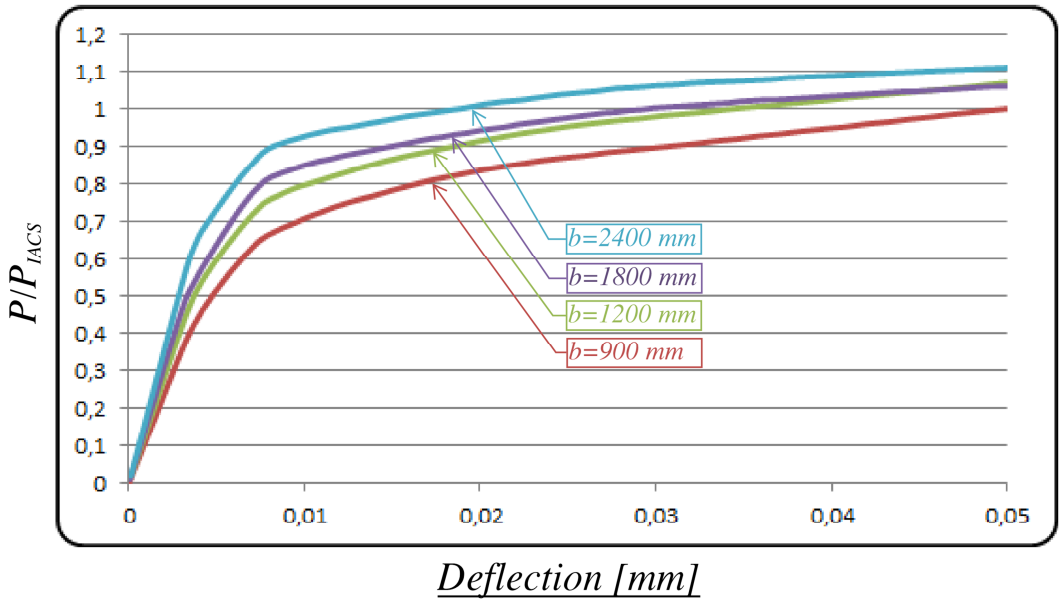

Figure 50: USFOS resistance predictions for a plate field with scantlings 2400x800x35 subjected to ice patches with increasing breadth b.

From figure 50 it is observed that the roof-top collapse mechanism adopted by IACS tends to overestimate the plate field capacity as the patch heights get smaller relative to the plate field height. This could be due to the fact that the collapse mechanism described by figure 46, assuming the existence of yield lines along the unsupported patch edges, does not represent the real plastic collapse mechanism of a plate field, especially for smaller patch heights relative to plate field height.

The IACS plate field capacity for the case of b=900 mm, is about 35% more than the USFOS pressure capacity , fig. 50, corresponding to a dearth of plate thickness requirement of about 19,7%.

The roof-top mechanism hinge lines orientation is depending on the ratio of the ice patch height "*b*" to the stiffener spacing "*s*", as b/s becomes smaller than 1 the yield line pattern rotate 90^{o} relative to the original orientation for b/s>1, fig.51.

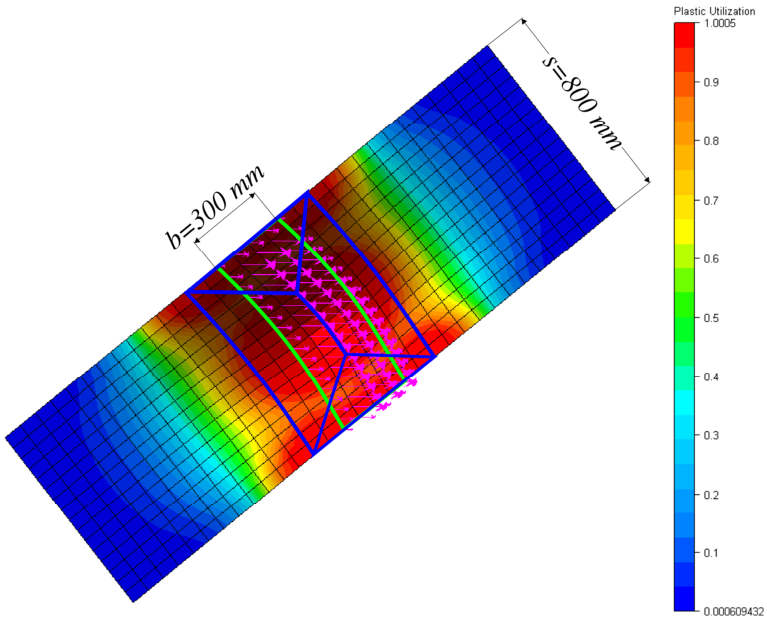

Figure 51: Plate collapse patterns and the corresponding roof-top collapse mechanism for a patch with b<0,5S.

In this case the roof-top collapse pressure capacity becomes:

$$P_u = \frac{4t^2}{S^2}\left(\frac{S}{b} + 0{,}5\right)^2 \tag{82}$$

Figure 52 represents the predicted USFOS capacity for the 2400x800x35 plate field with an ice patch height of $b = 300\ mm$, and a material with yield stress of 400MPa.

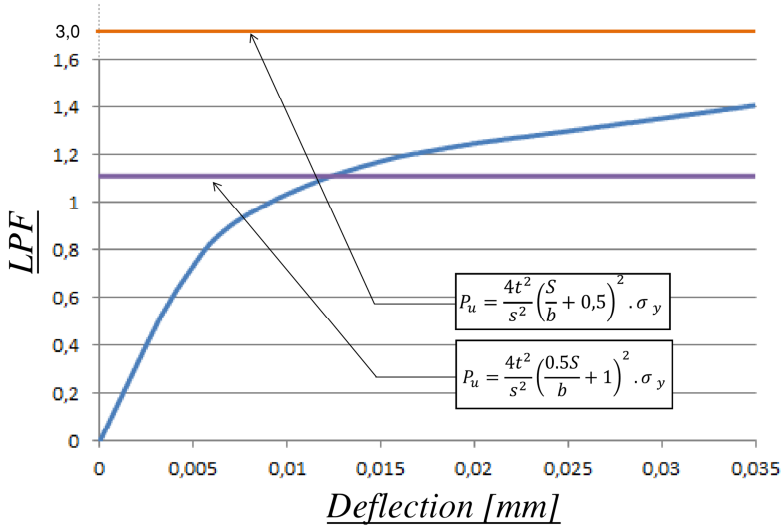

Figure 52: The roof-top capacity and USFOS resistance for a plate field with scantlings 2400x800x35 subjected to an ice patch with breadth b=300mm

From figure 52,it is seen that the roof top collapse mechanism for the case of $b \leq 0{,}5s$ considering equation (82) overestimates the capacity of the plate filed dramatically, this is due to the same assumption of the existence of yield lines along the patch unsupported edges. It is noticed from figure 51, for small b/S ratios, that the real collapse mechanism is more like a three hinge lines mechanism rather than the roof top collapse mechanism.

However, the pressure capacity, for the case of small s/b ratios, considering equation (80) seems to fit the IACS result pretty well. Nevertheless, it is not straightforward to conclude that equation (80) is to be used also in the case of $b \leq 0{,}5s$, this has to be investigated by running several

nonlinear analyses considering a range of plate field aspect ratios. Fortunately, for an ice going vessel, it is very frequent that $\frac{1}{3\bar{b}^2} \ll 1$.

For the special case where $b \leq s$, the net thickness requirement has to be specially considered, and the plate field capacity could be estimated using a non-linear FE tool such as USFOS.

6.3.3.2 The IACS plate capacity and plate file aspect ratio effect

Ref. Jørgen Amdahl [6], and from the collapse pressure expression, equation (80), we can see that the ultimate pressure capacity consists of the plate strip solution of a collapse load, $\frac{4\sigma_y t^2}{s^2}$, multiplied with the ice patch aspect ration factor $\left(\frac{0.5S}{b} + 1\right)^2$.

The plate thickness requirement for transversally stiffened plate, equation (80), does not depend on the **palte field aspect ratio**, but on the **patch aspect ratio only**, i.e. by applying a patch load of dimension bxS, the capacity of a plate field bxSxt and LxSxt, where L>S as illustrated by figure 53, will be the same.

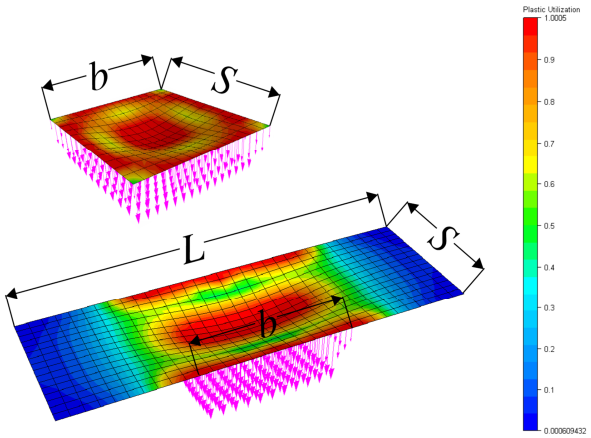

Figure 53: Patch loaded plate with b=l and b<<L

To investigate the effect of the case where the ice patch load has the same dimensions as plate field, fig. 53, a USFOS non-linear analysis is conducted for two plate fields with the same thickness t=35 and spacing S=800 but with different spans L=900 and L=2400 as shown by figure 53. The patch load applied on both plate fields is the same width b=900. The ,material slected is with yield stress 400 MPa. Boundary conditions for both plates are horizontally free, fixed transversally and rotationally.

It is found from figure 54 that the capacity of the 900x800x35 plate field is significantly heiger than the capacity of the 2400x800x35 plate filed, disporving what is anticipated by equation 80. It is also noticed that the capacity of the 900x800 plate field is quite closer to the IACS plate filed capacity, eq. 80.

One can say, based on figure 54 and equation (80) that the plate IACS capacity where b<L, assumes that the plate is supported fictitiously along the unsupported patch edges reguardless of the length of the plate, hence, introdusing a fictious line hinge along the unsupported patch edges. it is easily seen, from figure 54, that the effect of the plate field aspect ratio is quite significant, explaining once more the overestimated results of the IACS plate capacity shown by figure 50.

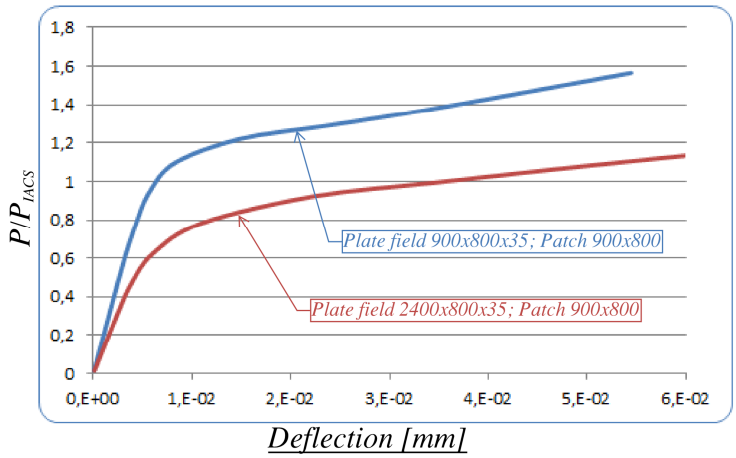

Figure 54: USFOS resistance prediction of a 900x800x35 and 2400x800x35 plate filed, applying a patch load with b=900 mm.

By extracting the normalized USFOS capacities from figure 50, for ice patch breadths 900 mm, 1200 mm, 1800 mm and 2400 mm, and plotting them versus the ratio of the patch breadths b to the plate length L, b/L, a linear relationship between $\frac{P_{USFOS}}{P_{IACS}}$ and $\frac{b}{L}$ can be approximated as shown by figure 55.

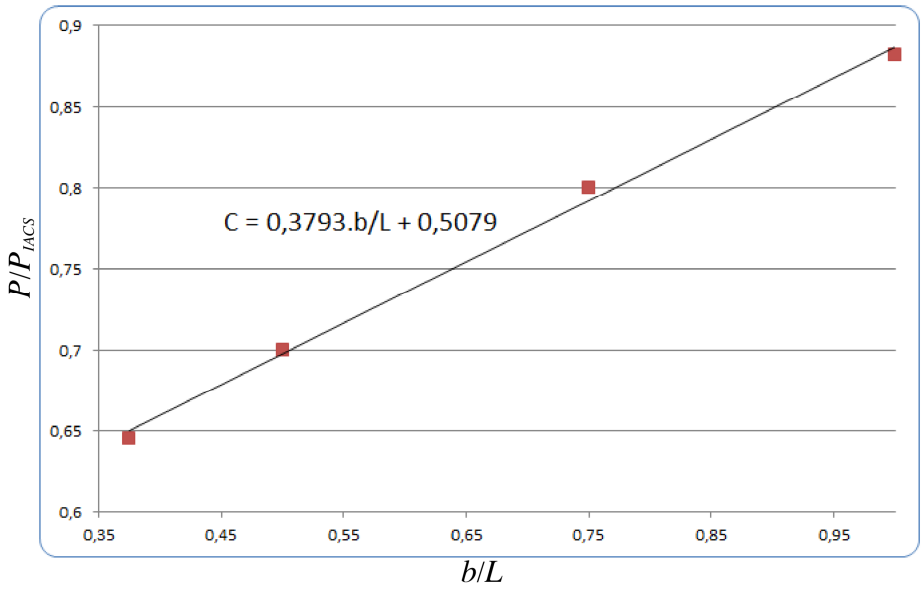

Figure 55: Plott of $\frac{P_{USFOS}}{P_{IACS}}$ versus $\frac{b}{L}$ for plate field with scantlings 2400x800x35 and boundary conditions transversally fixed, horizontally free and rotationally clamped.

The C factor, as expressed in figure 55, may be considered as a calibration factor to compensate for the IACS plate filed capacity overestimation, and equation (80) may be rewritten as follow:

$$t_{net} = \frac{S}{2}\sqrt{\frac{P_u}{C.\sigma_y}}.\frac{1}{\frac{0.5S}{b}+1} \tag{83}$$

Where:

$$C = 0{,}38\frac{b}{L} + 0{,}51$$

b = Ice patch breadth

L= plate field length

This way both the plate filed acpect ratio and the patch aspect ratio will have a countribution in defining the plate field pressure capacity.

6.3.3.3 IACS capacity versus Søreide plastic plate capacity

The simplified plastic collapse mechanism adopted by Søreide [1] is for a clamped plate, horizontally free and under uniformly distributed load. The corresponding plate capacity reads:

$$\overline{P}_S = \frac{P_{u,S} S^2}{\sigma_y t^2} = \frac{12\left(1+\frac{S}{L}\right)}{3-\frac{S}{L}} \tag{84}$$

Equation (84) is based on the assumption that the angel α described by figure 46 is 45^o regardless of the plate field and the patch aspect ratio considered. Søreide has investigated the influence of this assumption by comparing equation (84) with an exact upper bound Wood solution and lower bound equilibrium solution, ref. [1], without any significant discrepancies.

Equation (84) can be compared with the IACS plate capacity for longitudinally stiffened plates, if we neglect the orientation factor, i.e.:

$$\overline{P}_{IACS} = \frac{P_u S^2}{\sigma_y t^2} = 4\left(\frac{S}{2L}+1\right)^2 \tag{85}$$

The corresponding exact solution for a longitudinally stiffened plate according to equation (78) is:

$$\overline{P}_{u;exact} = \frac{8}{\sqrt{3}}\left(\frac{S}{\sqrt{3}L}+\sqrt{\frac{1}{3}\left(\frac{S}{L}\right)^2+1}\right)^2 \tag{86}$$

The aspect ration $\frac{S}{L}$ is for the most of the cases within the range $0{,}4 < AR_p < 1$, according to DNV rules for ships. It is seen from figure 56 that equation 85 and 86 represents respectively a lower bound and an upper bound solution for equation (84), and deviate strongly from the simplified Søreide solution as the plate field aspect ratio gets closer to 1, i.e. a square plate field.

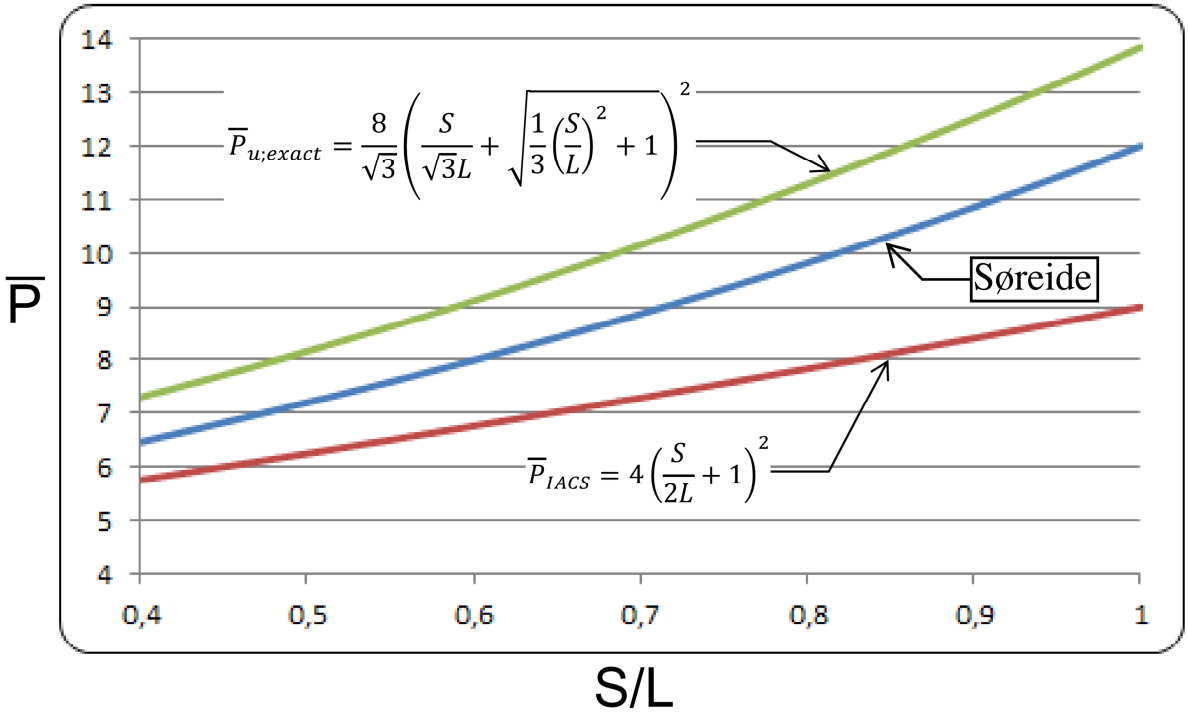

Figure 56: Plot of the normalized collapse capacity according to Søreide [1] and top roof collapse mechanism versus plate field aspect ratio.

6.3.3.4 Plate boundary conditions

According to Jørgen Amdahl [6], the boundary conditions for a plate element subjected to patch load depends on both the orientation of the patch relative to the plate field, and the topography of the structure, i.e. whether longitudinally or transversally stiffened plate as illustrated by figure 57.

For a transversally stiffened plate under patch load, the edges of the plate may be considered as transversally fixed, with edges forced to be straight. This is the case of relatively weaker stiffeners.

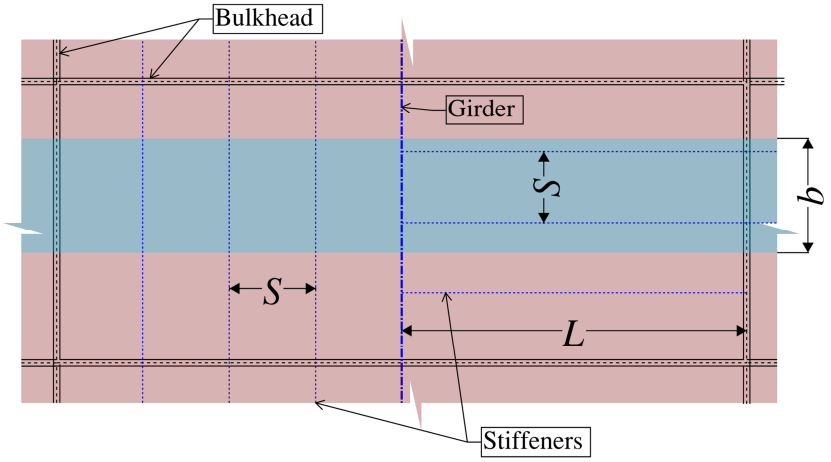

Figure 57: Various Boundary Conditions for Plate Elements within a stiffened panel. (Jørgen Amdahl, MTS-2009.05.18)

However, and because the ice patch is more or less continuous in the longitudinal direction, the part of the plate edge within the supported ice patch edge with breadth b will be restricted to rotate due to symmetrical load on both sides of the stiffener. The boundary conditions in this part of the plate field may be regarded as clamped. Fig.58

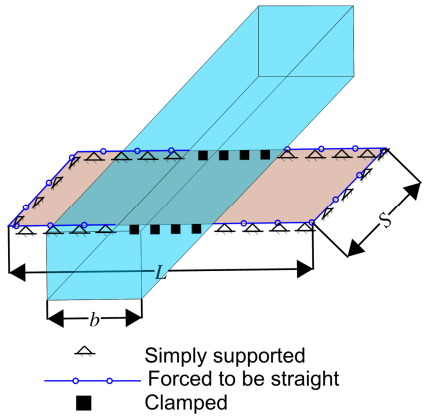

Figure 58: Boundary conditions of a transversally stiffened plate subjected to an ice patch

In the case of strong transverse stiffeners/girders the plate edges may be considered as restrained and totally clamped edges around the plate field could be the most appropriate boundary condition.

For longitudinally stiffened plates under patch load, we may consider the plate as constrained with horizontally free longitudinal edges but forced to be straight. The short edges may be seen as clamped due to the symmetric ice load on both sides of the girder/bulkhead, fig. 59.

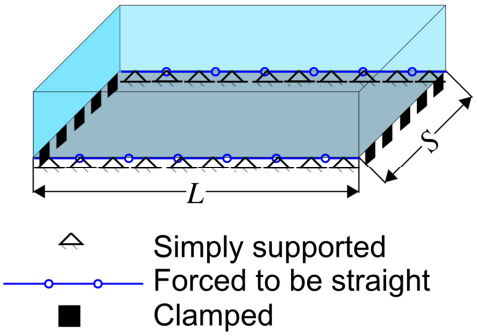

Figure 59: Boundary conditions of a longitudinally stiffened plate subjected to an ice patch

To investigate the case of transversally stiffened plate under patch load, a nonlinear USFOS analysis of a plate field subjected to an ice patch has been carried out with five different boundary

conditions. The plate field considered in this analysis is 2400x800x21. The ice patch breadth is b=900 mm and the material selected is with a yield stress of 400 MPa.

The different boundary conditions specified for this analysis are defined as follow:

BC1: Transversally fixed, horizontally and rotationally free, but rotationally clamped along the supported edges of the patch. Fig.58

BC2: Transversally fixed, horizontally and rotationally free with edges forced to be straight, but rotationally clamped along the supported edges of the patch, fig. 58

BC3: Transversally fixed, horizontally free and rotationally clamped.

BC4: Transversally fixed, horizontally free and rotationally clamped, with edges forced to be straight.

BC5: Totally clamped edges.

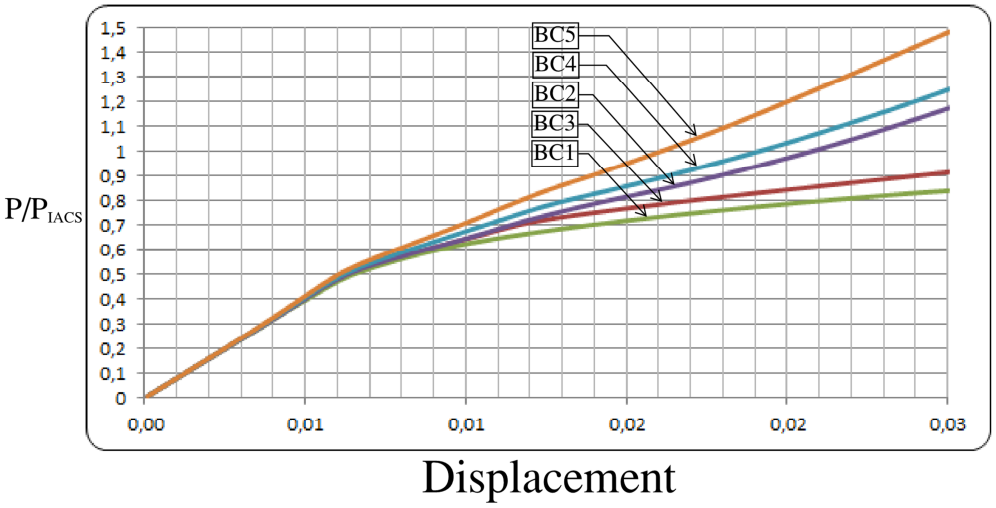

Figure 60: USFOS predictions of resistance for a 2400x800x21 plate field considering different boundary conditions.

It is seen from figure 60 that the capacity of the plate considering all the boundary conditions possible is below the capacity of the plate with totally clamped edges. It is also seen from the same figure that the closest plate capacity to the IACS capacity is the capacity for the case of totally clamped plate.

Provided that the stiffeners are capable of supporting the plate boundary, it is concluded that the totally clamped boundary condition may be regarded as the most realistic one.

Address:
NTNU
Department of Marine Technology
N-7491 Trondheim

Location
Marinteknisk Senter
O. Nielsens vei 10

Tel. +47 73 595501
Fax +47 73 595697

7. Longitudinal strength

7.1 Introduction

The collision scenario considered in the IACS polar rules for the longitudinal strength assessment with respect to ice load is a head-on ramming scenario, this scenario results in a vertical beaching force at the stem creating a global bending moment and a shear force along the hull girder.

As the vessel approaches level ice with a certain speed, the stem tends to penetrate the ice edge to a certain depth, at the same time the bow of the vessel rides on the ice to a certain height before the ice sheet failure, depending on the stem shape, ice strength and thickness, ships velocity and displacement.

The resulting bending moment distribution along the hull girder has a maximum shifted toward the bow compared to the wave bending moment. Moreover, the shear force due to ice vertical force is not anymore zero at the FP but 100% the design vertical ice force. Fig. (61).

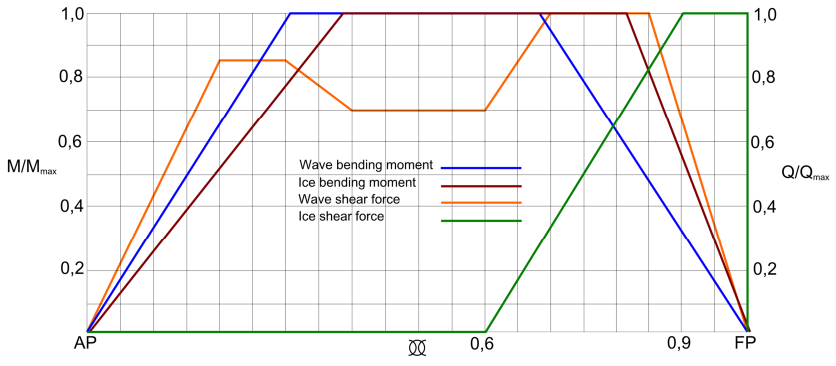

Figure 61: Shear and moment distribution due to waves and ice load according to DNV rules Pt.3 Ch.1 Sec.5 B200 and IACS polar rules for ships.

7.2 Vertical ice force as a result of the head-on ramming scenario

In order to derive an expression of the maximum head-on ramming force and the resulting hull girder bending moment, two complimentary methods were adopted by Claude Daley, Kaj Riska and Geoffery Smith [14], a numerical method denoted the Sii (Ship-ice-interaction)-2D method and an analytical method. These two methods are combined to create a user friendly algebraic expression of the design vertical ice force at the bow in terms of ships and ice parameters.

The Sii-2D method is a time step numerical integration approach used to simulate the ramming based on the mass/stiffness discretization model described by figure 62, It is proven by earlier work, reference [14], that this method can reproduce results very close to full-scale data.

The Sii-2D method consists of solving equilibrium equations in a stepwise manner involving the following forces:

- Bow heave stiffness, K_y, and the corresponding mass, M_y, and damping C_y.
- Surge mass, M_x and damping C_x.
- As the ice may break flexurally depending on the ice thickness, strength and bow shape, the model includes both the elastic and the crushing ice stiffness, respectively K_{el} and K_{cr}, together with the bow angles γ and α defined by figure 3.

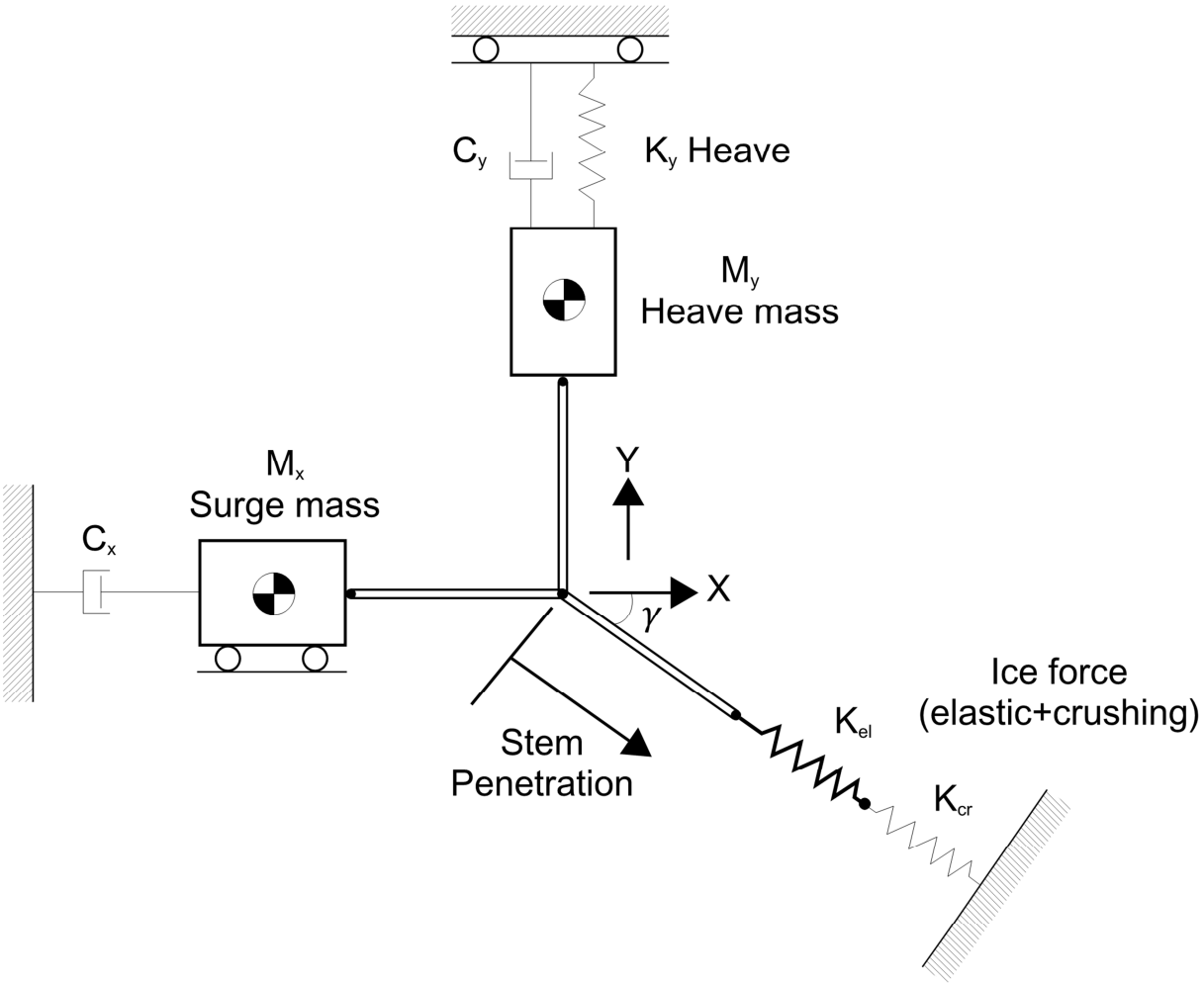

Figure 62: Idealization of ramming mechanics used in Sii_2D (Claude Daley, Kaj Riska and Geoffrey Smith [14])

The analytical method in the other hand, according to Daley, is based mainly on solving the energy equation, equation (87), to express the vertical penetration of the ice edge as a function of the vertical bow force.

$$KE = PE + IE \tag{87}$$

Where:

$KE =$ The kinetic energy

$PE =$ The potential energy

$IE =$ The ice indentation energy

This analytical approach allows for establishing a close form design equation valid for head-on rams in **very thick ice**, equation (88), where the variables are ship and ice parameters:

$$F_{IB} = C.\kappa^{a}.sin^{b}(\gamma).(D.K_h)^{0,5}.V \quad (88)$$

Where:

- γ is the stem angle, fig. 3.
- α is the waterline angle, fig. 3.
- κ is the normalized ice strength = $\frac{K_{Ice}}{K_h}$.
- K_h is the vertical stiffness at the bow = $\rho.g.A_{wp}$.
- $K_{Ice} = \frac{p_I\sqrt{2}\tan(\alpha)}{\sin(\gamma)\sqrt{\cos(\gamma)\sqrt{\tan^2(\alpha)+\sin^2(\gamma)}}}$ according to Claude Daley, Kaj Riska and Geoffery Smith [14].
- p_I is the ice pressure constant.
- V is the ship velocity.
- D is the ship displacement.
- A_{wp} is the waterplane area.
- a, b and C are constant to be determined.

Equation (88) is then harmonized by modifying the constants a, b and C in such a way to fit with the data extracted from the Sii-2D simulation, as shown by figure 63.

The final expression of the maximum vertical bow force is found by Claude Daley, Kaj Riska and Geoffery Smith as follow:

$$F_{IB} = 0{,}534.\kappa^{0{,}15}.sin^{0{,}2}(\gamma).(D.K_h)^{0{,}5}.p_I.V \quad (89)$$

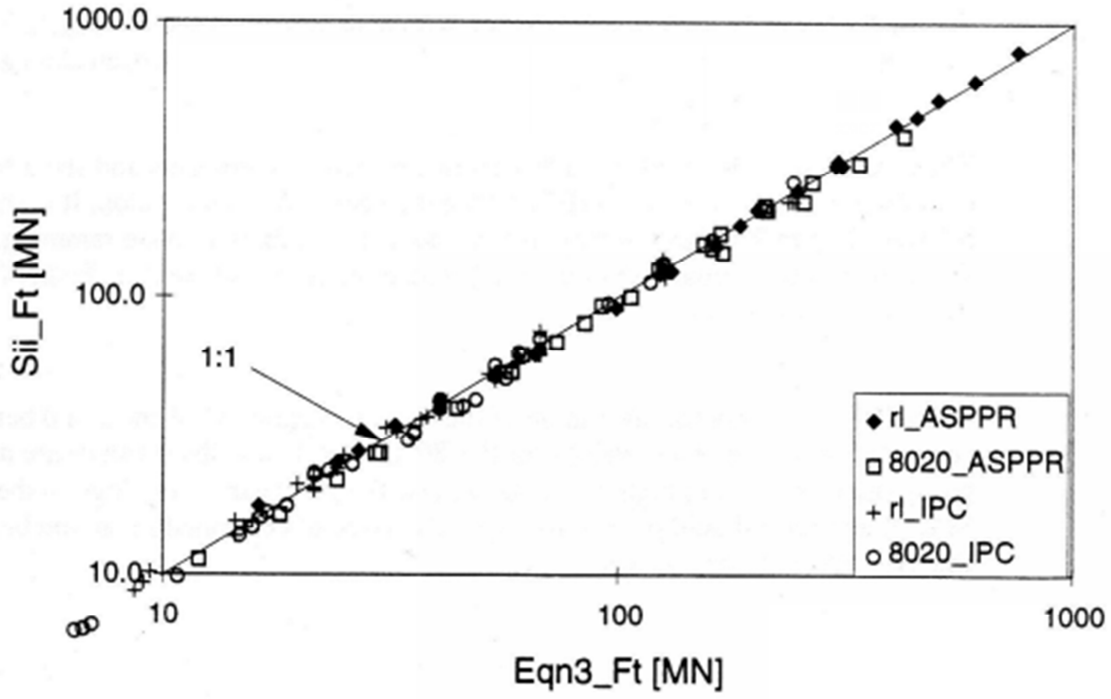

Figure 63: Comparison of equation (88) with the Sii-2D model results (log scale).

(Claude Daley, Kaj Riska and Geoffery Smith [14])

The essential assumption of very thick ice considered in the derivation of equation (89) is not always true, and the ice flow thickness may be small enough to allow a flexural failure of ice before any substantial ice crushing. Hence, the final vertical bow force to include this failure mode has to become as follow:

$$F_{IB} = min\begin{cases} 0{,}534.\kappa^{0{,}15}.sin^{0{,}2}(\gamma).(D.K_h)^{0{,}5}.p_I.V \\ 1{,}2.\sigma_f.{h_{ice}}^2 \end{cases} \quad (90)$$

Equation (90), is implemented in the UR rules in a simplified way, by introducing flexural and longitudinal Strength class factors accounting for all the class dependent parameters. The UR rule equation for vertical bow force is as follow:

$$F_{IB} = min\begin{cases} 0{,}534.{K_I}^{0{,}15}.sin^{0{,}2}(\gamma).(D.K_h)^{0{,}5}.CF_L \\ 1{,}2.CF_F \end{cases} \quad (91)$$

Where:

- $CF_L = {p_I}^{0{,}15}.V$, longitudinal Strength class factors.
- CF_F flexural class factors as defined by table (2).
- $K_I = \frac{K_f}{K_h}$ explained by the following:

According to Daley, reference [14], K_f is the stem indentation parameter in the ice, depending both on stem form and ice strength. In other words, the vertical force is a function of the ice pressure constant p_I and the area A_v, which is the vertical projection of the contact area between the stem and the ice edge, fig.64. The vertical force is then obtained as:

$$F_{IB} = p_I.{A_v}^{1+ex} \quad (92)$$

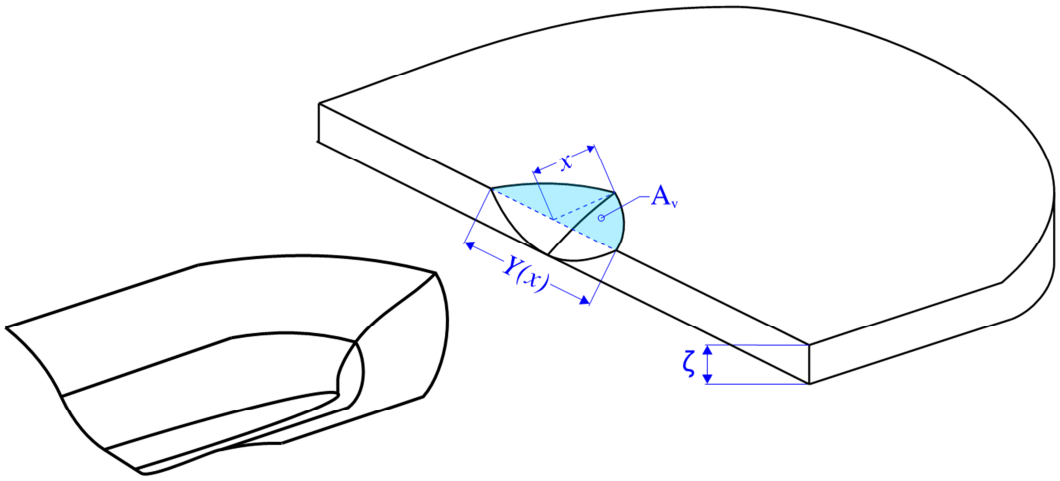

Figure 64: Head on ramming scenario with an infinite ice floe and the geometry of the resulting Ice edge indentation.

The bow shape dependent vertical area, A_v ,is obtained by introducing functions describing the water line shape at the bow area, as illustrated by figure 65 and 66.

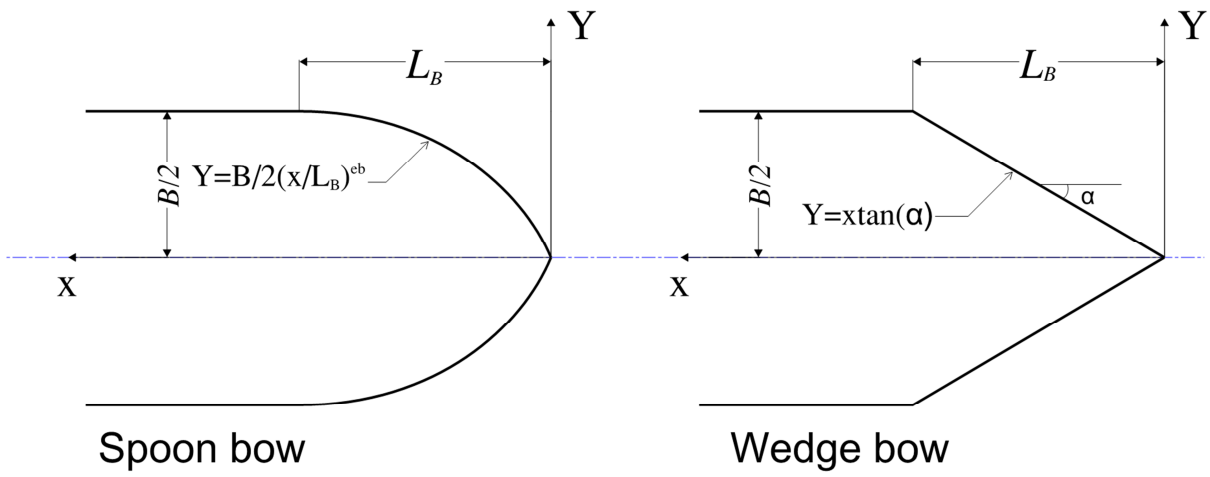

Figure 65: Bow shape definition (IACS Requirements for Polar Class, 2011)

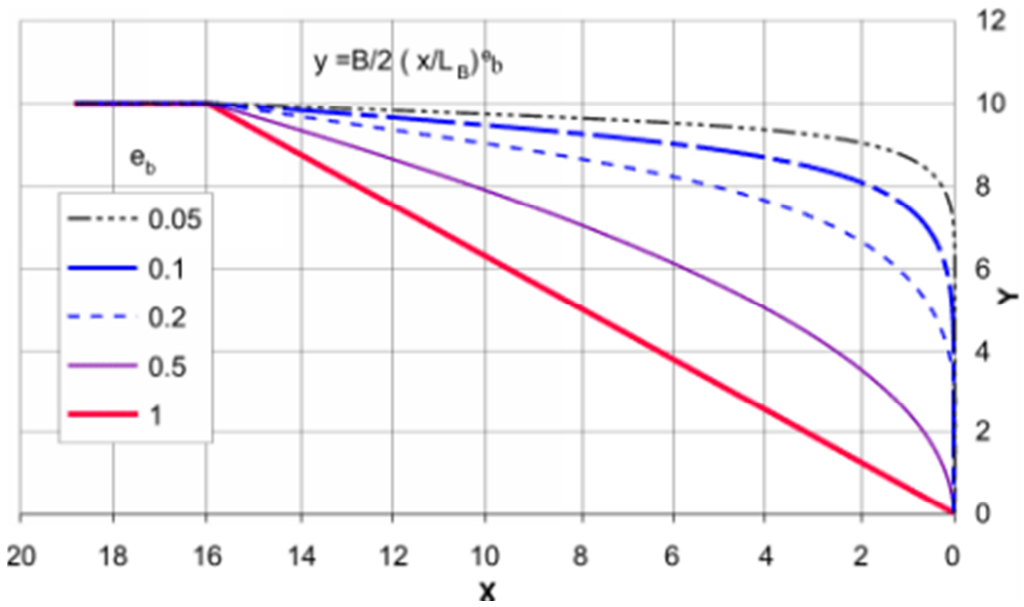

Figure 66: Illustration of e_b Effect on the Bow Shape for B = 20 and LB =16

(IACS Requirements for Polar Class, 2011)

- For a blunt bow, according to figure 65 and 66:

$$y(x) = \frac{B}{2}.\left(\frac{x}{L_B}\right)^{e_b} = C.B^{1-e_b}.x^{e_b} \quad (93)$$

Where:

$$C = \frac{1}{2\left(\frac{L_B}{B}\right)^{e_b}}$$

e_b is a bow shape exponent describing the water plane form as shown by figure 66.

Considering equation (93), the vertical area A_v is obtained as follow:

$$A_v = 2\int_0^x y(x)dx = \frac{2C}{1+e_b} B^{1-e_b}.x^{1+e_b} \quad (94)$$

- For a wedge bow form, according to figure 65, the vertical area becomes simply:

$$A_v = \tan(\alpha).x^2 \quad (95)$$

Apparently the above two A_v expressions, (94) and (95) together with the exponent ex included in equation 92, seems to be the radical behind the expression of K_f included in the UR rules and expressed as follow:

a) For the case of a blunt bow form

$$K_f = \left(\frac{2 \cdot C \cdot B^{1-e_b}}{1+e_b}\right)^{0.9} \cdot tan(\gamma_{stem})^{-0.9(1+e_b)} \quad (96)$$

b) For the case of wedge bow form ($\alpha_{stem} < 80^o$), $e_b = 1$, K_f is simplified to become:

$$K_f = \left(\frac{tan(\alpha_{stem})}{tan^2(\gamma_{stem})}\right)^{0.9} \quad (97)$$

In figure 67, the maximum sagging wave bending moment according to DNV rules Pt.3 Ch.1 Sec.5 B201 and the IACS maximum design vertical ice bending moment are plotted versus ships length for 6 different vessels

The ship lengths together with all the corresponding hull parameters for the calculation of the sagging bending moments are summarized by table 5.

Table 5: Hull parameters necessary for the calculation of sagging bending moments

Vessels	L	B	D	C_B	C_{WP}	γ	α	Δ [ton]	A_{wp} [m^2]
V1	100	14,3	5,4	0,72	0,8	30	30	5699	1144
V2	150	21,4	8,2	0,72	0,8	30	30	19425	2568
V3	210	30	11,3	0,72	0,8	30	30	52538	5040
V4	242	34,6	13	0,72	0,8	30	30	80332	6699
V5	270	38,6	14,5	0,72	0,8	30	30	111526	8338
V6	333	47,6	17,9	0,72	0,8	30	30	209392	12681

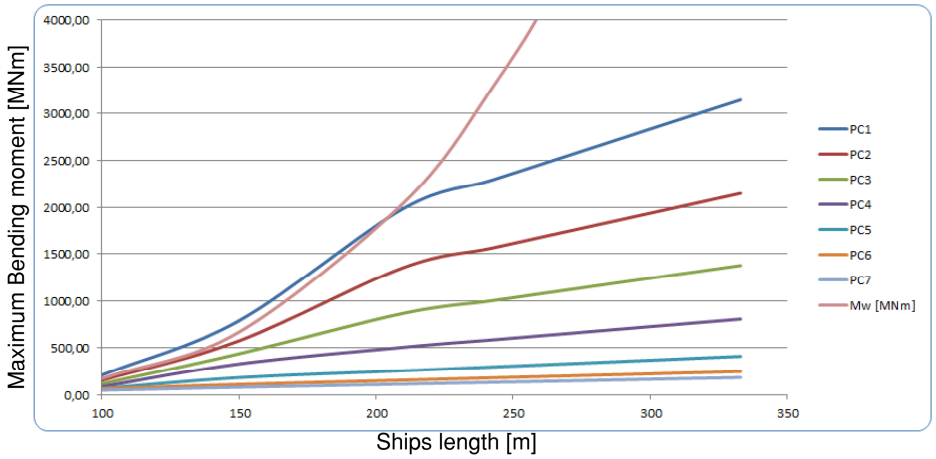

Figure 67: Plot of the maximum ice bending moment according to IACS Req. 2006/Rev.2, 2010, I2.13.4.1, equation 13, and the maximum wave bending moment in sagging according to DNV rules Pt.3 Ch.1 Sec.5 B 201, versus the lengths of the vessels listed in table 4.

As it is seen from figure 67, the ice bending moment is not an issue for vessels with length above 200 m regardless of the PC class assigned. For ships with Length 200 m and below, the ice bending moment may be the governing factor with respect to global strength, especially for the case of very high PC classes.

In the other hand, the ice shear force is to be taken in consideration in the forward part of the vessel, i.e. from the stem and to a position about 0.8 L from AP, regardless of the vessel size and the PC class assigned.

Address:
NTNU
Department of Marine Technology
N-7491 Trondheim

Location
Marinteknisk Senter
O. Nielsens vei 10

Tel. +47 73 595501
Fax +47 73 595697

8. Steel weight increase due to class increase

8.1 Introduction

Steel weight increase due to class increase could be an important issue for designers to deal with especially in a predesign phase of the vessel, as it may influence the vessel speed and the transported payload weight of the vessel. Hence, investigating the implication of choosing a class notation PC_{i-1} rather than PC_i in terms of steel weight may be crucial for the whole design.

To have a realistic feeling of class increase impact in terms of steel weight, let's consider a ship in a predesign phase with the following preliminary specifications, taken from the existing design ***S. A. AGULHAS II***, *POLAR SUPPLY AND RESEARCH VESSEL*:

- Class notation: **1A1 PC-5 WINTERIZED BASIC Passenger Ship LFL* COMF-V(2)C(2) HELDK-SHF DEICE RP E0 DYNPOS-AUT NAUT-AW CLEAN DESIGN DAT(-35 °C) BIS TMON**
- DWT: 4,780 tons
- Overall length of 134.2 m
- Beam B=22 m
- Depth D=10.55 metres
- Displacement $\Delta = 14.2\ Kt$.
- Transversally stiffening.
- Frame spacing S=400 mm.
- Values of the normal frame angle at upper ice waterline, β', and the upper ice waterline angle α, as shown in figure 3, are specified in table 6.

Address:
NTNU
Department of Marine Technology
N-7491 Trondheim

Location
Marinteknisk Senter
O. Nielsens vei 10

Tel. +47 73 595501
Fax +47 73 595697

In this report, only the plate and framing requirement are considered for the weight increase estimation due to class increase.

The frame span in the bow region is set to be 2400 mm and in the non-bow region as 1200mm, this choice is made mainly to include the effect of the curvature of the hull in the bow, as the frame span is larger than the vertical distance between decks or stringers.

To simplify the calculations, it is also assumed that the ship is transversally stiffened with frame spacing of 400 mm all over the ice reinforced area; this assumption is not conservative since the frame spacing in the bow and the stern regions tends to be larger due to the curvature of the hull. In addition, assumptions about the material propriety and measurement of the hull shape parameter are summarized in table 6.

Table 6: Hull parameters necessary for the calculation plate and framing requirement

Displacement Δ [kt]	14,2
Yield stress σ_f [MPa]	500
Frame span a[m]	2,4
Transverse frame spacing s[m]	0,4
Ship length, measured on the upper ice waterline L[m]	122
Distance from the forward perpendicular (FP) to station under consideration in the bow region x [m], see fig.8	5,5
Waterline angle α [°], see fig.3	31
Normal frame angle β' [°], see fig.3	49,4
Calculated shape coefficient fa_i [-], see fig.8	0,39
Calculated ice normal force F_i [MN], see fig.8	38,05
Line load Q_i [MN/m]	10,08
Pressure P_i [MPa]	15,14

8.2 Steel weight increase due to plate thickness requirement

The Weight increase due to plate thickness requirement as we increase the class has been calculated by estimating the areal of each hull area using the shell expansion drawing for the above selected vessel. Fig.68

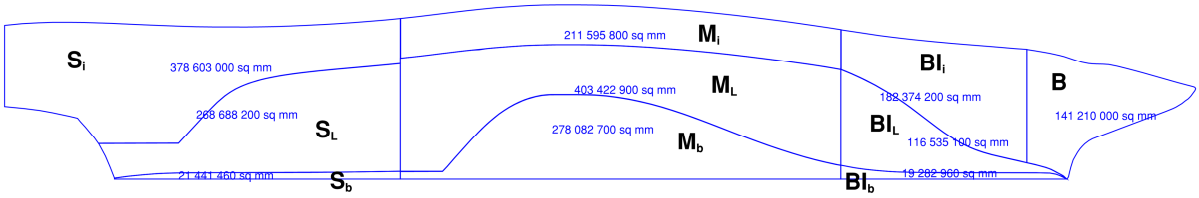

Figure 68: Areal of the ice areas mesured directly from shell expansion drawing of the *S. A. AGULHAS II, POLAR SUPPLY AND RESEARCH VESSEL*

The weight of the total required shell plate within the ice reinforced area, corresponding to each polar class, is summarized in table 7.

From table 7, it is noted that for a transversally stiffened shell, the weight can roughly jump from 217 tons to 763 tons by going from PC7 to PC1, given that the selected material is extra high strength steel with yield stress of 500MPa.

If instead the material selected for a transversally stiffened shell is a high strength structural steel with yield point of 355 MPa, denoted NV-36, the weight can roughly jump from 257 tons to 906 tons by going from PC7 to PC1. About 19% steel weight increase if we keep the class unchanged and go from NVA-500 to NV-36.

Table 7: Calculation results of steel weight increase due to plate requirement by going from PC7 to PC1.

		Weight increase due to thickness requirement													
		Transverse stiffeneing							Long. Stiffeneing						
	Areal [mm^2]	PC1	PC2	PC3	PC4	PC5	PC6	PC7	PC1	PC2	PC3	PC4	PC5	PC6	PC7
B	141209800	70	56	47	41	35	30	28	93	76	65	57	50	43	39
Bi_i	182374100	86	67	56	47	41	39	36	114	91	77	65	58	55	51
BI_L	116535300	48	37	31	26	22	18	16	64	51	43	36	31	25	23
Bi_b	19281040	7	5	4	4	3	2	2	9	7	6	5	4	3	3
M_i	211595700	86	66	51	45	37	30	27	108	85	67	58	49	40	37
M_L	403 422 900	138	105	83	68	55	43	39	174	135	109	89	73	56	52
M_b	278082800	74	59	45	0	0	0	0	93	76	59	0	0	0	0
S_i	378602900	159	123	100	83	66	51	43	200	158	130	109	88	67	58
S_L	268687800	87	66	52	42	33	28	26	110	85	68	55	44	37	35
S_b	22916040	7	5	4	3	2	0	0	8	6	5	4	3	0	0
Sum [ton]		763	591	473	358	295	241	217	976	771	629	478	400	325	297

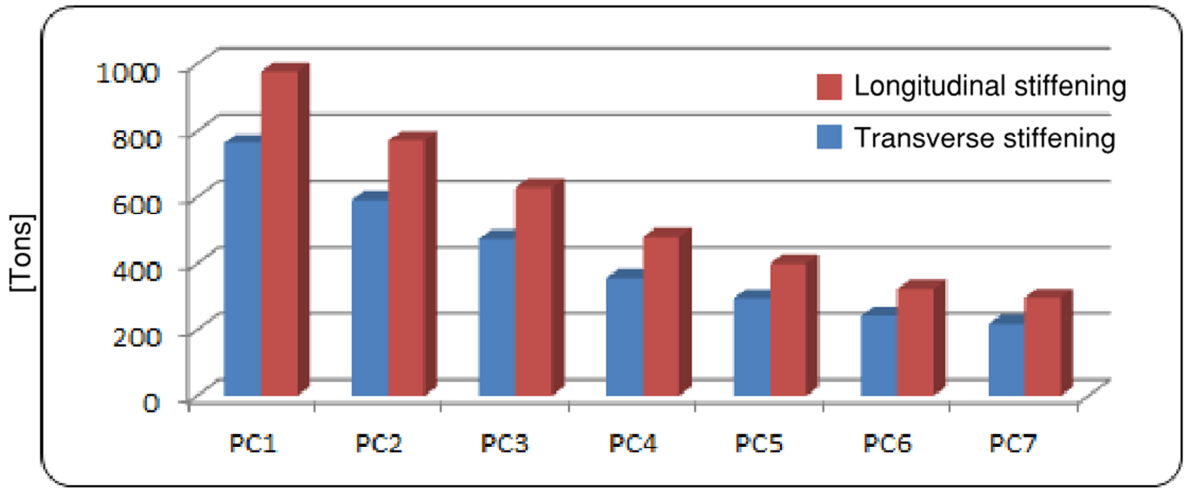

Figure 69: Steel weight from plating polar class requirement within the ice reinforced area for a longitudinally and a transversally stiffened shell, considering the hull form of the *S. A. AGULHAS II, POLAR SUPPLY AND RESEARCH VESSEL*

It is also noted from figure 69 that steel weight from shell plate requirement within the ice reinforced area for a longitudinally stiffened hull is significantly higher than the case of transversally stiffened hull, about 33% higher regardless of the assigned polar class, this makes

the weight increase concern due to class increase even worse for larger vessels where longitudinal strength is a major consideration and longitudinal stiffening is quite common.

8.3 Steel weight increase due to framing requirement

For transverse stiffeners, the calculation of the required plastic section modulus is not straight forward, as a set of frame parameters has to be predetermined. One must first determine almost the complete frame geometry to calculate the following:

- Shear area ration of minimum to actual shear area, $\frac{A_0}{A_w}$

  Where: $A_0 = \frac{PbS\sqrt{3}}{2\sigma_y}$ and A_w= net web cross-sectional area
- The ratio of flange and plate plastic section modulus to the cross section plastic modulus, $k_z = \frac{z_p}{Z_p}$

This makes the calculation of framing contribution to weight increase when increasing the class quite complicated and the resulting steel weight increase due to framing requirement as we increase the class are presented in table 8.

The calculations in table 8 are carried out considering the following:

- $A_w \geq A_0$
- The cross section plastic modulus considered is exactly the required one, $Z_p = Z_{p\,req.}$ considering both the centrally and the off-center (asymmetrical) patch loaded frame.
- Framing – Structural stability

The number of stiffeners, n, included in table 7 is estimated by the following:

$$n_{Stiffener} = \frac{the\ areal\ of\ the\ ice\ reiforced\ area}{s.l}$$

Where S is the stiffener spacing and l is the span.

Table 8: Calculation results of steel weight increase due to framing requirement by going from PC7 to PC1.

		B	Bi_i	BI_L	Bi_b	M_i	M_L	M_b	S_i	S_L	S_b	Sum [ton]
Weight increase due to transverse framing requirement [ton]	Areal [mm^2]	1,41E+08	1,82E+08	1,17E+08	1,93E+07	2,12E+08	4,03E+08	2,78E+08	3,79E+08	2,69E+08	2,29E+07	
	n stiffeners	147	190	243	40	441	840	579	789	560	48	
	PC1	40	41	16	2	30	44	20	56	28	2	556
	PC2	27	27	11	1	20	28	15	37	18	1	371
	PC3	20	20	8	1	14	21	11	28	13	1	275
	PC4	17	17	7	1	11	16	0	21	10	1	199
	PC5	14	15	5	1	9	12	0	16	7	0	157
	PC6	12	14	4	0	7	8	0	10	5	0	121
	PC7	11	13	4	0	6	7	0	8	5	0	107

From table 8 it is seen that the weight steel of the required framing cross section within the ice reinforced area is jumping from 107 tons to 556 tons by increasing the class from PC7 to PC1, given that the selected material is extra high strength steel with yield stress of 500MPa.

8.4 Total steel weight increase by going from PC7 to PC1

Considering the above selected ship and the material proprieties specified in table 6, a total steel weight increase by going from PC7 to PC1, considering both plate and framing requirement, is found to be roughly about 1000 tons, fig. 70. If we consider the depth increase due to this weight increase, the stringers and web-frames requirements, we can state with good confidence that the total steel weight will increase more than the result anticipated by table 7 and 8.

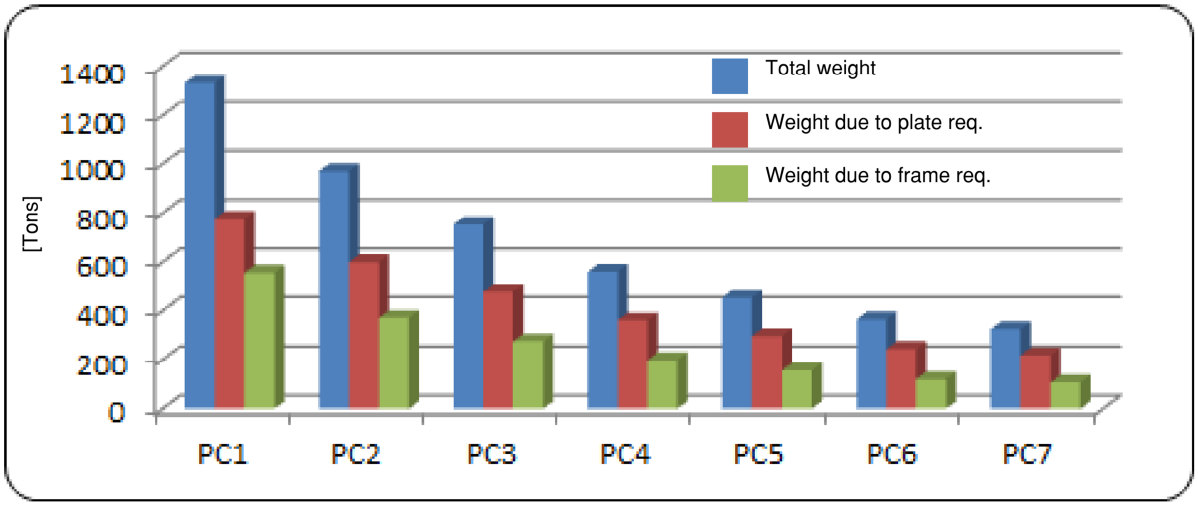

Figure 70: Total Steel weight from polar class requirement of shell plating and framing within the ice reinforced area for a transversally stiffened shell with frame spacing of S=400 mm, considering the hull form of the *S. A. AGULHAS II, POLAR SUPPLY AND RESEARCH VESSEL*

This increase in steel weight is approximately equivalent to 7 fully filled water ballast tanks of size 10m x10m x1,5 m and about 21% the deadweight of the ship. The corresponding estimated value in case of lower material strength such as NV-36 is more than 25 % the deadweight , which is a quite significant steel weight increase.

The total percentage steel weight increase by going stepwise from PC7 to PC1, regardless of the material selected for the plate, is as presented by figure 71.

In many cases the designer has to decrease load elsewhere in the vessel to compensate for the loss of the operability and/or the profitability of the vessel due to this effect.

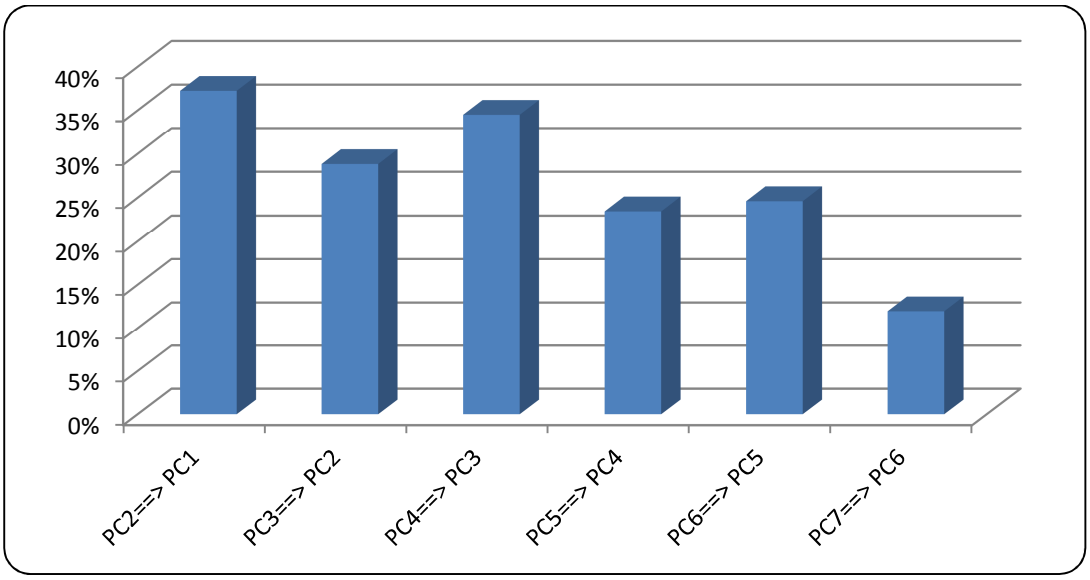

Figure 71: Total steel weight increase by going stepwise from PC7 to PC1

9. Validity of the IACS unified Rules for design of a moored Arctic FPSO/driller.

For hips intended for navigation in ice-infested polar waters, the task has been to determine the scantlings such that the structure can resist the maximum pressures and forces as the ship is crushing and/or bending the ice. However, for a moored FPSO/Driller the task is to determine the structure resistance to the ice maximum pressures and forces as drifting ice is crushing and/or bending itself to the structure.

In the case of a ship shaped FPSO, it is convenient to distinguish between the situation where the vessel is moored and under transit. For the case of a moored FPSO, the vessel velocity as a class dependent factor is irrelevant. The factors that are predetermined as a result of the assigned polar class are ice thickness, strength and ice drifting velocity, which can be determined from the environmental data available for the area considered.

The only remaining factor designers have the possibility to play with to reduce or optimize the ice/hull interactions is the hull shape and the arrangement of the mooring system.

As the ice drift direction is always changing due to wind and current, the design of a suitable mooring system is crucial for an arctic ship shaped FPSO. The mooring system has to be arranged to avoid direct impact of ice with the mooring lines, and to ensure the best ice vaning position, which is the ability of the vessel together with the mooring system to secure heading towards the ice drift direction, this way the FPSO capability of breaking ice will be greatly improved.

Address:
NTNU
Department of Marine Technology
N-7491 Trondheim

Location
Marinteknisk Senter
O. Nielsens vei 10

Tel. +47 73 595501
Fax +47 73 595697

In a transit situation the FPSO should be considered as a normal ice going vessel to a certain extent and should be reinforced accordingly, i.e according to the IACS Polar Class for ships.

However, in a moored situation, the applicability of the IACS PC rules to an arctic FPSO is not straight forward, as it is not simple to determine the contact area, $A = \frac{WH}{2}$, equation (5), of the wedge base, fig. (2), which is a result of balancing the kinetic energy with the ice crushing energy. The mass involved in the kinetic energy is not any more the ships displacement, but the drifting ice sheet mass.

In the case of a moored FPSO, the hull structure should be able to withstand the ice line loads acting simultaneously in the horizontal plane at the water level on both sides of the hull.

As mentioned earlier, the design normal ice force is the minimum between the crushing and the flexural force, equation (16), reproduced here as equation (98):

$$fa = min\begin{cases} \dfrac{1.2CF_F}{sin(\beta')CF_c.M_{ship}^{0.64}} \\ \dfrac{\left(0.097 - 0{,}68\left(\frac{x}{L} - 0.15\right)^2\right)\alpha}{\sqrt{\beta'}} \\ 0.6 \end{cases} \tag{98}$$

It is seen from equation (98) that if it is possible to keep the flexural force lower than the crushing one for a predetermined class dependent ice thickness, i.e. providing for a hull structure with relatively large β', the IACS rules becomes directly applicable to a moored polar FPSO, and the normal ice force becomes totally flexural as follow:

$$Fn = \frac{1.2\sigma_f {h_{ice}}^2}{sin(\beta')} \tag{99}$$

The flexural part of the normal ice load is already accounted for in the bow area when considering a FPSO in transit, eq. (98). In a moored situation, the normal ice load, eq. (99), is to be fully accounted for in the stern and the mid-ship area, i.e. without considering the hull area

factor AF. This load might have a higher value than the Non-Bow normal ice force, eq. (26), considered in the transit case.

From equation (30) and (99), the corresponding line load within a Non-Bow area becomes:

$$Q_{NonBow} = \frac{714.{\sigma_f}^{0,61}.CF_D}{sin(\beta')^{0,61}}.{h_{ice}}^{1,22}\left[\frac{KN}{m}\right] \qquad (100)$$

The remaining question is to which extent the angle of outboard flare at the water level, β', can be increased to ensure a totally flexural ice failure within the midship area.

For a conventional hull shape, i.e. a ship shaped FPSO, the angle β' in the mid-ship area at the upper ice waterline is normally very small, i.e. almost vertical ship side. However, in the stern area where β' is large, the line load in equation (100) may be more relevant, depending on the operational mode intended for the vessel. For a double-acting concept, the line load, eq. (100), is not the governing load in the stern area; in this case the stern will be regarded as a bow.

The challenge of ice line load when a vessel is trapped between moving ice floes, is already dealt with in DNV Rules for ARCTIC VESSELS AND ICE BREAKING SERVICE, Pt.5 Ch.1 Sec.4 D300. The ice floes are mainly driven by wind and tides (often many miles distant), resulting to a huge load that may put the whole hull integrity in jeopardy. The vessels shall withstand line loads acting simultaneously in the horizontal plane at the water level on both sides amidships.

Given that the outboard flare angle, β_f, is not to be taken less than 10^o, the horizontal component of the ice pressure, q, is then limited by the presence of the vertical component, resulting in the flexural failure of ice. The value of bending moment induced by this vertical component of the ice pressure is obtained as follow:

$$q.\sin(\beta_f).a = \frac{\sigma_{ice}{h_{ice}}^2}{6} \qquad (101)$$

Address:
NTNU
Department of Marine Technology
N-7491 Trondheim

Location
Marinteknisk Senter
O. Nielsens vei 10

Tel. +47 73 595501
Fax +47 73 595697

Where a is the arm where the ice sheet is expected to crack due to bending, which is estimated to be as follow, according to background for "*DNV HULL STRUCTUREAL RULES"* by Christian Mürer (1995):

$$a = \frac{\sigma_{ice}\sqrt{h_{ice}}}{1000} \tag{102}$$

Combining (101) and (102), the design line loads is then obtained as:

$$q = \frac{165}{\sin(\beta_f)}(h_{ice})^{1.5} \left[\frac{\text{KN}}{\text{m}}\right] \tag{103}$$

$$= 950.(h_{ice})^{1.5} \left[\frac{\text{KN}}{\text{m}}\right] \text{ for vertical side shells } (\beta_f < 10^o)$$

Where:

h_{ice} = average ice thickness

β_f = angle of outboard flare at the waterlevel. The outboard flare angle shall not be taken less than 10^o.

To investigate the relevancy of line loads stated by, eq. (30), (100) and (103), two different hull shapes are considered:'

- A ship shaped FPSO with the same hull form as the S. A. AGULHAS II, POLAR SUPPLY AND RESEARCH VESSEL, where the ship side is almost vertical.
- A non-conventional hull shape, the conical drilling unit KULLUK, the first floating drilling vessel designed and constructed for extended season drilling operations in deep arctic waters, where $\beta' \approx 45^o$. Fig. (72).

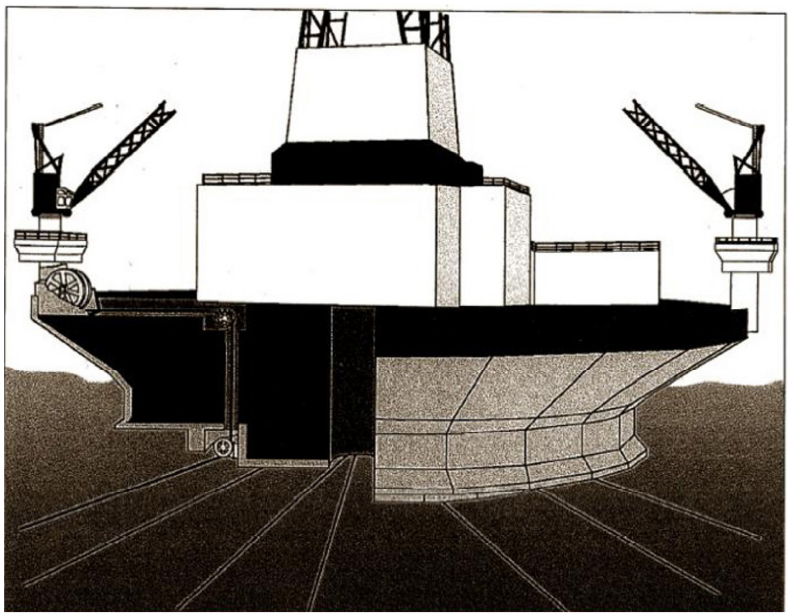

Figure 72: Schematic illustration of the KULLUK (Marine Exchange of Alaska, http://www.mxak.org)

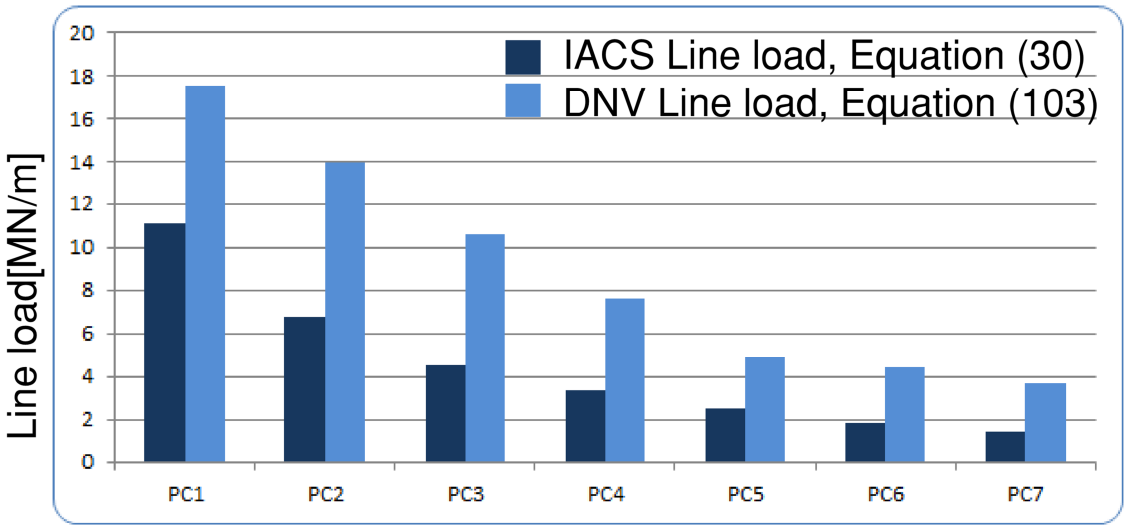

Figure 73: Comparison of ICAS line load, eq. (30) and DNV line load, Pt.5 Ch.1 Sec.4 D300 for the S. A. AGULHAS II, POLAR SUPPLY AND RESEARCH VESSEL where ship side is almost vertical, i.e. $\beta' = 0^o$

Address:
NTNU
Department of Marine Technology
N-7491 Trondheim

Location
Marinteknisk Senter
O. Nielsens vei 10

Tel. +47 73 595501
Fax +47 73 595697

From figure 73, it is seen that the IACS line load, eq.(30), **where the AF factor, hull area factor, is not considered**, is significantly lower than the DNV line load stated by equations (103). The line load, eq.(100), is not considered in this equation as it is not relevant, i.e. $\beta' = 0^o$.

The governing ice line load in the midship area in the case of a ship shaped FPSO may be the DNV line load, eq.(103). However, in the stern area the case may be different as $\beta' \neq 0^o$, and line load, eq.(100) may have to be considered.

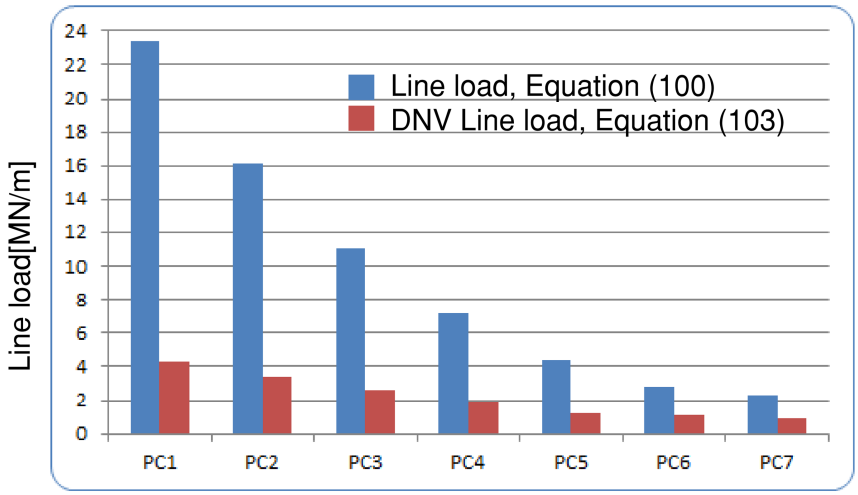

Figure 74: ICAS line load, eq. (100) versus DNV line load, Pt.5 Ch.1 Sec.4 D300, considering a non-conventional hull shape with an outboard flare at the water level of 45°.

From figure 74 we can see that for the case of a non-conventional FPSO, **where β' is large enough to ensure a flexural ice failure**, the governing load in the non-bow region is the line load stated by equation (100) where the AF factor is not considered.

From both cases, figure (73) and (74), it is noticed that the governing load can be either the DNV line load, eq. (103) or the line load stated by equation (100), depending on the angle of outboard flare at the water level, β'. A general expression of line load to be applied in the now-bow region for a ship shaped or a non-conventional hull shape polar FPSO may be expressed as follow:

$$Q_{NonBow} = \begin{cases} max \begin{cases} \dfrac{714.\sigma_f{}^{0,61}.CF_D}{sin(\beta')^{0,61}}.(h_{ice})^{1,22} \\ \dfrac{165}{\sin(\beta_f)}(h_{ice})^{1.5} \end{cases} & \left[\dfrac{KN}{m}\right] \\ 950.(h_{ice})^{1.5} \ \left[\dfrac{\mathrm{KN}}{\mathrm{m}}\right] \text{ for vertical side shells } (\beta_f < 10^o) \end{cases} \quad (104)$$

Given that the worst case line load scenario is considered as discussed above, the remaining challenge is the strength of the mooring system and its connection to the hull. The whole concept should be developed to avoid that the mooring lines bears the brunt of the total ice load. According to Satish Prabhakar, Alec van Nes and Rafael Corona (Ice Engineering, 2009), this could be assured by providing for an efficient ice management combined with good mooring arrangement system such as:

- Icebreaker surveillance to reduce ice actions.
- Internal turret mooring system.
- Azimuth thrusters to clear the ice and to ensure ice vaning.

10. Conclusion

The roof top collapse mechanism adopted by IACS for the derivation of plate thickness requirement seems to overestimate the pressure capacity of a plate field. By running several FE plate fields analysis, it was noticed that the actual collapse mechanism, depending on the plate filed aspect ratio, the patch load aspect ratio and the boundary conditions, may vary between the following collapse mechanisms:

- Roof-top collapse mechanism.
- Double-diamond collapse mechanism, proposed by Lin Hong [7].
- Three parallel hinge lines, proposed by Nyseth and Holtsmark [21].

A varying collapse mechanism makes the derivation of a close form expression of thickness requirement even more complicated. To overcome this overestimation, one can either consider all the above mentioned three collapse mechanisms and select the corresponding minimum pressure capacity or consider only the roof top collapse mechanism and use the calibration "C" factor, eq. (83), to compensate for the IACS overestimation of the plate field capacity.

As discussed earlier, the IACS 3 hinge collapse mechanism together with the assumptions made, may overestimate the pressure capacity for an ice patch loaded frame, depending on the cross section considered and the ratio $\frac{b}{L}$. However, this overestimation may have been already compensated for in the rules by considering the estimation of the design ice patch and/or introducing Peak Pressure Factors PPF.

The steel weight increase due to class increase may be crucial in a pre-design phase of a polar ship, this factor affects the design of polar vessel differently, depending of the nature of the mission, i.e. the design of an offshore support vessel or an FPSO is not as affected by steel weight

increase as a tanker or a bulk carrier. For transportation purposes, using the trans-Arctic routes around the year is already a challenge in terms of, among others, increased fuel consumption due to ice resistance. Increasing the weight due to class increase will reduce the loading capacity of the ship and increase the hull resistance even more.

Moored polar FPSO that can function under all Arctic conditions is a feasible project, which requires special considerations with respect to design and ice management assistance. The assistance of icebreakers around the field of a moored polar FPSO together with good ice threat assessment and detection of hazardous ice features are very necessary factors to operate a polar FPSO in a safe manner. The remaining question is about the profitability of the whole process.

In my opinion, a ship shaped arctic FPSO is a better alternative, as the vessel will have the ability to move more efficiently both in open waters and to a certain extent in ice infested waters compared to a non-conventional hull solution. This can be achieved by meeting the following three conditions:

- A ship-shaped FPSO with an effective ice breaking bow, and a reinforced now-bow regions according to the early discussed line loads, eq. (104).
- A suitable mooring arrangement.
- And an effective ice management system to anticipate ice floes and to evade/counter them.

11. Recommendations to further work

An alternative collapse mechanism for a **transversally stiffened** plate field that may have to be assessed against the FE plate pressure capacity is the **Modified Roof-Top** mechanism. This mechanism is simply the conventional roof-top mechanism without the hinge lines along the unsupported patch edges, fig. (75). For the case of longitudinally stiffened plate filed, the conventional roof top collapse mechanism seems to give acceptable result, fig. (50).

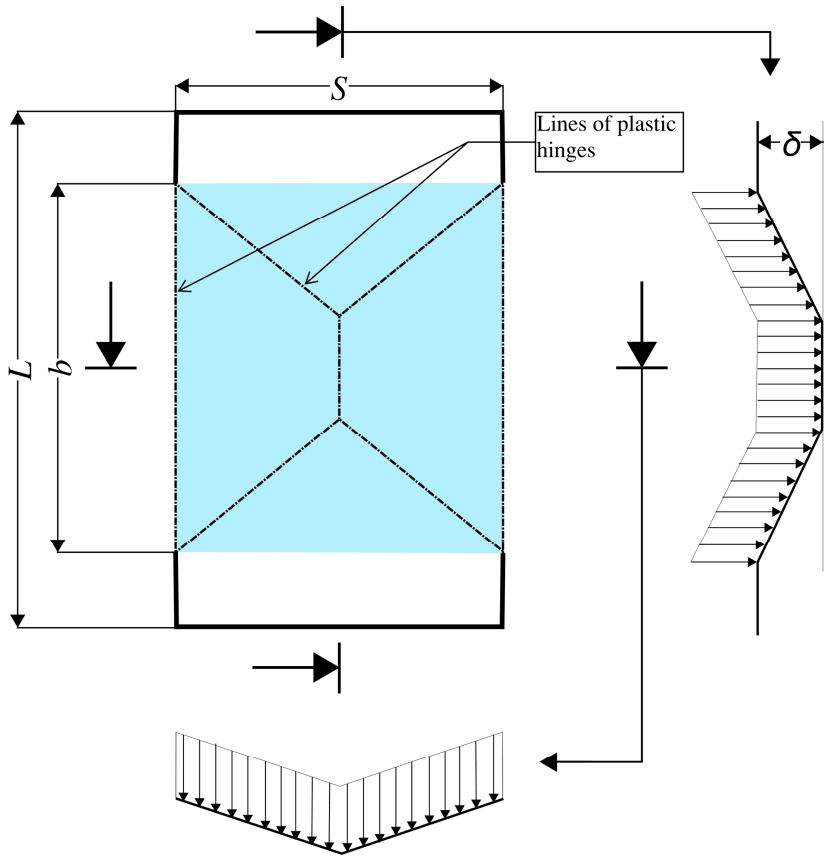

Figure 75: Modified Roof-Top Mechanism

The total reserve resistance, eq. (48), may have to be studied more thoroughly, i.e. numerically and/or analytically, to get a better overview on the variation of the total reserve resistance with respect to the following ratios:

- $\frac{b}{L}$, ratio of the ice patch breadth to the frame span.
- k_w, ratio of the web modulus.
- k_z, ratio of z_p to Z_P.

In the case of a polar FPSO, the line load proposed in equation (104) may have to be studied thoroughly. Equation (100) and (103) may have to be compared considering a range of angles of outboard flare at the water level, $\beta' \in [0^o; 45^o]$ for different hull structures. This comparison may lead to a more simplified line load equation to be applied at the non-bow regions for a polar FPSO, rather than equation (104).

12. References

[1] Tore H. Søreide. Ultimate Load Analysis Of Marine Structures. 2. Opplag 1985.

[2] DERIVATION AND USE OF FORMULATIONS FOR FRAMING DESIGN IN THE POLAR CLASS UNIFIED REQUIREMENTS. By Kendrick, AMARK Inc. and Daley, Daley R&E. January, 2000.

[3] IACS Unified Requirements for Polar Ships. Background Notes to: Shell Plating Thickness. By Evgeny Appolonov Krylov, Shipbuilding Research Institute. March 2000.

[4] IACS Unified Requirements for Polar Ships. Background Notes to: Design Ice Loads. By Claude Daley, Memorial University. February 2000.

[5] Det Norske Veritas. PART 5 CHAPTER 1. Ships for Navigation in Ice. JANUARY 2012.

[6] TMR4205 Buckling and Ultimate Strength of Marine Structures. By Professor Jørgen Amdahl :

- Chapter 3: Buckling of Stiffened Plates. MTS-2009.05.18.
- Chapter 6: Design considerations for stiffened plates subjected to ice action. MTS 2007-01-26.
- Chapter 7: Plastic Methods of Analysis. MTS 2007-01-10.

[7] 7Simplified Analysis and Design of Ships subjected to Collision and Grounding. By Lin Hong. Thesis for the degree of doctor philosophiae. Trondheim, Norway, December 2008.

[8] Conceptual Framework for an Ice Load Model by Claude Daley and Kaj Riska.

[9] Derivation of plastic framing requirements for polar ships. By C.G.Daley. Faculty of Engineering and Applied Science, Memorial University, St. John's, Canada A1B 3X5. 15 February 2002.

[10] ENERGY BASED ICE COLLISION FORCES. By Claude Daley. Memorial University of Newfoundland, St. John's, Newfoundland, Canada A1C 3X5, 1999.

[11] "www.usfos.com"

[12]"http://www.offshoremoorings.org/Moorings/2009/Group02_Prabhakar/OffshoreMooringsWEBSITE25sept2009/FPSO_Specific_Design.htm"

[13] DNV HULL STRUCTURAL RULES, Development, Background, Motives, by Christian Mürer, 1995.

[14] Ice Forces and Ship Response during Ramming and Shoulder Collisions, Phase III-Harmonization of Polar Ship Rules, by Claude Daley, Kaj Riska and Geoffrey Smith.

[15] The IACS Unified Requirements for Polar Ships, I1(August 2006) (Rev.1Jan2007) (Corr.1 Oct 2007).

[16] Background Notes to Hull Area Definition, Extents and Factors. By James Bond American Bureau of Shipping, March 2000.

[17] EN 1993-1-1 (2005) (English): Eurocode 3: Design of steel structures - Part 1-1: General rules and rules for buildings [Authority: The European Union Per Regulation 305/2011, Directive 98/34/EC, Directive 2004/18/EC]

[18] OFFSHORE STANDARD, DNV-OS-C101, DESIGN OF OFFSHORE STEEL STRUCTURES, GENERAL (LRFD METHOD), APRIL 2011.

[19] USFOS USER'S MANUAL, Modelling, MARINTEK 1999-02-17

[20] T. Moan and S. Sævik Chapter 12 - Nonlinear Analysis

[21] Nyseth H. and Holtsmark G. Analytical plastic capacity formulation for plates subject to ice loads and similar types of patch loadings. In: Proc of 25th OMAE, Hamburg, Germany, 12p.

Appendix A: Bending moment calculations for a frame subjected to an ice patch

The bending moments for a patch loaded frame are calculated using the *Displacement Method on Matrix Form* and considering the discretization shown by figure (A.1)

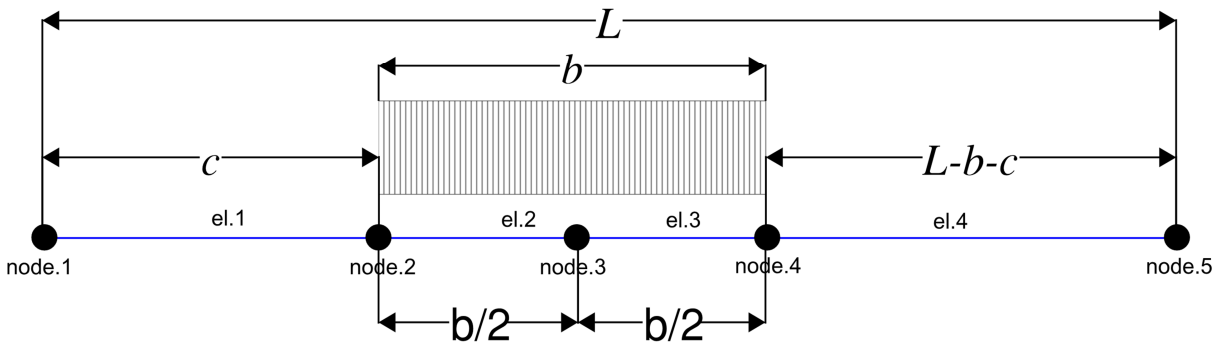

Figure A.1: discretization of a frame subjected to a centrally patch load.

The calculations are carried out using the following Matlab script:

```
syms L b q E I real
c=(L-b)/2;
d=c;
e=b/2;
K1=E*I/c^3*[[12 -6*c -12 -6*c];[-6*c 4*c^2 6*c 2*c^2];[-12 6*c 12 6*c];[-6*c 2*c^2 6*c 4*c^2]];
K2=E*I/e^3*[[12 -6*e -12 -6*e];[-6*e 4*e^2 6*e 2*e^2];[-12 6*e 12 6*e];[-6*e 2*e^2 6*e 4*e^2]];
K3=E*I/e^3*[[12 -6*e -12 -6*e];[-6*e 4*e^2 6*e 2*e^2];[-12 6*e 12 6*e];[-6*e 2*e^2 6*e 4*e^2]];
K4=E*I/d^3*[[12 -6*d -12 -6*d];[-6*d 4*d^2 6*d 2*d^2];[-12 6*d 12 6*d];[-6*d 2*d^2 6*d 4*d^2]];
.....Clamped ends.....
a1_clamped=[[0 0 0 0 0 0];[0 0 0 0 0 0];[1 0 0 0 0 0];[0 1 0 0 0 0]];
a2_clamped=[[1 0 0 0 0 0];[0 1 0 0 0 0];[0 0 1 0 0 0];[0 0 0 1 0 0]];
```

```
a3_clamped=[[0 0 1 0 0 0];[0 0 0 1 0 0];[0 0 0 0 1 0];[0 0 0 0 0 1]];
a4_clamped=[[0 0 0 0 1 0];[0 0 0 0 0 1];[0 0 0 0 0 0];[0 0 0 0 0 0]];
K_tot_clamped=a1_clamped'*K1*a1_clamped+a2_clamped'*K2*a2_clamped+a3_clamped'*K3*a3_clamped+a4_cl
amped'*K4*a4_clamped;
R_2_clamped=a2_clamped'*[q*e/2 -q*e^2/12 q*e/2 q*e^2/12]';
R_3_clamped=a3_clamped'*[q*e/2 -q*e^2/12 q*e/2 q*e^2/12]';
R_clamped=-(R_2_clamped+R_3_clamped);
r_clamped=K_tot_clamped^-1*R_clamped;
S_1_clamped=simplify(K1*a1_clamped*r_clamped)
S_2_clamped=simplify(K2*a2_clamped*r_clamped)
S_3_clamped=simplify(K3*a3_clamped*r_clamped)
S_4_clamped=simplify(K4*a4_clamped*r_clamped)

.....Simply supported.....
a1_free=[[0 0 0 0 0 0 0 0];[1 0 0 0 0 0 0 0];[0 1 0 0 0 0 0 0];[0 0 1 0 0 0 0 0]];
a2_free=[[0 1 0 0 0 0 0 0];[0 0 1 0 0 0 0 0];[0 0 0 1 0 0 0 0];[0 0 0 0 1 0 0 0]];
a3_free=[[0 0 0 1 0 0 0 0];[0 0 0 0 1 0 0 0];[0 0 0 0 0 1 0 0];[0 0 0 0 0 0 1 0]];
a4_free=[[0 0 0 0 0 1 0 0];[0 0 0 0 0 0 1 0];[0 0 0 0 0 0 0 0];[0 0 0 0 0 0 0 1]];
K_tot_free=a1_free'*K1*a1_free+a2_free'*K2*a2_free+a3_free'*K3*a3_free+a4_free'*K4*a4_free;
R2_free=a2_free'*[q*e/2 -q*e^2/12 q*e/2 q*e^2/12]';
R3_free=a3_free'*[q*e/2 -q*e^2/12 q*e/2 q*e^2/12]';
R_free=-(R2_free+R3_free);
r_free=K_tot_free^-1*R_free;
S1_free=simplify(K1*a1_free*r_free)
S2_free=simplify(K2*a2_free*r_free)
S3_free=simplify(K3*a3_free*r_free)
S4_free=simplify(K4*a4_free*r_free)
```

The resulting bending moments at the center and the ends for both simply supported and clamped patch loaded frame are as summarized by figure (A.2)

From figure (A.2), q_2 and q_3 can be obtained as

$$q_2 = \frac{M_{p,red}24L}{b(3L^2 - b^2)}$$

$$q_3 = -\frac{8\left(\frac{A(6L^2b - 6Lb^2 + 2b^3)}{2b(3L^2 - b^2)} - 1\right)}{b(2L - b)}M_p$$

Where:

$$M_{p,red} = \sigma_y . Z_p . A \text{ and } A = \left[1 - k_w + k_w\sqrt{1 - \left(\frac{A_0}{A_w}\right)^2}\right]$$

$$M_p = \sigma_y . Z_p$$

The critical patch line load is then obtained by the sum of the line loads q_2 and q_3, i.e. $q_c = q_2 + q_3$

And the frame line load plastic capacity yields:

$$q_c = \frac{8(A+1)}{b(2L-b)}\sigma_y . Z_p$$

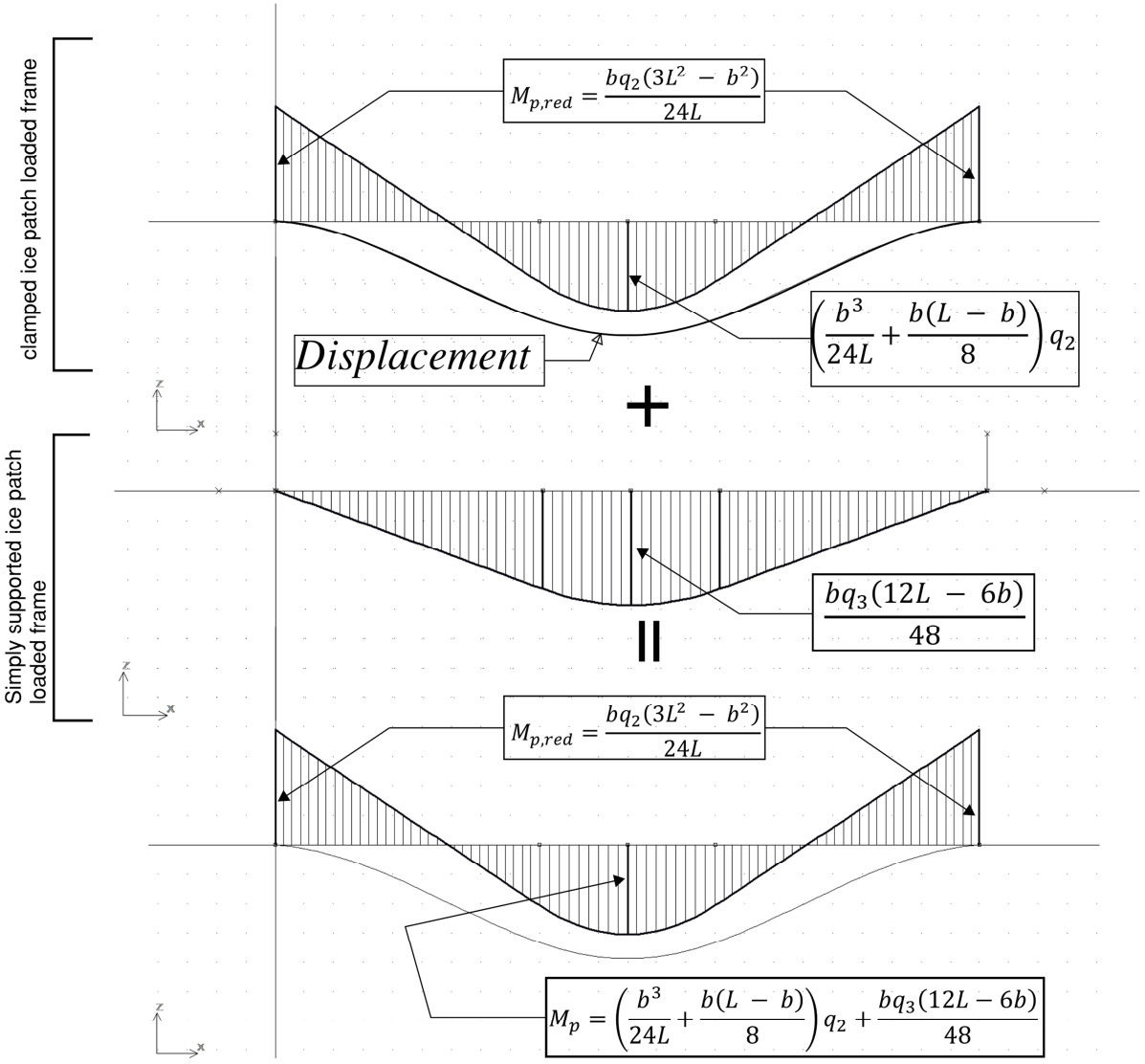
clamped ice patch loaded frame
$M_{p,red} = \frac{bq_2(3L^2 - b^2)}{24L}$
Displacement
$\left(\frac{b^3}{24L} + \frac{b(L-b)}{8}\right)q_2$
+
Simply supported ice patch loaded frame
$\frac{bq_3(12L - 6b)}{48}$
=
$M_{p,red} = \frac{bq_2(3L^2 - b^2)}{24L}$
$M_p = \left(\frac{b^3}{24L} + \frac{b(L-b)}{8}\right)q_2 + \frac{bq_3(12L-6b)}{48}$

Figure A.2:

Appendix B: Plots of the ratios $\frac{q_c}{q_y\alpha}$, $\frac{q_{c,lim}}{q_y\alpha}$ and $\frac{d\left(\frac{q_c}{q_y\alpha}\right)}{db}$ versus $\frac{b}{L}$ for different cross sections and spans.

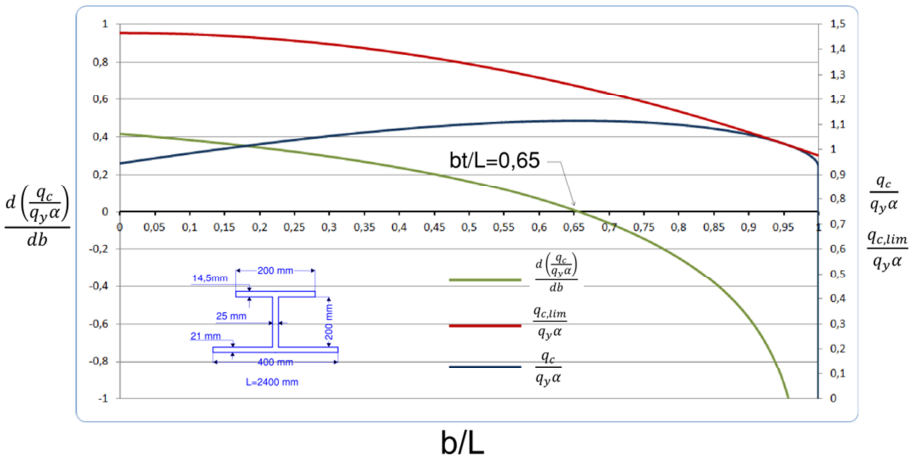

Figure B.1

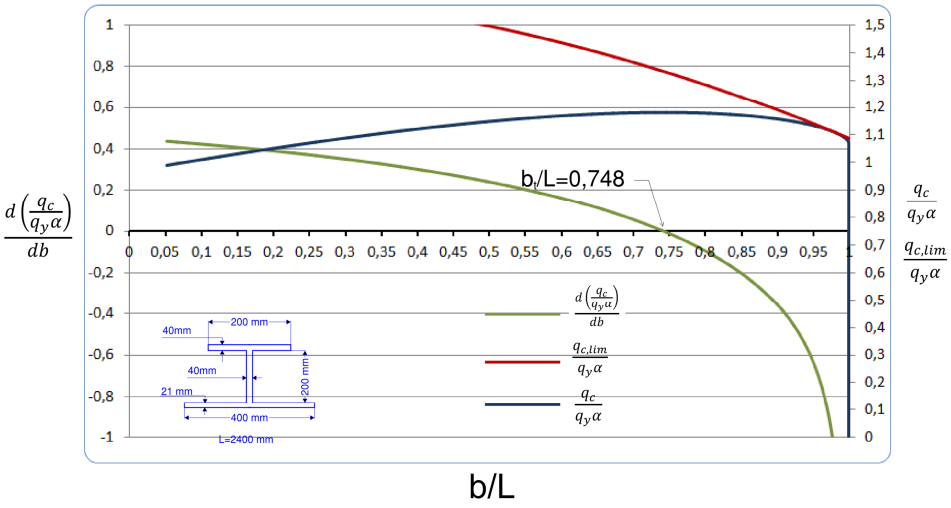

Figure B.2

Address:
NTNU
Department of Marine Technology
N-7491 Trondheim

Location
Marinteknisk Senter
O. Nielsens vei 10

Tel. +47 73 595501
Fax +47 73 595697

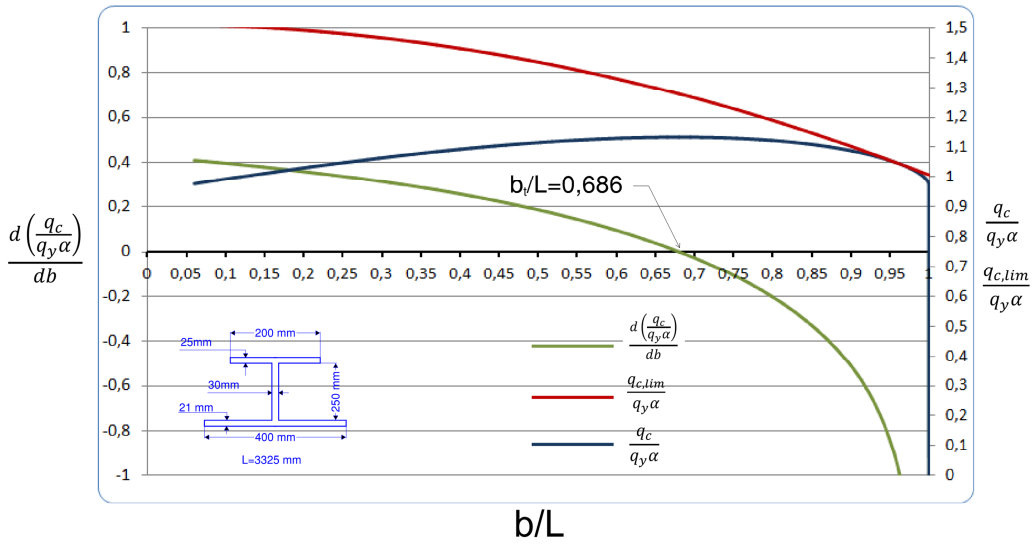

Figure B.3

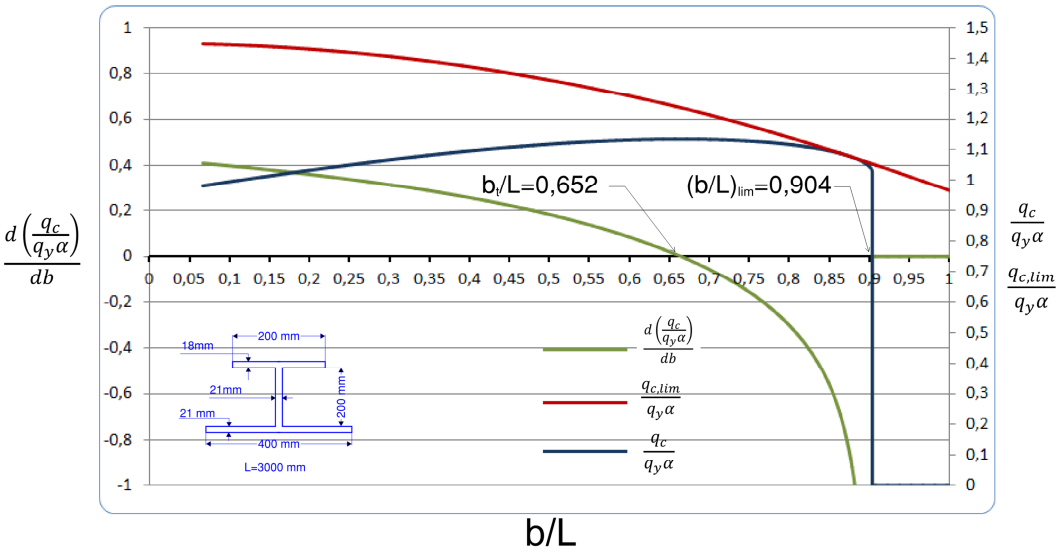

Figure B.4

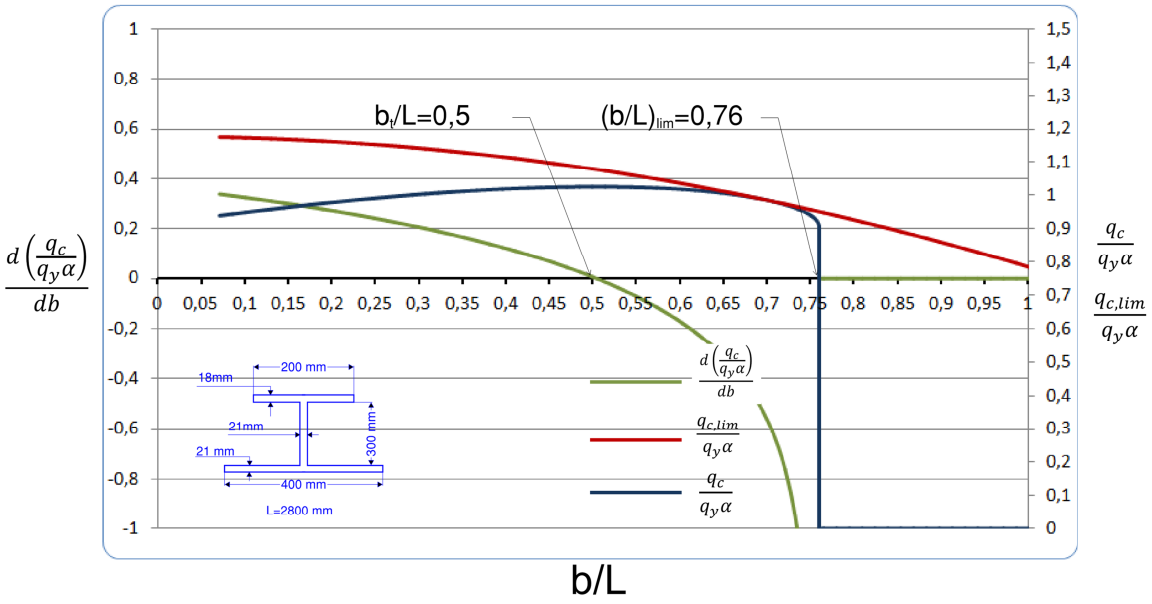

Figure B.5

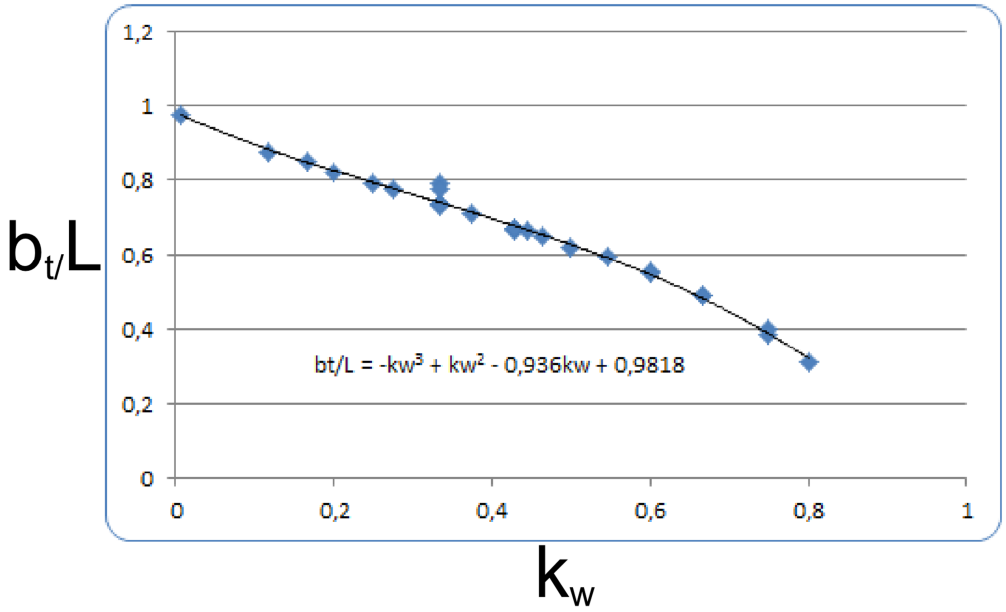

Figure B.6: Plot of the ratios of the ice patch breadth b_t, where the total reserve resistance is maximum, to the span L, i.e. $\frac{b_t}{L}$, versus k_w for different cross sections and spans.

Appendix C:

C.1 Calculations of the frame capacity considering the four hinge collapse mechanism

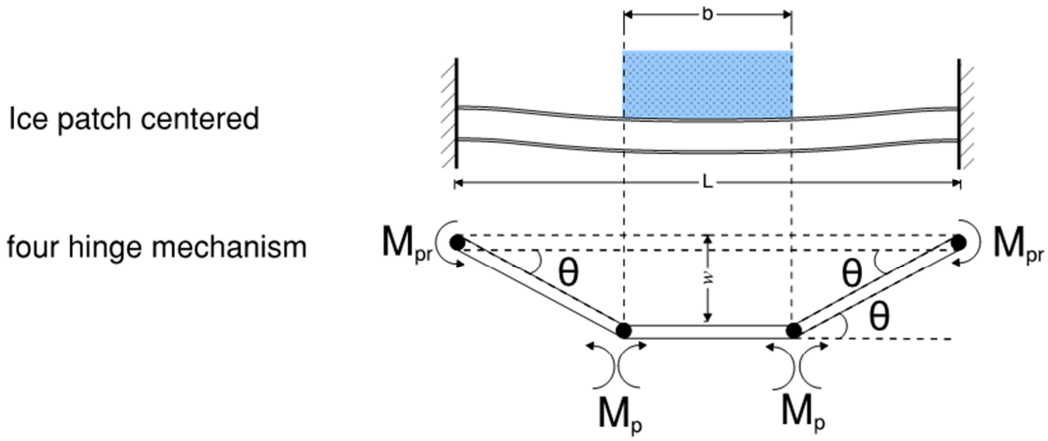

Figure C.1: Four hinges Collapse mechanisms for centrally patch loaded frame with fixed ends

From figure C.1 the external work:

$$W_e = P.S.b.\theta.\frac{L-b}{2}$$

And the internal work:

$$\boldsymbol{W_i = 2.M_{pr}.\theta + 2.M_p.\theta}$$

Where:

$$M_{p,red} = \sigma_y.Z_p.A$$

Address:
NTNU
Department of Marine Technology
N-7491 Trondheim

Location
Marinteknisk Senter
O. Nielsens vei 10

Tel. +47 73 595501
Fax +47 73 595697

$$A = \left[1 - k_w + k_w\sqrt{1 - \left(\frac{A_0}{A_w}\right)^2}\right]$$

$$M_p = \sigma_y . Z_p$$

$$A_0 = \frac{PbS\sqrt{3}}{2\sigma_y}$$

$$k_w = \frac{Z_w}{Z_p}$$

By enforcing that $\boldsymbol{W_e = W_i}$, the plastic section modulus yields:

$$\begin{cases} Z_{p,req} = P_c . b . S\left(1 - \frac{b}{L}\right)\frac{L}{4\sigma_y}A_1 \\ Where\ A_1 = \dfrac{1}{\left[2 - k_w\left(1 - \sqrt{1 - \left(\frac{A_0}{A_w}\right)^2}\right)\right]} \end{cases}$$

And the corresponding pressure capacity is obtained, parallel to the capacity equations derived by C.G.Daley [2] for the 3 hinges collapse mechanism, as follow:

$$P_{Cenrally} = \frac{(2-k_w)+k_w\sqrt{1-48Z_{pns}(1-k_w)}}{12Z_{pns}k_w^2+1}\left(\frac{Z_p\sigma_y 4}{SbL\left(1-\frac{b}{L}\right)}\right) \leq 2\frac{A_w\sigma_y}{\sqrt{3}Sb}$$

Where:

$$Z_{pns} = \left(\frac{Z_p}{A_w L\left(1-\frac{b}{L}\right)}\right)^2$$

Address:
NTNU
Department of Marine Technology
N-7491 Trondheim

Location
Marinteknisk Senter
O. Nielsens vei 10

Tel. +47 73 595501
Fax +47 73 595697

C.2 Plots of the capacity ratio $\frac{P_{Cenrally,4h}}{P_{Cenrally,3h}}$ versus $\frac{b}{L}$

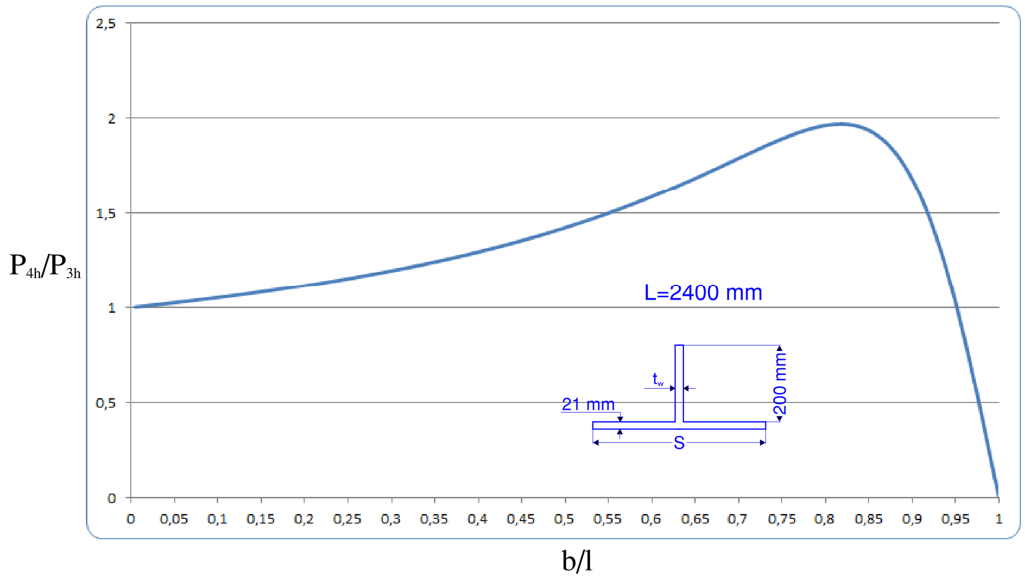

Figure C.2

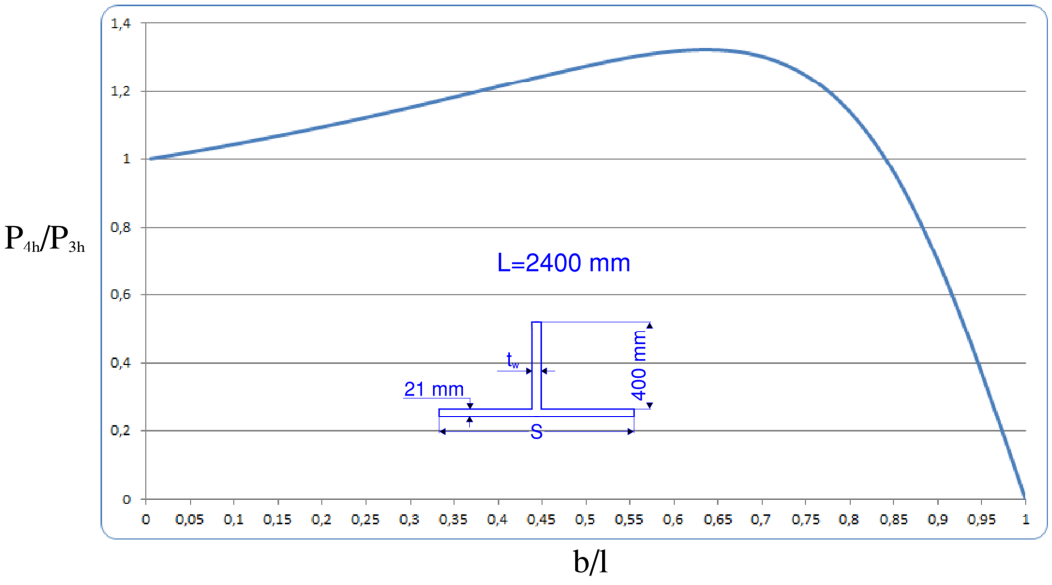

Figure C.3

Address:
NTNU
Department of Marine Technology
N-7491 Trondheim

Location
Marinteknisk Senter
O. Nielsens vei 10

Tel. +47 73 595501
Fax +47 73 595697

NTNU
Norwegian University of Science and Technology
Department of Marine Technology

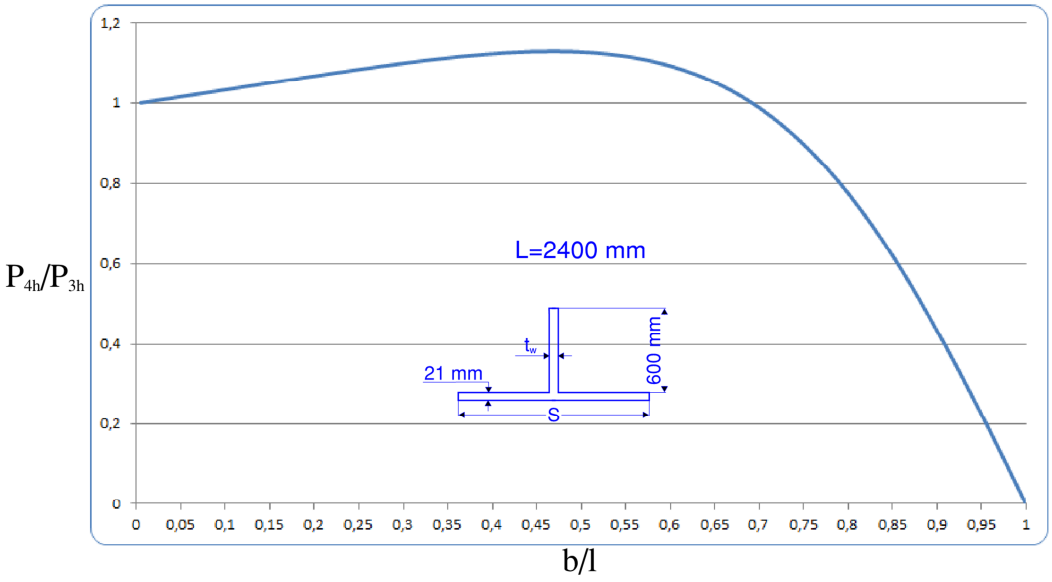

Figure C.4

Address:
NTNU
Department of Marine Technology
N-7491 Trondheim

Location
Marinteknisk Senter
O. Nielsens vei 10

Tel. +47 73 595501
Fax +47 73 595697